

# World Journal of *Radiology*

*World J Radiol* 2017 February 28; 9(2): 27-90



## Editorial Board

2014-2017

The *World Journal of Radiology* Editorial Board consists of 365 members, representing a team of worldwide experts in radiology. They are from 36 countries, including Afghanistan (1), Argentina (2), Australia (5), Austria (7), Belgium (2), Brazil (8), Canada (6), Chile (1), China (43), Croatia (1), Denmark (4), Egypt (6), France (5), Germany (22), Greece (10), India (12), Iran (6), Ireland (2), Israel (3), Italy (47), Japan (13), Netherlands (1), New Zealand (1), Pakistan (1), Poland (2), Portugal (1), Serbia (1), Singapore (3), Slovakia (1), South Korea (18), Spain (4), Sweden (2), Switzerland (4), Thailand (1), Turkey (26), United Kingdom (11), and United States (82).

### EDITORS-IN-CHIEF

Kai U Juergens, *Bremen*  
Edwin JR van Beek, *Edinburgh*  
Thomas J Vogl, *Frankfurt*

### GUEST EDITORIAL BOARD MEMBERS

Wing P Chan, *Taipei*  
Chung-Huei Hsu, *Taipei*  
Chin-Chang Huang, *Taipei*  
Tsong-Long Hwang, *Taoyuan*  
Jung-Lung Hsu, *Taipei*  
Chia-Hung Kao, *Taichung*  
Yu-Ting Kuo, *Tainan*  
Hon-Man Liu, *Taipei*  
Hui-Lung Liang, *Kaohsiung*  
Chun Chung Lui, *Kaohsiung*  
Sen-Wen Teng, *Taipei*  
Yung-Liang (William) Wan, *Taoyuan*

### MEMBERS OF THE EDITORIAL BOARD



#### Afghanistan

Takao Hiraki, *Okayama*



#### Argentina

Patricia Carrascosa, *Vicente Lopez*  
Maria C Ziadi, *Rosario*



#### Australia

Lourens Bester, *Sydney*  
Gemma A Figtree, *Sydney*

Stuart M Grieve, *Sydney*  
Wai-Kit Lee, *Fitzroy*  
Prabhakar Ramachandran, *Melbourne*



#### Austria

Herwig R Cerwenka, *Graz*  
Gudrun M Feuchtnner, *Innsbruck*  
Benjamin Henninger, *Innsbruck*  
Rupert Lanzenberger, *Vienna*  
Shu-Ren Li, *Vienna*  
Veronika Schopf, *Vienna*  
Tobias De Zordo, *Innsbruck*



#### Belgium

Steve Majerus, *Liege*  
Kathelijne Peremans, *Merelbeke*



#### Brazil

Clerio F Azevedo, *Rio de Janeiro*  
Patrícia P Alfredo, *São Paulo*  
Eduardo FC Fleury, *São Paulo*  
Edward Araujo Júnior, *São Paulo*  
Wellington P Martins, *Ribeirao Preto*  
Ricardo A Mesquita, *Belo Horizonte*  
Vera MC Salemi, *São Paulo*  
Claudia Szobot, *Porto Alegre*  
Lilian YI Yamaga, *São Paulo*



#### Canada

Marie Arsalidou, *Toronto*  
Otman A Basir, *Waterloo*

Tarik Zine Belhocine, *Toronto*  
James Chow, *Toronto*  
Tae K Kim, *Toronto*  
Anastasia Oikonomou, *Toronto*



#### China

Hong-Wei Chen, *Wuxi*  
Feng Chen, *Hangzhou*  
Jian-Ping Chu, *Guangzhou*  
Guo-Guang Fan, *Shenyang*  
Bu-Lang Gao, *Shijiazhuang*  
Qi-Yong Gong, *Chengdu*  
Ying Han, *Beijing*  
Xian-Li Lv, *Beijing*  
Yi-Zhuo Li, *Guangzhou*  
Xiang-Xi Meng, *Harbin*  
Yun Peng, *Beijing*  
Jun Shen, *Guangzhou*  
Ze-Zhou Song, *Hangzhou*  
Wai Kwong Tang, *Hong Kong*  
Gang-Hua Tang, *Guangzhou*  
Jie Tian, *Beijing*  
Lu-Hua Wang, *Beijing*  
Xiao-bing Wang, *Xi'an*  
Yi-Gen Wu, *Nanjing*  
Kai Wu, *Guangzhou*  
Hui-Xiong Xu, *Shanghai*  
Zuo-Zhang Yang, *Kunming*  
Xiao-Dan Ye, *Shanghai*  
David T Yew, *Hong Kong*  
Ting-He Yu, *Chongqing*  
Zheng Yuan, *Shanghai*  
Min-Ming Zhang, *Hangzhou*  
Yudong Zhang, *Nanjing*  
Dong Zhang, *Chongqing*  
Wen-Bin Zeng, *Changsha*

Yue-Qi Zhu, *Shanghai*



**Croatia**

Goran Kusec, *Osijek*



**Denmark**

Poul E Andersen, *Odense*

Lars J Petersen, *Aalborg*

Thomas Z Ramsøy, *Frederiksberg*

Morten Ziebell, *Copenhagen*



**Egypt**

Mohamed F Bazeed, *Mansoura*

Mohamed Abou El-Ghar, *Mansoura*

Reem HA Mohamed, *Cairo*

Mohamed R Nouh, *Alexandria*

Ahmed AKA Razek, *Mansoura*

Ashraf A Zytoon, *Shebin El-Koom*



**France**

Sabine F Bensamoun, *Compiègne*

Romarc Loffroy, *Dijon*

Stephanie Nougaret, *Montpellier*

Hassane Oudadesse, *Rennes*

Vincent Vinh-Hung, *Fort-de-France*



**Germany**

Henryk Barthel, *Leipzig*

Peter Bannas, *Hamburg*

Martin Beeres, *Frankfurt*

Ilja F Ciernik, *Dessau*

A Dimitrakopoulou-Strauss, *Heidelberg*

Peter A Fasching, *Erlangen*

Andreas G Schreyer, *Regensburg*

Philipp Heusch, *Duesseldorf*

Sonja M Kirchhoff, *Munich*

Sebastian Ley, *Munich*

Adel Maataoui, *Frankfurt am Main*

Stephan M Meckel, *Freiburg*

Hans W Muller, *Duesseldorf*

Kay Raum, *Berlin*

Dirk Rades, *Luebeck*

Marc-Ulrich Regier, *Hamburg*

Alexey Surov, *Halle*

Martin Walter, *Magdeburg*

Axel Wetter, *Essen*

Christoph Zilkens, *Düsseldorf*



**Greece**

Panagiotis Antoniou, *Thessaloniki*

Nikos Efthimiou, *Athens*

Dimitris Karnabatidis, *Patras*

George Latsios, *Athens*

Stylianios Megremis, *Iraklion*

Alexander D Rapidis, *Athens*

Kiki Theodorou, *Larissa*

Ioannis A Tsalafoutas, *Athens*

Evanthia E Tripoliti, *Ioannina*

Athina C Tsili, *Ioannina*



**India**

Ritesh Agarwal, *Chandigarh*

Chandan J Das, *New Delhi*

Prathamesh V Joshi, *Mumbai*

Naveen Kalra, *Chandigarh*

Chandrasekharan Kesavadas, *Trivandrum*

Jyoti Kumar, *New Delhi*

Atin Kumar, *New Delhi*

Kaushala P Mishra, *Allahabad*

Daya N Sharma, *New Delhi*

Binit Sureka, *New Delhi*

Sanjay Sharma, *New Delhi*

Raja R Yadav, *Allahabad*



**Iran**

Majid Assadi, *Bushehr*

SeyedReza Najafizadeh, *Tehran*

Mohammad Ali Oghabian, *Tehran*

Amir Reza Radmard, *Tehran*

Ramin Sadeghi, *Mashhad*

Hadi Rokni Yazdi, *Tehran*



**Ireland**

Tadhg Gleeson, *Wexford*

Frederik JAI Vernimmen, *Cork*



**Israel**

Dafna Ben Bashat, *Tel Aviv*

Amit Gefen, *Tel Aviv*

Tamar Sella, *Jerusalem*



**Italy**

Adriano Alippi, *Rome*

Dante Amelio, *Trento*

Michele Anzidei, *Rome*

Filippo F Angileri, *Messinas*

Stefano Arcangeli, *Rome*

Roberto Azzoni, *San Donato milanese*

Tommaso V Bartolotta, *Palermo*

Tommaso Bartalena, *Imola*

Livia Bernardin, *San Bonifacio*

Federico Boschi, *Verona*

Sergio Casciaro, *Lecce*

Emanuele Casciani, *Rome*

Musa M Can, *Napoli*

Alberto Cuocolo, *Napoli*

Michele Ferrara, *Coppito*

Mauro Feola, *Fossano*

Giampiero Francica, *Castel Volturno*

Luigi De Gennaro, *Rome*

Giulio Giovannetti, *Pisa*

Francesca Iacobellis, *Napoli*

Formato Invernizzi, *Monza Brianza*

Francesco Lassandro, *Naples*

Lorenzo Livi, *Florence*

Pier P Mainenti, *Napoli*

Laura Marzetti, *Chieti*

Giuseppe Malinverni, *Crescentino*

Enrica Milanese, *Turin*

Giovanni Morana, *Treviso*

Lorenzo Monti, *Milan*

Silvia D Morbelli, *Genoa*

Barbara Palumbo, *Perugia*

Cecilia Parazzini, *Milan*

Stefano Pergolizzi, *Messina*

Antonio Pinto, *Naples*

Camillo Porcaro, *Rome*

Carlo C Quattrocchi, *Rome*

Alberto Rebonato, *Perugia*

Giuseppe Rizzo, *Rome*

Roberto De Rosa, *Naples*

Domenico Rubello, *Rovigo*

Andrea Salvati, *Bari*

Sergio Sartori, *Ferrara*

Luca M Sconfienza, *Milano*

Giovanni Storto, *Rionero*

Nicola Sverzellati, *Parma*

Alberto S Tagliafico, *Genova*

Nicola Troisi, *Florence*



**Japan**

Yasuhiko Hori, *Chiba*

Hidetoshi Ikeda, *Koriyama*

Masahito Kawabori, *Sapporo*

Tamotsu Kamishima, *Sapporo*

Hiro Kiyosue, *Yufu*

Yasunori Minami, *Osaka-sayama*

Yasuhiro Morimoto, *Kitakyushu*

Satoru Murata, *Tokyo*

Shigeki Nagamachi, *Miyazaki*

Hiroshi Onishi, *Yamanashi*

Morio Sato, *Wakayama Shi*

Yoshito Tsushima, *Maebashi*

Masahiro Yanagawa, *Suita*



**Netherlands**

Willem Jan van Rooij, *Tilburg*



**New Zealand**

W Howell Round, *Hamilton*



**Pakistan**

Wazir Muhammad, *Abbottabad*



**Poland**

Maciej S Baglaj, *Wroclaw*

Piotr Czauderna, *Gdansk*



### Portugal

Joao Manuel RS Tavares, *Porto*



### Serbia

Olivera Ciraj-Bjelac, *Belgrade*



### Singapore

Gopinathan Anil, *Singapore*

Terence KB Teo, *Singapore*

Cher Heng Tan, *Singapore*



### Slovakia

Stefan Sivak, *Martin*



### South Korea

Ki Seok Choo, *Busan*

Seung Hong Choi, *Seoul*

Dae-Seob Choi, *Jinju*

Hong-Seok Jang, *Seoul*

Yong Jeong, *Daejeon*

Chan Kyo Kim, *Seoul*

Se Hyung Kim, *Seoul*

Joong-Seok Kim, *Seoul*

Sang Eun Kim, *Seongnam*

Sung Joon Kwon, *Seoul*

Jeong Min Lee, *Seoul*

In Sook Lee, *Busan*

Noh Park, *Goyang*

Chang Min Park, *Seoul*

Sung Bin Park, *Seoul*

Deuk Jae Sung, *Seoul*

Choongsoo Shin, *Seoul*

Kwon-Ha Yoon, *Iksan*



### Spain

Miguel A De Gregorio, *Zaragoza*

Antonio Luna, *Jaén*

Enrique Marco de Lucas, *Santander*

Fernando Ruiz Santiago, *Granada*



### Sweden

Dmitry Grishenkov, *Stockholm*

Tie-Qiang Li, *Stockholm*



### Switzerland

Nicolau Beckmann, *Basel*

Christian Boy, *Bern*

Giorgio Treglia, *Bellinzona*

Stephan Ulmer, *Kiel*



### Thailand

Sirianong Namwongprom, *Chiang Mai*



### Turkey

Kubilay Aydin, *Istanbul*

Ramazan Akdemir, *Sakarya*

Serhat Avcu, *Ankara*

Ayşe Aralasmak, *Istanbul*

Oktay Algin, *Ankara*

Nevbahar Akcar, *Meselik*

Bilal Battal, *Ankara*

Zulkif Bozgeyik, *Elazig*

Nazan Ciledag, *Aakara*

Fuldem Y Donmez, *Ankara*

Gulgun Engin, *Istanbul*

Ahmet Y Goktay, *Izmir*

Oguzhan G Gumustas, *Bursa*

Kaan Gunduz, *Ankara*

Pelin Ozcan Kara, *Mersin*

Kivanc Kamburoglu, *Ankara*

Ozgur Kilickesmez, *Istanbul*

Furuzan Numan, *Istanbul*

Cem Onal, *Adana*

Ozgur Oztekin, *Izmir*

Seda Ozbek (Boruban), *Konya*

Selda Sarikaya, *Zonguldak*

Figen Taser, *Kutahya*

Baran Tokar, *Eskisehir*

Ender Uysal, *Istanbul*

Ensar Yekeler, *Istanbul*



### United Kingdom

Indran Davagnanam, *London*

M DC Valdés Hernández, *Edinburgh*

Alan Jackson, *Manchester*

Suneil Jain, *Belfast*

Long R Jiao, *London*

Miltiadis Krokidis, *Cambridge*

Pradesh Kumar, *Liverpool*

Peter D Kuzmich, *Derby*

Georgios Plataniotis, *Brighton*

Vanessa Sluming, *Liverpool*



### United States

Garima Agrawal, *Saint Louis*

James R Brasic, *Baltimore*

Rajendra D Badgaiyan, *Buffalo*

Ulas Bagci, *Bethesda*

Anat Biegon, *Stony Brook*

Ramon Casanova, *Winston Salem*

Wenli Cai, *Boston*

Zheng Chang, *Durham*

Corey J Chakarun, *Long Beach*

Kai Chen, *Los Angeles*

Hyun-Soon Chong, *Chicago*

Marco Cura, *Dallas*

Ravi R Desai, *Bensalem*

Delia DeBuc, *Miami*

Carlo N De Cecco, *Charleston*

Timm-Michael L Dickfeld, *Baltimore*

Subba R Digumarthy, *Boston*

Huy M Do, *Stanford*

Todd A Faasse, *Grand Rapids*

Salomao Faintuch, *Boston*

Girish M Fatterpekar, *New York*

Dhakshinamoorthy Ganesan, *Houston*

Robert J Griffin, *Little Rock*

Andrew J Gunn, *Boston*

Sandeep S Hedgire, *Boston*

Timothy J Hoffman, *Columbia*

Mai-Lan Ho, *San Francisco*

Juebin Huang, *Jackson*

Abid Irshad, *Charleston*

Matilde Inglese, *New York*

El-Sayed H Ibrahim, *Jacksonville*

Paul R Julsrud, *Rochester*

Pamela T Johnson, *Baltimore*

Ming-Hung Kao, *Tempe*

Sunil Krishnan, *Houston*

Richard A Komoroski, *Cincinnati*

Sandi A Kwee, *Honolulu*

King Kim, *Ft. Lauderdale*

Guozheng Liu, *Worcester*

Yiyan Liu, *Newark*

Venkatesh Mani, *New York*

Lian-Sheng Ma, *Pleasanton*

Rachna Madan, *Boston*

Zeyad A Metwalli, *Houston*

Yilong Ma, *Manhasset*

Hui Mao, *Atlanta*

Feroze B Mohamed, *Philadelphia*

Gul Moonis, *Boston*

John L Noshier, *New Brunswick*

Rahmi Oklu, *Boston*

Aytekun Oto, *Chicago*

Bishnuhari Paudyal, *Philadelphia*

Rajul Pandya, *Youngstown*

Chong-Xian Pan, *Sacramento*

Jay J Pillai, *Baltimore*

Neal Prakash, *Duarte*

Reza Rahbar, *Boston*

Ali S Raja, *Boston*

Gustavo J Rodriguez, *El Paso*

David J Sahn, *Portland*

Steven Schild, *Scottsdale*

Ali R Sepahdari, *Los Angeles*

Li Shen, *Indianapolis*

JP Sheehan, *Charlottesville*

Atul B Shinagare, *Boston*

Sarabjeet Singh, *Boston*

Charles J Smith, *Columbia*

Kenji Suzuki, *Chicago*

Monvadi Srichai-Parsia, *Washington*

Sree H Tirumani, *Boston*

Hebert A Vargas, *New York*

Sachit Verma, *Philadelphia*

Yoichi Watanabe, *Minneapolis*

Li Wang, *Chapel Hill*

Carol C Wu, *Boston*

Shoujun Xu, *Houston*

Min Yao, *Cleveland*

Xiaofeng Yang, *Atlanta*

Qingbao Yu, *Albuquerque*

Aifeng Zhang, *Chicago*

Chao Zhou, *Bethlehem*

Hongming Zhuang, *Philadelphia*



**EDITORIAL**

- 27 Evaluation of response to immune checkpoint inhibitors: Is there a role for positron emission tomography?  
*Bauckneht M, Piva R, Sambuceti G, Grossi F, Morbelli S*

**REVIEW**

- 34 Potential role of imaging in assessing harmful effects on spermatogenesis in adult testes with varicocele  
*Tsili AC, Xiropotamou ON, Sylakos A, Maliakas V, Sofikitis N, Argyropoulou MI*

**MINIREVIEWS**

- 46 Magnetic resonance enterography in Crohn's disease: How we do it and common imaging findings  
*Mantarro A, Scalise P, Guidi E, Neri E*

**ORIGINAL ARTICLE****Basic Study**

- 55 Radiology education in Europe: Analysis of results from 22 European countries  
*Rehani B, Zhang YC, Rehani MM, Palkó A, Lau L, Lette MNM, Dillon WP*
- 63 Radiation dose enhancement in skin therapy with nanoparticle addition: A Monte Carlo study on kilovoltage photon and megavoltage electron beams  
*Zheng XJ, Chow JCL*

**Retrospective Study**

- 72 Magnetic resonance imaging in the assessment of brain involvement in alcoholic and nonalcoholic Wernicke's encephalopathy  
*Sparacia G, Anastasi A, Speciale C, Agnello F, Banco A*

**Observational Study**

- 79 Feasibility of imaging superficial palmar arch using micro-ultrasound, 7T and 3T magnetic resonance imaging  
*Pruzan AN, Kaufman AE, Calcagno C, Zhou Y, Fayad ZA, Mani V*
- 85 Gastric blunt traumatic injuries: A computed tomography grading classification  
*Solazzo A, Lassandro G, Lassandro F*

## Contents

*World Journal of Radiology*  
Volume 9 Number 2 February 28, 2017

### ABOUT COVER

Editorial Board Member of *World Journal of Radiology*, Nicola Sverzellati, MD, Academic Research, Department of Surgical Sciences, Section of Radiology, University of Parma, 43121 Parma, Italy

### AIM AND SCOPE

*World Journal of Radiology* (*World J Radiol*, *WJR*, online ISSN 1949-8470, DOI: 10.4329) is a peer-reviewed open access academic journal that aims to guide clinical practice and improve diagnostic and therapeutic skills of clinicians.

*WJR* covers topics concerning diagnostic radiology, radiation oncology, radiologic physics, neuroradiology, nuclear radiology, pediatric radiology, vascular/interventional radiology, medical imaging achieved by various modalities and related methods analysis. The current columns of *WJR* include editorial, frontier, diagnostic advances, therapeutics advances, field of vision, mini-reviews, review, topic highlight, medical ethics, original articles, case report, clinical case conference (clinicopathological conference), and autobiography.

We encourage authors to submit their manuscripts to *WJR*. We will give priority to manuscripts that are supported by major national and international foundations and those that are of great basic and clinical significance.

### INDEXING/ABSTRACTING

*World Journal of Radiology* is now indexed in PubMed, PubMed Central.

### FLYLEAF

I-III Editorial Board

### EDITORS FOR THIS ISSUE

Responsible Assistant Editor: *Xiang Li*  
Responsible Electronic Editor: *Huan-Liang Wu*  
Proofing Editor-in-Chief: *Lian-Sheng Ma*

Responsible Science Editor: *Jin-Xin Kong*  
Proofing Editorial Office Director: *Xiu-Xia Song*

NAME OF JOURNAL  
*World Journal of Radiology*

ISSN  
ISSN 1949-8470 (online)

LAUNCH DATE  
January 31, 2009

FREQUENCY  
Monthly

EDITORS-IN-CHIEF  
**Kai U Juergens, MD, Associate Professor, MRT** und PET/CT, Nuklearmedizin Bremen Mitte, ZEMODI - Zentrum für morphologische und molekulare Diagnostik, Bremen 28177, Germany

**Edwin JR van Beek, MD, PhD, Professor**, Clinical Research Imaging Centre and Department of Medical Radiology, University of Edinburgh, Edinburgh EH16 4TJ, United Kingdom

**Thomas J Vogl, MD, Professor, Reader in Health Technology Assessment**, Department of Diagnostic and Interventional Radiology, Johann Wolfgang Goethe University of Frankfurt, Frankfurt 60590,

Germany

EDITORIAL BOARD MEMBERS  
All editorial board members resources online at <http://www.wjnet.com/1949-8470/editorialboard.htm>

EDITORIAL OFFICE  
Xiu-Xia Song, Director  
*World Journal of Radiology*  
Baishideng Publishing Group Inc  
8226 Regency Drive, Pleasanton, CA 94588, USA  
Telephone: +1-925-2238242  
Fax: +1-925-2238243  
E-mail: [editorialoffice@wjnet.com](mailto:editorialoffice@wjnet.com)  
Help Desk: <http://www.wjnet.com/esps/helpdesk.aspx>  
<http://www.wjnet.com>

PUBLISHER  
Baishideng Publishing Group Inc  
8226 Regency Drive,  
Pleasanton, CA 94588, USA  
Telephone: +1-925-2238242  
Fax: +1-925-2238243  
E-mail: [bpgoffice@wjnet.com](mailto:bpgoffice@wjnet.com)  
Help Desk: <http://www.wjnet.com/esps/helpdesk.aspx>  
<http://www.wjnet.com>

PUBLICATION DATE  
February 28, 2017

COPYRIGHT  
© 2017 Baishideng Publishing Group Inc. Articles published by this Open-Access journal are distributed under the terms of the Creative Commons Attribution Non-commercial License, which permits use, distribution, and reproduction in any medium, provided the original work is properly cited, the use is non commercial and is otherwise in compliance with the license.

SPECIAL STATEMENT  
All articles published in journals owned by the Baishideng Publishing Group (BPG) represent the views and opinions of their authors, and not the views, opinions or policies of the BPG, except where otherwise explicitly indicated.

INSTRUCTIONS TO AUTHORS  
<http://www.wjnet.com/bpg/gerinfo/204>

ONLINE SUBMISSION  
<http://www.wjnet.com/esps/>

## Evaluation of response to immune checkpoint inhibitors: Is there a role for positron emission tomography?

Matteo Bauckneht, Roberta Piva, Gianmario Sambuceti, Francesco Grossi, Silvia Morbelli

Matteo Bauckneht, Roberta Piva, Gianmario Sambuceti, Silvia Morbelli, Nuclear Medicine Unit, IRCCS San Martino-IST, University of Genoa, 16132 Genoa, Italy

Francesco Grossi, Lung Cancer Unit, IRCCS San Martino-IST, University of Genoa, 16132 Genoa, Italy

**Author contributions:** Morbelli S conceived and designed the study; Bauckneht M and Morbelli S drafted the manuscript; Bauckneht M and Piva R prepared the tables and figures; Sambuceti G and Grossi F critically revised the manuscript; all the authors approved the final version of the paper.

**Conflict-of-interest statement:** The authors have no conflicts of interest related to this publication to disclose.

**Open-Access:** This article is an open-access article which was selected by an in-house editor and fully peer-reviewed by external reviewers. It is distributed in accordance with the Creative Commons Attribution Non Commercial (CC BY-NC 4.0) license, which permits others to distribute, remix, adapt, build upon this work non-commercially, and license their derivative works on different terms, provided the original work is properly cited and the use is non-commercial. See: <http://creativecommons.org/licenses/by-nc/4.0/>

**Manuscript source:** Invited manuscript

**Correspondence to:** Silvia Morbelli, MD, PhD, Nuclear Medicine Unit, IRCCS San Martino-IST, University of Genoa, Largo R. Benzi 10, 16132 Genova, Italy. [silviadaniela.morbelli@hsanmartino.it](mailto:silviadaniela.morbelli@hsanmartino.it)  
Telephone: +39-010-5552026  
Fax: +39-010-5556911

Received: August 20, 2016

Peer-review started: August 23, 2016

First decision: October 21, 2016

Revised: November 2, 2016

Accepted: November 27, 2016

Article in press: November 29, 2016

Published online: February 28, 2017

such as immune checkpoint inhibitors (ICPIs) have demonstrated significant antitumor activity across a wide range of solid tumors. In the clinical practice, the radiological effect of immunotherapeutic agents has raised several more relevant and complex challenges for the determination of their imaging-based response at single patient level. Accordingly, it has been suggested that the conventional Response Evaluation Criteria in Solid Tumors assessment alone, based on dimensional evaluation provided by computed tomography (CT), tends to underestimate the benefit of ICPIs at least in a subset of patients, supporting the need of immune-related response criteria. Different from CT, very few data are available for the evaluation of immunotherapy by means of  $^{18}\text{F}$ -fluoro-2-deoxy-D-glucose positron emission tomography (FDG-PET). Moreover, since the antineoplastic activity of ICPIs is highly related to the activation of T cells against cancer cells, FDG accumulation might cause false-positive findings. Yet, discrimination between benign and malignant processes represents a huge challenge for FDG-PET in this clinical setting. Consequently, it might be of high interest to test the complex and variegated response to ICPIs by means of PET and thus it is worthwhile to ask if a similar introduction of immune-related PET-based criteria could be proposed in the future. Finally, PET might offer a new insight into the biology and pathophysiology of ICPIs thanks to a growing number of non-invasive immune-diagnostic approaches based on non-FDG tracers.

**Key words:** Immune checkpoint inhibitors; Positron emission tomography; Computed tomography;  $^{18}\text{F}$ -fluoro-2-deoxy-D-glucose; Non- $^{18}\text{F}$ -fluoro-2-deoxy-D-glucose tracers

© **The Author(s) 2017.** Published by Baishideng Publishing Group Inc. All rights reserved.

**Core tip:** In the clinical practice, the radiological interpretation of immunotherapy effects represents a huge challenge at single patient level. However, although the computed tomography-based response

### Abstract

Strategies targeting intracellular negative regulators

evaluation for immune checkpoint inhibitors (ICPIs) is feasible thanks to the introduction of immune-related response criteria, very few data are available for the potential role of  $^{18}\text{F}$ -fluoro-2-deoxy-D-glucose positron emission tomography (FDG-PET). Due to the intrinsic nature of FDG accumulation pathophysiology, it might be central to test the complex and variegated response to ICPIs by means of PET. Finally, PET might offer a new insight into the biology of ICPIs thanks to a growing number of non-invasive immune-diagnostic approaches based on non-FDG tracers.

Bauckneht M, Piva R, Sambuceti G, Grossi F, Morbelli S. Evaluation of response to immune checkpoint inhibitors: Is there a role for positron emission tomography? *World J Radiol* 2017; 9(2): 27-33 Available from: URL: <http://www.wjgnet.com/1949-8470/full/v9/i2/27.htm> DOI: <http://dx.doi.org/10.4329/wjr.v9.i2.27>

## TEXT

The function of the immune system is characterized by multiple checkpoints aiming to avoid its over-activation against healthy cells (self-tolerance)<sup>[1]</sup>. Cancer cells may take advantage of these checkpoints to escape detection by the immune system. Some of these checkpoints such as cytotoxic T-lymphocyte-associated antigen 4 (CTLA-4) and programmed cell death protein 1 (PD-1) have been extensively studied as targets in the frame of the so-called cancer immunotherapy<sup>[1]</sup>. CTLA-4 counteracts the activity of the T cell co-stimulatory receptor CD28 and actively delivers inhibitory signals to the T cell<sup>[2]</sup>. PD-1 has two ligands, PD1 ligand 1 (PDL1) and PDL2, and its inhibitory effect is accomplished through a dual mechanism of promoting apoptosis in antigen specific T-cells in lymph nodes while simultaneously reducing apoptosis in regulatory T cells (suppressor T cells)<sup>[3]</sup>. In the last few years, the blockade of immune checkpoints has disclosed the potential of the antitumor immune response in a fashion that is transforming human cancer therapeutics. CTLA4 antibodies such as ipilimumab and tremelimumab have been tested in the last ten years in different types of cancer, starting with patients with advanced melanoma<sup>[4]</sup>. Ipilimumab was the first therapy to demonstrate a survival benefit for patients with metastatic melanoma. In a study by Hodi *et al.*<sup>[5]</sup>, ipilimumab significantly improved overall survival in patients with previously treated metastatic melanoma and the drug was approved by the United States Food and Drug Administration (FDA) for the treatment of advanced melanoma in 2011<sup>[5]</sup>. Similarly, nivolumab, a humanized anti-PD-1 monoclonal antibody, has demonstrated durable responses in several phase III trials and has received FDA approval in specific clinical settings in patients with melanoma, renal cell cancer, Hodgkin's lymphoma, bladder cancer, and non-small cell lung cancer (NSCLC)<sup>[6-9]</sup>. Figure 1 summarizes the

mechanisms of action of the two FDA approved immune checkpoint inhibitors (ICPIs).

## Evaluation of response to ICPIs

Historically, the Response Evaluation Criteria in Solid Tumors (RECIST) has been validated and used to evaluate antitumor responses to chemotherapeutic agents<sup>[10]</sup> (Table 1 for a more detailed description). These criteria are based on dimensional evaluation and rely on the fact that the cytotoxic effect of chemotherapeutic agents tends to translate into measurable effects in terms of tumor shrinkage from baseline. Furthermore, published studies indicated that achieving a response according to RECIST criteria is predictive of remission and improved survival in specific settings<sup>[11]</sup>. Conversely, both RECIST and their revised 1.1 version assumed that an early increase in tumor growth and/or the appearance of new lesions correspond to progressive disease (PD), testifying drug failure and indicating the need of ongoing treatment cessation<sup>[10]</sup>.

Some exceptions for the use of these criteria have been already suggested in patients treated with target therapies such as tyrosine kinase inhibitors as in this group of patients the lack of tumor shrinkage in the presence of a stable disease has been identified as a potential surrogate end point for improved clinical outcome<sup>[12]</sup>. However, in the clinical practice, the radiological effect of immunotherapeutic agents has raised several more relevant and complex challenges for the determination of their imaging-based response at single patient level<sup>[13]</sup>. In published studies, while some patients have responded to ICPIs with the expected tumor shrinkage (chemo-like response) or with a stable disease (target therapy-like response), other distinct immune-related patterns of response have been identified. In particular, an initial increase in tumor size, development of new lesions and then a delayed objective response were also observed in patients treated with immunotherapeutic agents<sup>[13]</sup>. Specifically, in some patients, the initial increase in total tumor burden was proven to be due to inflammatory cell infiltrates by means of biopsy. In these patients the initial pseudo-progression was followed by a decrease in tumor burden or even disease regression.

As RECIST criteria were not suitable to catch these atypical responses, the so-called immune-related response criteria (irRC) have been proposed to provide more rigorous characterization of all patterns of response observed in the phase II development program for ipilimumab in melanoma<sup>[13-15]</sup> (Table 1). The main differences between RECIST 1.1 and irRC rely on the fact that, according to irRC, appearance of new lesions (PD according to the RECIST criteria) will only result in progressive disease in case of a significant ( $\geq 25\%$ ) increase in total tumor burden with respect to baseline. Moreover, different from conventional criteria, if irRC-based PD is evident, it requires further confirmation after one month with the aim of capturing



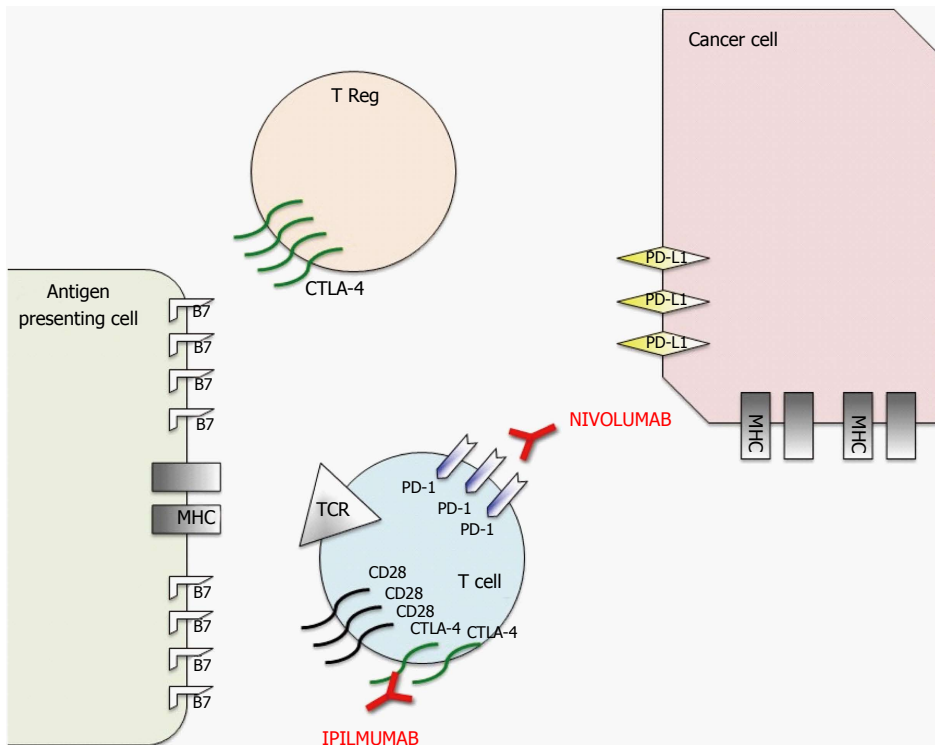


**Figure 1 Schematic representation of mechanism of action of nivolumab and ipilimumab, two Food and Drug Administration approved immune checkpoint inhibitors.** To prevent autoimmunity, numerous checkpoint pathways regulate the activation of T cells at multiple steps (process known as peripheral tolerance). Central in this process are the cytotoxic T-lymphocyte-associated antigen 4 (CTLA-4) and programmed death 1 (PD-1) immune checkpoints pathways. CTLA-4 is potentially able to stop autoreactive T cells at the initial stage of naive T-cell activation, typically in lymph nodes, while PD-1 regulates previously activated T cells at the later stages of an immune response in peripheral tissues. The binding between T-cell receptor (TCR), which is expressed on T cell surface, with major histocompatibility complex (MHC) expressed on antigen presenting cells (APCs) provides specificity to T-cell activation. However, T cell activation requires more than one stimulatory signal. Among them a central role is played by the binding between B7 molecules (APC) with CD28 (T-Cell). CTLA-4 is a CD28 homolog which does not produce a stimulatory signal but inhibits TCR-MHC binding and thus the T-Cell activation. Different from T-cells in which the amount of CTLA-4 is low, T-Regs highly express CTLA-4. In these cells CTLA-4 might play a role in their suppressive functions. PD-1 is a member of the B7/CD38 family of protein, which is able to bind with two different ligands: Programmed death ligand 1 (PD-L1) and programmed death ligand 2 (PD-L2). PD-1 activation in a T-cell prevents the phosphorylation of key TCR signaling intermediates and thus T-cell activation, resulting in suboptimal control of infections and cancers. Therefore, even though they act at different phases of T-cell activation, the negative effect of PD-1 and CTLA-4 on T-cell activity is similar. Moreover, different from CTLA-4, PD-1 expression is not specific in T-cells, but can be observed also in B-cells and myeloid cells. The rationale for immune checkpoint inhibition (represented in red) for cancer treatment is that CTLA-4 and PD1 pathways are strictly related to cancer survival and thus targeting these molecules or their ligands with monoclonal antibodies permits to impact on cancer growth. Therefore, even if the exact mechanism of action of these monoclonal antibodies in the antitumor response remains unclear, research data suggest that it is at least partially related to an activation and proliferation of T-cells regardless of TCR specificity (due to the inhibition of the inhibitory activity of these checkpoints), which enhances the anti-cancer immune reaction.

delayed response.

Recently, Hodi *et al*<sup>[16]</sup> evaluated atypical response patterns and reported the overall survival data in correlation with irRC and RECIST criteria in the context of a retrospective analysis of 327 melanoma patients treated with the PD-1 inhibitor pembrolizumab. This study indicated that the conventional RECIST assessment alone tends to underestimate the benefit of PD-1 inhibitor therapy in a subset of patients, supporting a need of immune-related response evaluation<sup>[16]</sup>. IrRC are thus increasingly proposed, but they have not been validated yet in the context of clinical trials and most trials involving ICPIs continue to use RECIST 1.1 to obtain standardized endpoints for regulatory approvals<sup>[15]</sup>.

However, although the irRC seem better than RECIST, the former has some limitations. The irRC use the bidimensional measurements in line with WHO criteria that are now rarely used in clinical trials and replaced by the unidimensional measurement of the

larger axis of target lesions (RECIST 1.0 and 1.1). The bidimensional measurements introduce a greater variability than unidimensional measurements and make it difficult to compare the responses with studies using the RECIST criteria.

### **Is there a role for <sup>18</sup>F-fluoro-2-deoxy-D-glucose positron emission tomography in the evaluation of ICPIs?**

While optimal CT-based response criteria for ICPIs are in the path of their identification, very few data are available for the evaluation of immunotherapy by means of <sup>18</sup>F-fluoro-2-deoxy-D-glucose positron emission tomography (<sup>18</sup>F-FDG-PET), one of the most used imaging techniques in oncology. <sup>18</sup>F-FDG-PET is currently the most widely used molecular imaging modality in the clinical practice for staging and restaging of several cancers. <sup>18</sup>F-FDG-PET is clinically indicated before and after treatment in patients with Hodgkin's lymphoma and NSCLC and it is used in patients with melanoma for

**Table 1** Key features of positron emission tomography Response Criteria in Solid Tumors, European Organization for Research and Treatment of Cancer 1999, Response Evaluation Criteria in Solid Tumors 1.1 and immune related Response Criteria

Category	PERCIST	EORTC 1999	RECIST 1.1	irRC
Target lesions	The hottest single tumor lesion (SUL peak) at baseline <sup>18</sup> F-FDG PET	The most <sup>18</sup> F-FDG-avid lesions (SUV BSA). Number of lesions not specified	Maximum, 5	Maximum, 15 lesions
New lesion	Results in progressive disease at first appearance	Results in progressive disease at first appearance	Results in progressive disease at first appearance	Up to 10 new visceral and 5 cutaneous lesions may be added to the sum of the products of the two largest perpendicular diameters of all index lesions at any time point
Complete response	CMR: Complete resolution of <sup>18</sup> F-FDG uptake within the target lesion (< mean liver activity and indistinguishable from background/blood pool and no new <sup>18</sup> F-FDG-avid lesions)	CMR: Complete absence of <sup>18</sup> F-FDG uptake	Disappearance of all target and nontarget lesions Nodes must regress to < 10 mm short axis No new lesions Confirmation required	
Partial response	PMR: A reduction of a minimum of 30% in the target tumor <sup>18</sup> F-FDG SUL peak	PMR: A decrease in SUV > 25%	≥ 30% decrease in tumor burden compared to baseline Confirmation required	≥ 50% decrease in tumor burden compared with baseline <sup>1</sup> Confirmation required
Progressive disease	PMD: A 30% increase in <sup>18</sup> F-FDG SUL peak or advent of new <sup>18</sup> F-FDG-avid lesions	PMD: An increase in SUV > 25% or appearance of new lesions	≥ 20% + 5 mm absolute increase in tumor burden compared with nadir Appearance of new lesions or progression of nontarget lesions	≥ 25% increase in tumor burden compared with baseline, nadir or reset baseline <sup>1</sup> New lesions added to tumor burden Confirmation required
Stable disease	SMD: Disease other than CMR, PMR or PMD	SMD: Increase in SUV by < 25% or decrease in SUV by < 15%	Neither partial response nor progressive disease	

<sup>1</sup>If an increase in tumor burden is observed at the first scheduled assessment, the baseline is reset to the value observed at the first assessment. PERCIST: PET Response Criteria in Solid Tumors; EORTC: European Organization for Research and Treatment of Cancer; RECIST: Response Evaluation Criteria in Solid Tumors; irRC: Immune related Response Criteria; CMR: Complete metabolic response; PMR: Partial metabolic response; PMD: Progressive metabolic disease; SMD: Stable metabolic disease; SUL: SUV normalized to lean body mass; SUV BSA: SUV normalized for body surface area; SUV: Standardized uptake value.

specific clinical indications<sup>[17-19]</sup>. The use of <sup>18</sup>F-FDG-PET in post-treatment settings is based on the assumption that tumor size changes are only the final step in a sequence of complex metabolic and functional processes during and after treatment<sup>[20]</sup>. Two different types of criteria have been proposed for the identification of <sup>18</sup>F-FDG-PET-based response in solid tumors: The European Organization for Research and Treatment of Cancer (EORTC) and the PET Response Criteria in Solid Tumors (PERCIST) criteria<sup>[21,22]</sup> (Table 1). Both criteria target the most metabolically active part of patient's tumor burden, which is regarded as the most viable and aggressive disease site. In both cases, the so-called standardized uptake value (SUV) is measured at baseline and after treatment. However, they differ for some relevant aspects. The EORTC criteria were published in 1999 and are based on the evaluation of a lesion-specific region of interest (ROI) chosen as the most <sup>18</sup>F-FDG-avid at baseline and followed in the after-treatment scans<sup>[22]</sup>. The PERCIST criteria were proposed in 2009 by Wahl *et al.*<sup>[21]</sup> and rely on the use of a 1 cm<sup>3</sup> ROI on the most <sup>18</sup>F-FDG-avid part of the single most metabolically active lesion at each PET/CT scan (which is not necessarily located in the same lesion in all scans).

Relatively few papers have compared the two

methods in solid tumors and good agreement, similar responses and survival outcomes have been highlighted in the available studies<sup>[23]</sup>. However, for the EORTC criteria, no recommendations on the number of target lesions or on whether computing SUV max or average SUV for response calculation are given while the PERCIST criteria recommend the use of lean body mass for SUV normalization (SUL). In this framework, some studies have demonstrated a higher accuracy with respect to RECIST for both metabolic response based criteria in patients treated with target therapies such as erlotinib. This finding is due to the relative lower tumor shrinkage characterizing this type of treatment<sup>[24]</sup>. Similarly, an <sup>18</sup>F-FDG-PET-based five-point scale (5-PS), the so-called Deauville criteria, has been demonstrated to be superior to CT-based response by scoring images in the assessment of response at the middle and end of treatment in HD patients<sup>[18]</sup>. Again these findings testify that functional changes always precede morphological changes in the course of pathological processes. In this regard it might be of interest to test the complex and variegated response to ICPIs by means of PET-based criteria. In fact, on one hand, functional imaging may capture different features of treatment with ICPIs in terms of entity and time course of response. On

the other hand, it has been reported that the initial increase in tumor size, later followed by tumor volume reduction in part of the patients treated with ICPIs, is due to inflammatory cell infiltrates. Accordingly, given the well-known high metabolic activity characterizing inflammatory cells, this feature may also hamper the evaluation of  $^{18}\text{F}$ -FDG-PET-based response to ICPIs. Sachpekidis *et al.*<sup>[20]</sup> evaluated the role of  $^{18}\text{F}$ -FDG-PET/CT after two cycles of ipilimumab in predicting the final response to therapy in 22 patients with metastatic melanoma. They evaluated response to treatment by means of the EORTC criteria and found that  $^{18}\text{F}$ -FDG-PET/CT after two cycles of ipilimumab is predictive of the final treatment outcome in patients with progressive metabolic disease (PMD) and stable metabolic disease (SMD)<sup>[20]</sup>. However, two patients were initially falsely classified as early SMD, but they later demonstrated new metastatic lesions, “upgrading” them to late PMD. Similarly, early evaluation by means of  $^{18}\text{F}$ -FDG-PET did not identify responders to treatment as the two patients eventually characterized with PMR were initially classified with early PMD due to new lesions<sup>[20]</sup>. In fact, both RECIST 1.1 and PET-based criteria consider the identification of new (metabolically active) lesions as progressive disease. Therefore, presently proposed PET-based metabolic criteria suffer from at least one of the same limitations that have resulted in the underestimation of response to treatment with ICPIs by means of RECIST 1.1. Similarly, in the phase 2 study by Younes *et al.*<sup>[9]</sup>, nivolumab resulted in frequent responses in patients with classical Hodgkin’s lymphoma after failure of ASCT and brentuximab vedotin. Most of these responses were maintained through the reported follow-up period with an acceptable safety profile. In this study  $^{18}\text{F}$ -FDG-PET was performed at baseline and at weeks 17 and 25. A negative  $^{18}\text{F}$ -FDG-PET scan, visually assessed by an independent radiological review committee (IRRC), was required for confirmation of complete remission. The study demonstrated a general reduction of tumor burden. Yet, discordance in complete remission between IRRC and investigator assessments was largely based on the interpretation of  $^{18}\text{F}$ -FDG-PET scans and standardized uptake values were not collected as part of this study. The vast majority of other available data on the potential utility of  $^{18}\text{F}$ -FDG-PET after ICPIs are case reports more often describing underlying challenges of monitoring radiologic response in these patients and showing  $^{18}\text{F}$ -FDG-PET features of inflammatory reactions. PET-highlighted autoimmune pancolitis, splenic sarcoidosis-like lesion and exacerbation of sarcoidosis as a potential confounder in the assessment of tumor response in a melanoma patient treated with ipilimumab have all been described<sup>[25-27]</sup>. Similarly, Koo *et al.*<sup>[26]</sup> illustrated a series of inflammatory reactions with avid FDG uptake in patients treated with ipilimumab, including those with thyroiditis, hypophysitis, granulomatous inflammation in the lymph nodes and skin, and enterocolitis.

Accordingly, the potential and challenges of  $^{18}\text{F}$ -FDG-

PET imaging in the evaluation of patients treated with ICPIs still need to be clarified and deeply addressed. Given the relatively greater experience of CT-based evaluation in this setting and the fact that irRC CT-based criteria seem to better in capturing response to ICPIs, it is worthwhile to ask if a similar modification of PET-based criteria could be proposed in the future.

### **Potential new PET-based approaches to evaluate the effect of ICPIs**

As mentioned above, due to its intrinsic nature,  $^{18}\text{F}$ -FDG-PET displays not only cancer cell’s metabolic activity but also inflammation. Since the antineoplastic activity of ICPIs is highly related to the activation of T cells against cancer cells,  $^{18}\text{F}$ -FDG accumulation might cause false-positive findings. Yet, discrimination between benign and malignant processes represents a huge challenge for  $^{18}\text{F}$ -FDG-PET in this clinical setting. Together with the need of the clinicians to discriminate between responders and non-responders, allowing individual therapy optimization and avoiding adverse effects brought about by ineffective therapy, several studies have been recently conducted to explore the possible role of non-FDG radiotracers in the field of ICPIs. These studies, mainly performed with labeled monoclonal antibodies, open the new era of the so-called “Immuno-PET”. Accordingly, in 2014, Higashikawa *et al.*<sup>[28]</sup> developed a molecular imaging probe that is able to evaluate CTLA-4 expression prior to CTLA-4 targeting in cancer. This  $^{64}\text{Cu}$  labeled radiotracer is basically composed of DOTA protein together with a CTLA-4 specific antibody and is able to display CTLA-4 expression *in vivo*. Similarly, specific experimental radiotracers were proposed for the visualization of PD-1 and PD-L1 cellular expression<sup>[29-32]</sup>. Maute *et al.*<sup>[29]</sup> measured PD-L1 expression by radiolabeling a PD-L1 high affinity protein (HAC) with  $^{64}\text{Cu}$  and tested its feasibility in a living mouse, while Hettich *et al.*<sup>[30]</sup> developed two  $^{64}\text{Cu}$  labeled immunoPET tracers for imaging of both PD-1 and PD-L1. Also one SPECT study with radiolabeled anti-murine PD-L1 in mice has been conducted<sup>[32]</sup>. More recently, a  $^{89}\text{Zr}$  labeled CD3 PET imaging agent was proposed by Larimer *et al.*<sup>[33]</sup>. CD3 is a part of the TCR complex that serves as a global T lymphocyte marker. By serving as a marker of total T-cell infiltration, CD3 may represent a more direct approach than pre-treatment biopsy or genetic screening to monitoring tumor immune response, by directly examining active recruitment of T cells responsible for cancer cell death. In this study the authors showed that CD3 PET imaging revealed two distinct groups of mice, stratified by PET signal intensity. While high-CD3 PET uptake was correlated with subsequent reduced tumor volume, low uptake was predictive of suboptimal response. Altogether these non-invasive approaches allow simultaneous imaging of the entire cancer mass and associated metastases, which may differ from the primary tumor in CTLA-4, PD-1 or PD-L1 expression status. Immune imaging can be used for repeated assessment of the same tumor at different

time points (e.g., before and after treatment), thereby yielding a richer set of diagnostic information that would be difficult or impossible to achieve with traditional approaches. Furthermore, although further investigations are needed before their potential introduction in the clinical setting, these non-invasive immune-diagnostic approaches might yield novel insights into the biology and pathophysiological importance of ICPIs as cancer therapeutics.

## REFERENCES

- Pardoll DM.** The blockade of immune checkpoints in cancer immunotherapy. *Nat Rev Cancer* 2012; **12**: 252-264 [PMID: 22437870 DOI: 10.1038/nrc3239]
- Walunas TL, Lenschow DJ, Bakker CY, Linsley PS, Freeman GJ, Green JM, Thompson CB, Bluestone JA.** CTLA-4 can function as a negative regulator of T cell activation. *Immunity* 1994; **1**: 405-413 [PMID: 7882171]
- Francisco LM, Sage PT, Sharpe AH.** The PD-1 pathway in tolerance and autoimmunity. *Immunol Rev* 2010; **236**: 219-242 [PMID: 20636820 DOI: 10.1111/j.1600]
- O'Day SJ, Hamid O, Urba WJ.** Targeting cytotoxic T-lymphocyte antigen-4 (CTLA-4): a novel strategy for the treatment of melanoma and other malignancies. *Cancer* 2007; **110**: 2614-2627 [PMID: 18000991 DOI: 10.1002/cncr.23086]
- Hodi FS, O'Day SJ, McDermott DF, Weber RW, Sosman JA, Haanen JB, Gonzalez R, Robert C, Schadendorf D, Hassel JC, Akerley W, van den Eertwegh AJ, Lutzky J, Lorigan P, Vaubel JM, Linette GP, Hogg D, Ottensmeier CH, Lebbé C, Peschel C, Quirt I, Clark JI, Wolchok JD, Weber JS, Tian J, Yellin MJ, Nichol GM, Hoos A, Urba WJ.** Improved survival with ipilimumab in patients with metastatic melanoma. *N Engl J Med* 2010; **363**: 711-723 [PMID: 20525992 DOI: 10.1056/NEJMoa1003466]
- Giri A, Walia SS, Gajra A.** Clinical Trials Investigating Immune Checkpoint Inhibitors in Non-Small-Cell Lung Cancer. *Rev Recent Clin Trials* 2016; **11**: 297-305 [PMID: 27457350]
- Carlo MI, Voss MH, Motzer RJ.** Checkpoint inhibitors and other novel immunotherapies for advanced renal cell carcinoma. *Nat Rev Urol* 2016; **13**: 420-431 [PMID: 27324121 DOI: 10.1038/nrurol.2016.103]
- Ball MW, Allaf ME, Drake CG.** Recent advances in immunotherapy for kidney cancer. *Discov Med* 2016; **21**: 305-313 [PMID: 27232516]
- Younes A, Santoro A, Shipp M, Zinzani PL, Timmerman JM, Ansell S, Armand P, Fanale M, Ratanatharathorn V, Kuruvilla J, Cohen JB, Collins G, Savage KJ, Trneny M, Kato K, Farsaci B, Parker SM, Rodig S, Roemer MG, Ligon AH, Engert A.** Nivolumab for classical Hodgkin's lymphoma after failure of both autologous stem-cell transplantation and brentuximab vedotin: a multicentre, multicohort, single-arm phase 2 trial. *Lancet Oncol* 2016; **17**: 1283-1294 [PMID: 27451390 DOI: 10.1016/S1470-2045(16)30167]
- Eisenhauer EA, Therasse P, Bogaerts J, Schwartz LH, Sargent D, Ford R, Dancey J, Arbuck S, Gwyther S, Mooney M, Rubinstein L, Shankar L, Dodd L, Kaplan R, Lacombe D, Verweij J.** New response evaluation criteria in solid tumours: revised RECIST guideline (version 1.1). *Eur J Cancer* 2009; **45**: 228-247 [PMID: 19097774 DOI: 10.1016/j.ejca.2008.10.026]
- von Minckwitz G, Sinn HP, Raab G, Loibl S, Blohmer JU, Eidtmann H, Hilfrich J, Merkle E, Jackisch C, Costa SD, Caputo A, Kaufmann M.** Clinical response after two cycles compared to HER2, Ki-67, p53, and bcl-2 in independently predicting a pathological complete response after preoperative chemotherapy in patients with operable carcinoma of the breast. *Breast Cancer Res* 2008; **10**: R30 [PMID: 18380893 DOI: 10.1186/bcr1989]
- Tsuji K, Shiraishi J, Tsuji T, Kurata T, Kawaguchi T, Kubo A, Takada M.** Is response rate increment obtained by molecular targeted agents related to survival benefit in the phase III trials of advanced cancer? *Ann Oncol* 2010; **21**: 1668-1674 [PMID: 20064832 DOI: 10.1093/annonc/mdp588]
- Wolchok JD, Hoos A, O'Day S, Weber JS, Hamid O, Lebbé C, Maio M, Binder M, Bohnsack O, Nichol G, Humphrey R, Hodi FS.** Guidelines for the evaluation of immune therapy activity in solid tumors: immune-related response criteria. *Clin Cancer Res* 2009; **15**: 7412-7420 [PMID: 19934295 DOI: 10.1158/1078-0432]
- Hodi FS, Sznol M, Kluger HM, McDermott DF, Carvajal RD, Lawrence DP, Topalian SL, Atkins MB, Powderly JD, Sharfman WH, Puzanov I, Smith DC, Leming PD, Lipson EJ, Taube JM, Anders R, Horak CE, Kollia G, Gupta AK, Sosman JA.** Long term survival of ipilimumab-naïve patients (pts) with advanced melanoma (MEL) treated with nivolumab (anti-PD-1, BMS-936558, ONO-4538) in a phase I trial. ASCO Annual Meeting 2014 May 30- Jun 3; Chicago, Illinois, USA. *J Clin Oncol* 2014; **32**: 5s (suppl; abstr 9002)
- Chiou VL, Burotto M.** Pseudoprogression and Immune-Related Response in Solid Tumors. *J Clin Oncol* 2015; **33**: 3541-3543 [PMID: 26261262 DOI: 10.1200/JCO.2015.61.6870]
- Hodi FS, Hwu WJ, Kefford R, Weber JS, Daud A, Hamid O, Patnaik A, Ribas A, Robert C, Gangadhar TC, Joshua AM, Hersey P, Dronca R, Joseph R, Hille D, Xue D, Li XN, Kang SP, Ebbinghaus S, Perrone A, Wolchok JD.** Evaluation of Immune-Related Response Criteria and RECIST v1.1 in Patients With Advanced Melanoma Treated With Pembrolizumab. *J Clin Oncol* 2016; **34**: 1510-1517 [PMID: 26951310 DOI: 10.1200/JCO.2015.64.0391]
- Gould MK, Donington J, Lynch WR, Mazzzone PJ, Midthun DE, Naidich DP, Wiener RS.** Evaluation of individuals with pulmonary nodules: when is it lung cancer? Diagnosis and management of lung cancer, 3rd ed: American College of Chest Physicians evidence-based clinical practice guidelines. *Chest* 2013; **143**: e93S-120S [PMID: 23649456 DOI: 10.1378/chest.12-2351]
- Cheson BD, Fisher RI, Barrington SF, Cavalli F, Schwartz LH, Zucca E, Lister TA.** Recommendations for initial evaluation, staging, and response assessment of Hodgkin and non-Hodgkin lymphoma: the Lugano classification. *J Clin Oncol* 2014; **32**: 3059-3068 [PMID: 25113753 DOI: 10.1200/JCO.2013.54.8800]
- Morbelli S, Capitanio S, De Carli F, Bongioanni F, De Astis E, Miglino M, Verardi MT, Buschiazzo A, Fiz F, Marini C, Pomposelli E, Sambucetti G.** Baseline and ongoing PET-derived factors predict detrimental effect or potential utility of 18F-FDG PET/CT (FDG-PET/CT) performed for surveillance in asymptomatic lymphoma patients in first remission. *Eur J Nucl Med Mol Imaging* 2016; **43**: 232-239 [PMID: 26283504 DOI: 10.1007/s00259-015-3164-9]
- Sachpekidis C, Larribere L, Pan L, Haberkorn U, Dimitrakopoulou-Strauss A, Hassel JC.** Predictive value of early 18F-FDG PET/CT studies for treatment response evaluation to ipilimumab in metastatic melanoma: preliminary results of an ongoing study. *Eur J Nucl Med Mol Imaging* 2015; **42**: 386-396 [PMID: 25359635 DOI: 10.1007/s00259-014-2944-y]
- Wahl RL, Jacene H, Kasamony Y, Lodge MA.** From RECIST to PERCIST: Evolving Considerations for PET response criteria in solid tumors. *J Nucl Med* 2009; **50** Suppl 1: 122S-150S [PMID: 19403881 DOI: 10.2967/jnumed.108.057307]
- Young H, Baum R, Cremerius U, Herholz K, Hoekstra O, Lammertsma AA, Pruim J, Price P.** Measurement of clinical and subclinical tumour response using [18F]-fluorodeoxyglucose and positron emission tomography: review and 1999 EORTC recommendations. European Organization for Research and Treatment of Cancer (EORTC) PET Study Group. *Eur J Cancer* 1999; **35**: 1773-1782 [PMID: 10673991]
- Skougaard K, Nielsen D, Jensen BV, Hendel HW.** Comparison of EORTC criteria and PERCIST for PET/CT response evaluation of patients with metastatic colorectal cancer treated with irinotecan and cetuximab. *J Nucl Med* 2013; **54**: 1026-1031 [PMID: 23572497 DOI: 10.2967/jnumed.112.111757]
- Stefano A, Russo G, Ippolito M, Cosentino S, Murè G, Baldari S, Sabini MG, Sardina D, Valastro LM, Bordonaro R, Messa C, Gilardi MC, Soto Parra H.** Evaluation of erlotinib treatment response in non-small cell lung cancer using metabolic and anatomic criteria. *Q*



- J Nucl Med Mol Imaging* 2014 May 9; Epub ahead of print [PMID: 24809275]
- 25 **Goethals L**, Wilgenhof S, De Geeter F, Everaert H, Neyns B. 18F-FDG PET/CT imaging of an anti-CTLA-4 antibody-associated autoimmune pancolitis. *Eur J Nucl Med Mol Imaging* 2011; **38**: 1390-1391 [PMID: 21365253 DOI: 10.1007/s00259-011-1749-5]
  - 26 **Koo PJ**, Klingensmith WC, Lewis KD, Bagrosky BM, Gonzalez R. Anti-CTLA4 antibody therapy related complications on FDG PET/CT. *Clin Nucl Med* 2014; **39**: e93-e96 [PMID: 23657138 DOI: 10.1097/RLU.0b013e318292a775]
  - 27 **Perng P**, Marcus C, Subramaniam RM. (18)F-FDG PET/CT and Melanoma: Staging, Immune Modulation and Mutation-Targeted Therapy Assessment, and Prognosis. *AJR Am J Roentgenol* 2015; **205**: 259-270 [PMID: 26204273 DOI: 10.2214/AJR.14.13575]
  - 28 **Higashikawa K**, Yagi K, Watanabe K, Kamino S, Ueda M, Hiromura M, Enomoto S. 64Cu-DOTA-anti-CTLA-4 mAb enabled PET visualization of CTLA-4 on the T-cell infiltrating tumor tissues. *PLoS One* 2014; **9**: e109866 [PMID: 25365349]
  - 29 **Maute RL**, Gordon SR, Mayer AT, McCracken MN, Natarajan A, Ring NG, Kimura R, Tsai JM, Manglik A, Kruse AC, Gambhir SS, Weissman IL, Ring AM. Engineering high-affinity PD-1 variants for optimized immunotherapy and immuno-PET imaging. *Proc Natl Acad Sci USA* 2015; **112**: E6506-E6514 [PMID: 26604307 DOI: 10.1073/pnas.1519623112]
  - 30 **Hettich M**, Braun F, Bartholomä MD, Schirmbeck R, Niedermann G. High-Resolution PET Imaging with Therapeutic Antibody-based PD-1/PD-L1 Checkpoint Tracers. *Theranostics* 2016; **6**: 1629-1640 [PMID: 27446497 DOI: 10.7150/thno.15253]
  - 31 **Heskamp S**, Hobo W, Molkenboer-Kuennen JD, Olive D, Oyen WJ, Dolstra H, Boerman OC. Noninvasive Imaging of Tumor PD-L1 Expression Using Radiolabeled Anti-PD-L1 Antibodies. *Cancer Res* 2015; **75**: 2928-2936 [PMID: 25977331 DOI: 10.1158/0008-5472.CAN-14-3477]
  - 32 **Josefsson A**, Nedrow JR, Park S, Banerjee SR, Rittenbach A, Jammes F, Tsui B, Sgouros G. Imaging, Biodistribution, and Dosimetry of Radionuclide-Labeled PD-L1 Antibody in an Immunocompetent Mouse Model of Breast Cancer. *Cancer Res* 2016; **76**: 472-479 [PMID: 26554829 DOI: 10.1158/0008-5472.CAN-15-2141]
  - 33 **Larimer BM**, Wehrenberg-Klee E, Caraballo A, Mahmood U. Quantitative CD3 PET Imaging Predicts Tumor Growth Response to Anti-CTLA-4 Therapy. *J Nucl Med* 2016; **57**: 1607-1611 [PMID: 27230929 DOI: 10.2967/jnumed.116.173930]

**P- Reviewer:** Morris DLL, Palumbo B **S- Editor:** Ji FF

**L- Editor:** Wang TQ **E- Editor:** Wu HL



## Potential role of imaging in assessing harmful effects on spermatogenesis in adult testes with varicocele

Athina C Tsili, Olga N Xiropotamou, Anastasios Sylakos, Vasilios Maliakas, Nikolaos Sofikitis, Maria I Argyropoulou

Athina C Tsili, Olga N Xiropotamou, Vasilios Maliakas, Maria I Argyropoulou, Department of Clinical Radiology, University of Ioannina, Medical School, University Campus, 45110 Epirus, Greece

Anastasios Sylakos, Nikolaos Sofikitis, Department of Urology, University of Ioannina, Medical School, University Campus, 45110 Epirus, Greece

**Author contributions:** Tsili AC and Xiropotamou ON contributed equally to this work; Tsili AC, Sofikitis N and Argyropoulou MI designed the research; Xiropotamou ON, Sylakos A and Maliakas V performed the research and analyzed the data; Tsili AC and Xiropotamou ON wrote the paper; all authors approved the final version of the article to be published.

**Conflict-of-interest statement:** The authors declare no conflicts of interest related to this publication.

**Open-Access:** This article is an open-access article which was selected by an in-house editor and fully peer-reviewed by external reviewers. It is distributed in accordance with the Creative Commons Attribution Non Commercial (CC BY-NC 4.0) license, which permits others to distribute, remix, adapt, build upon this work non-commercially, and license their derivative works on different terms, provided the original work is properly cited and the use is non-commercial. See: <http://creativecommons.org/licenses/by-nc/4.0/>

**Manuscript source:** Invited manuscript

**Correspondence to:** Athina C Tsili, MD, Assistant Professor, Department of Clinical Radiology, University of Ioannina, Medical School, University Campus, Ioannina, 45110 Epirus, Greece. [a\\_tsili@yahoo.gr](mailto:a_tsili@yahoo.gr)  
Telephone: +30-69-76510904  
Fax: +30-26-51007862

Received: August 10, 2016

Peer-review started: August 11, 2016

First decision: September 12, 2016

Revised: November 2, 2016

Accepted: December 16, 2016

Article in press: December 19, 2016

Published online: February 28, 2017

### Abstract

Varicocele is characterized by an abnormal dilatation and retrograde blood flow in the spermatic veins. Varicocele is the leading correctable cause of male infertility. Although it is highly prevalent in infertile men, it is also observed in individuals with normal fertility. Determining which men are negatively affected by varicocele would enable clinicians to better select those men who will benefit from treatment. To assess the functional status of the testes in men with varicocele, color Doppler sonographic parameters were evaluated. Testicular arterial blood flow was significantly reduced in men with varicocele, reflecting an impairment of spermatogenesis. An improvement in the testicular blood supply was found after varicocelectomy on spectral Doppler analysis. Testicular contrast harmonic imaging and elastography might improve our knowledge about the influence of varicocele on intratesticular microcirculation and tissue stiffness, respectively, providing possible information on the early damage of testicular structure by varicocele. Magnetic resonance imaging (MRI), with measurement of apparent diffusion coefficient has been used to assess the degree of testicular dysfunction and to evaluate the effectiveness of varicocele repair. Large prospective studies are needed to validate the possible role of functional sonography and MRI in the assessment of early defects of spermatogenesis in testes with varicocele.

**Key words:** Varicocele; Spermatogenesis; Diagnostic imaging; Ultrasonography; Doppler ultrasound imaging; Magnetic resonance imaging; Functional

© The Author(s) 2017. Published by Baishideng Publishing Group Inc. All rights reserved.

**Core tip:** Varicocele is known as one of the main causes of male infertility. However, many controversies exist regarding the effect of varicocele on male reproductive potential, which patients to treat and whether repair leads to an improvement of the fertility status. Non-

invasive imaging modalities, including functional sonography and magnetic resonance imaging, might provide useful information on the early damage of testicular structure by varicoceles, therefore helping clinicians target repair efforts to those men who will benefit from varicocele treatment.

Tsili AC, Xiropotamou ON, Sylakos A, Maliakas V, Sofikitis N, Argyropoulou MI. Potential role of imaging in assessing harmful effects on spermatogenesis in adult testes with varicocele. *World J Radiol* 2017; 9(2): 34-45 Available from: URL: <http://www.wjgnet.com/1949-8470/full/v9/i2/34.htm> DOI: <http://dx.doi.org/10.4329/wjr.v9.i2.34>

## INTRODUCTION

Male infertility is a social problem, representing the causal factor for infertility in 50% of cases and the sole cause in 30% of infertile couples<sup>[1-3]</sup>. Varicocele is the most common andrological disorder between adolescents and adult males. Its clinical significance is mainly related to fertility, as it represents the most common cause of impaired male fertility and the most common treatable cause of infertility<sup>[4-10]</sup>. The origin of the word varicocele comes from varico (a combining form meaning "varix" in Latin) and cele (a combining form meaning "tumor" in Greek) and dates to 1730-1740.

Varicocele has been one of the most controversial topics of debate in the fields of andrology and urology, regarding the effect of varicocele on male infertility and whether repair leads to improvement of fertility status<sup>[4-10]</sup>. While most men with varicocele are able to father children, most evidence suggests that varicocele has detrimental effects on male reproductive potential. A non-invasive imaging technique providing answers to questions regarding which patients with varicocele are at risk for infertility and which will benefit from varicocele repair, would be extremely useful.

## DEFINITION AND EPIDEMIOLOGY

Varicocele is clinically defined as an abnormal dilation of the veins of the pampiniform venous plexus and the testicular veins with continuous or intermittent reflux of venous blood<sup>[4,5,11]</sup>. Primary varicoceles are due to venous reflux into the pampiniform plexus from the internal spermatic vein because of incompetent venous valves, and they usually occur on the left side. Secondary varicoceles are the result of increased pressure in the testicular veins, which can be related to several causes, such as hydronephrosis, abdominal and retroperitoneal neoplasms, and the so-called nutcracker phenomenon, which involves compression of the left renal vein between the superior mesenteric artery and aorta<sup>[4,12-15]</sup>. Although varicoceles are almost always

more common and larger on the left side, they are bilateral in 50% of cases<sup>[14]</sup>. The uncommon, isolated right-sided varicocele always necessitates further investigation, as this finding may be associated with situs inversus or retroperitoneal malignancies<sup>[4,14]</sup>.

Varicocele epidemiology is incompletely understood<sup>[14]</sup>. A clinical varicocele is found in approximately 15% of all adult males, up to 35% of infertile men and 81% of men presenting with secondary infertility. When classified according to semen analysis parameters, 12% of infertile men with normal semen analyses and 25.4% of those with abnormal results were found to have clinical varicocele<sup>[4,5,8,12,14]</sup>. This disorder may be present at birth or in young children, but the incidence substantially increases in adolescents coinciding with pubertal development<sup>[4,5,14]</sup>. The prevalence of varicocele also increases with advancing age, with an increase of approximately 10% per decade of life, probably because of the aging of venous valves<sup>[14]</sup>.

An association between varicocele and varicose veins of the lower extremities and an inverse relationship between the prevalence of varicocele and body mass index have been suggested<sup>[4-16]</sup>. Hereditary factors may also play a role in the prevalence of varicocele<sup>[14,17]</sup>.

## ETIOLOGY AND PATHOGENESIS

The exact etiology of varicocele is still unknown, but it is probably multifactorial<sup>[4,5,12,13,18]</sup>. The cause for the high incidence of left varicocele is that the left internal spermatic vein runs vertically to drain into the ipsilateral renal vein at a right angle, when the man is in the standing position, and thus, the endoluminal pressure in the renal vein is transmitted backward, opposing flow from the internal spermatic vein. On the right side, the internal spermatic vein runs tangentially to join the inferior vena cava, resulting in less flow turbulence and back pressure in the vein and therefore in a lower incidence of venous dilation on the right side. However, Gat *et al*<sup>[19]</sup> reported that varicocele is mainly a bilateral disease, expressed earlier on the left side, with a right-sided venous return problem presenting in 86% of infertile men with clinically significant varicocele.

Several other theories related to the etiological factors of varicocele have been proposed, including the following: Incompetence or absence of venous valves in the spermatic veins, obstructed venous drainage, vascular contractions of the left testicular vein caused by catecholamines from the left adrenal gland and the so-called nutcracker phenomenon<sup>[4,5,12,13,18,20,21]</sup>.

## CLINICAL FINDINGS-CLASSIFICATION

Clinically, varicocele is characterized by an abnormal enlargement of the spermatic veins of the venous plexus, which drains the blood from the testes, associated with an anomalous intermittent or continuous backflow of blood into the plexus. In adult males, most cases are

asymptomatic, often revealed during an investigation related to infertility and/or because of an unfavorable outcome of semen analysis<sup>[5]</sup>. Rarely, it may present with scrotal pain or create esthetic problems or discomfort due to the presence of significant enlargement of the scrotum<sup>[5,12]</sup>.

Clinical varicocele was found to be a significant risk factor for decreased sperm count, motility and morphology in adult infertile men<sup>[22,23]</sup>. A study conducted by the World Health Organization (WHO) reported that both sperm concentration and motility were lower in men with varicocele compared to individuals without varicocele<sup>[22]</sup>. Recently, Agarwal *et al.*<sup>[23]</sup> in a systematic review assessing the effects of varicocele on semen parameters based on the new 2010 WHO laboratory criteria for the examination of the human semen, reported that varicocele was associated with reduced sperm count, motility and morphology<sup>[23]</sup>.

Physical examination represents the gold standard for the diagnosis of clinically significant varicoceles<sup>[5,8,12,24]</sup>. It is used by clinical urologists and pediatricians, consisting of palpation performed with the patient in the standing position and observation of the scrotum during the Valsalva maneuver. The classification system published by Dubin and Amelar in 1970 is the most commonly used and includes the following three degrees of varicocele: Grade 1, varicocele detectable by palpation only during the Valsalva maneuver; Grade 2, varicocele detectable by simple palpation; and, Grade 3, varicocele visible on inspection and palpation<sup>[24]</sup>. However, this system has limitations because its diagnostic accuracy is closely associated with physician's experience. A study involving experienced andrologists and clinicians identified a significant inter-observer and intra-observer variability in the grading of varicoceles based on the above classification<sup>[12]</sup>.

Histology from a testicular biopsy in men with varicocele has shown depressed spermatogenesis with maturation arrest, sloughing of the spermatogenic epithelium, profusion of Leydig cells, thickening of the tubular basement membrane and interstitial blood vessel wall with luminal narrowing, and increased deposition of interstitial fibrous tissue<sup>[25]</sup>.

## **PATHOPHYSIOLOGY**

The pathophysiology of impaired spermatogenesis in varicocele is multifactorial. A combination of several factors affects spermatogenesis and sperm function, and the relative involvement of these factors is different in each patient<sup>[4,7,8,25]</sup>. Several pathophysiologic mechanisms resulting in impairment of spermatogenesis in left varicocele have been proposed, including heat stress, notch signaling, cadmium accumulation, insufficiency of the hypothalamo-pituitary-gonadal axis, retrograde flow of adrenal or renal metabolites, possible disruptions of blood-testis barrier, testicular hypoxia and alterations in testicular extracellular fluid dynamics<sup>[4,7,8,25]</sup>. Interstitial

lesions, including the proliferation of Leydig cells, thickening of the tubular basement membrane and blood vessel wall with luminal narrowing, and increased deposition of interstitial collagen fibers may also play an important role in varicocele-related testicular dysfunction<sup>[25]</sup>.

Current evidence suggests the primary role of reactive oxygen species (ROS) and the resultant oxidative stress (OS) in the pathogenesis of varicocele-associated male infertility<sup>[4,7,8,18,25,26]</sup>. Excessive ROS has also been associated with sperm DNA fragmentation (SDF), which may mediate the clinical manifestation of poor sperm function and infertility related to varicocele<sup>[4,7,8,18,25-27]</sup>. A significantly less total acrosin activity in the spermatozoa of infertile men with varicocele and an abnormal retention of cytoplasmic droplets by human spermatozoa, which is negatively correlated with sperm motility, are other potential contributing factors for the diminished sperm function in individuals with varicocele<sup>[4,28]</sup>.

Using animal models, bilateral detrimental effects on testicular temperature, blood flow, and histology have been reported to occur in cases of unilateral varicocele, probably related either to the dilatation of the right testicular vein in individuals with left varicocele or the role of the sympathetic nervous system<sup>[4,29,30]</sup>. The development of a unilateral varicocele affecting bilateral Leydig cell secretory function results in a significant reduction in bilateral intratesticular testosterone content, which, in turn, affects the Sertoli cell secretory function and epididymal maturation process, all contributing to the reduced male reproductive potential<sup>[4]</sup>. Recent advances in biomolecular techniques and mass spectrometry equipment have allowed us to better understand the molecular pathways associated with varicocele and male infertility<sup>[25,31,32]</sup>.

## **DIAGNOSIS**

In the past, various diagnostic imaging modalities were used for the evaluation of varicoceles, including venography, scintigraphy, and thermography<sup>[33-35]</sup>. Labeled blood-pool scintigraphy was reported as an accurate and noninvasive method for the detection and grading of varicocele. The main contribution of radionuclide blood-pool imaging of the scrotum was in the detection and grading of subclinical varicocele in infertile men with no other cause of infertility. The technique was also accurate in the diagnosis of recurrent varicocele<sup>[33-35]</sup>. However, the above methods have been replaced by less invasive and more easily performed diagnostic tools, especially ultrasonographic examination of the scrotum.

Ultrasonography (US) is currently the most established and widely used modality for the study of varicoceles, with 97% sensitivity and 94% specificity in the diagnosis of clinical varicocele and 83%-95% sensitivity in the diagnosis of subclinical varicocele<sup>[5,12,13,33,36,37]</sup>. The classic US features of a varicocele is that of "multiple,



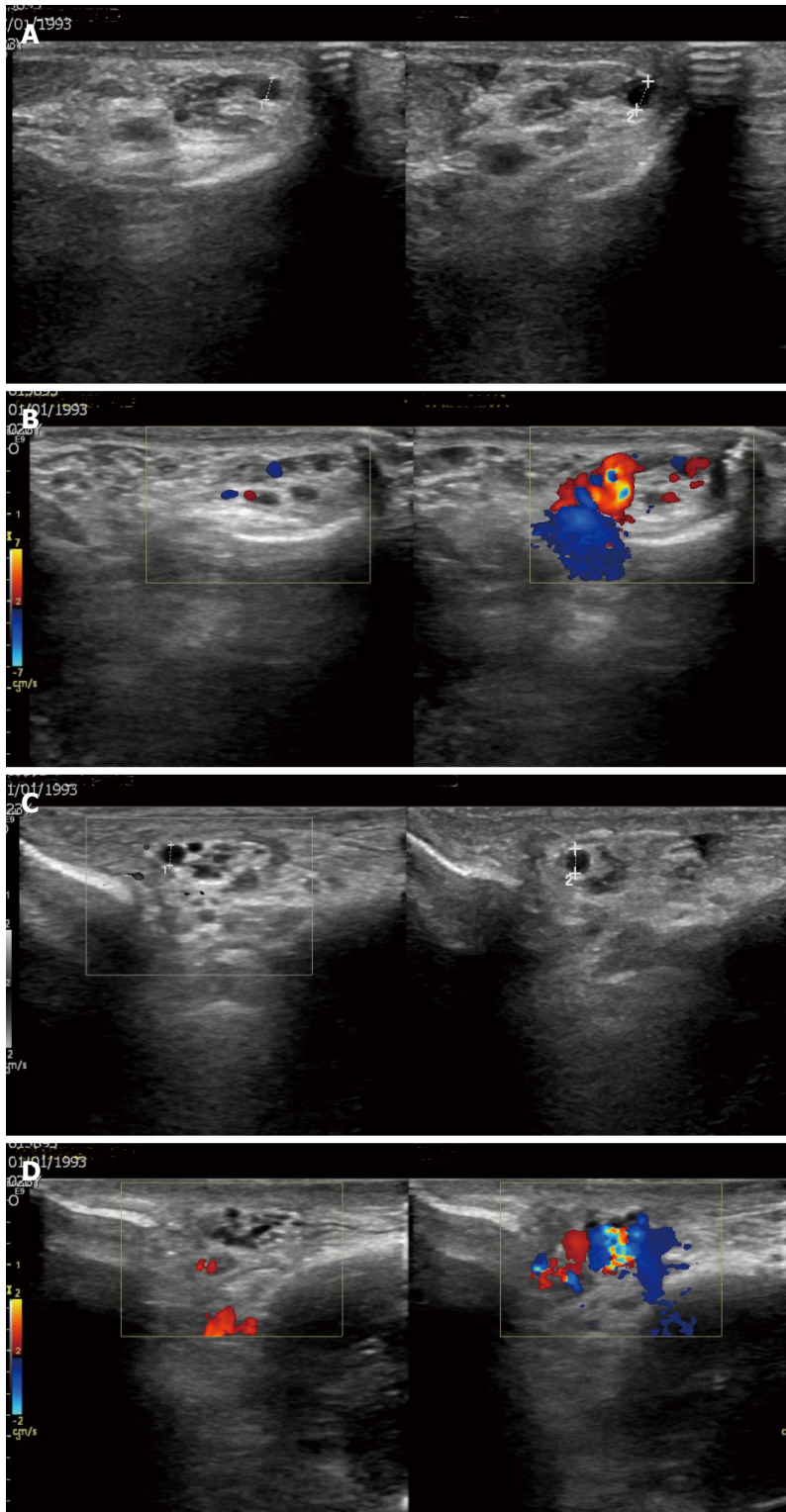


**Figure 1** A 24-year-old man with bilateral varicocele. A: Gray-scale sonographic images, longitudinal sections at the suprastesticular region of the left hemiscrotum at rest and during the Valsalva maneuver. The maximal diameter of the left spermatic veins is 2.5 mm at rest and 3.5 mm during the Valsalva maneuver; B: Color Doppler sonographic images, longitudinal sections same level show blood flow reversal after Valsalva maneuver; C: Gray-scale sonographic images, longitudinal sections at the right suprastesticular region. The maximal diameter of the right spermatic veins is 2.3 mm at rest and 2.8 mm during the Valsalva maneuver; D: Color Doppler sonographic images, longitudinal sections show flow reversal with Valsalva maneuver.

anechoic, serpiginous, tubular structures” near the superior and lateral aspects of the testis. Color, power, or spectral Doppler US with settings optimized for low flow velocities is used complimentary to aid in the diagnosis

of varicoceles. Typical Doppler findings include venous flow at rest, with intermittent or continuous flow reversal with Valsalva maneuver (Figures 1 and 2)<sup>[5,33]</sup>.

However, there are no homogeneous US criteria

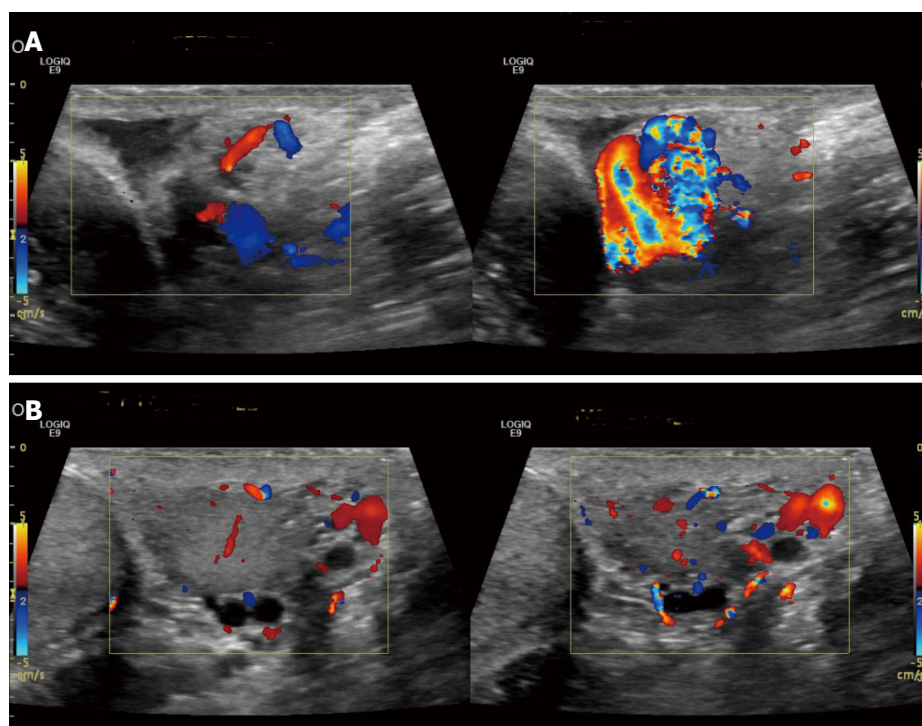


**Figure 2** A 36-year-old man with left varicocele. Color Doppler sonographic images, longitudinal sections at the level of the upper (A) and lower pole (B) of the left testis depict flow reversal seen during the Valsalva maneuver.

**Table 1** Sarteschi classification

Grade	Characteristics
1	Venous reflux at the emergence of the scrotal vein only during the Valsalva maneuver; hypertrophy of the venous wall without stasis
2	Supratesticular reflux only during the Valsalva maneuver; venous stasis without varicosities
3	Peritesticular reflux during the Valsalva maneuver; overt varicocele with early stage varices of the cremasteric vein
4	Spontaneous basal reflux that increases during the Valsalva maneuver; possible testicular hypotrophy, overt varicocele, varicosities in the pampiniform plexus
5	Spontaneous basal reflux that does not increase during the Valsalva maneuver; testicular hypotrophy, overt varicocele, varicosities in the pampiniform plexus

regarding the extent of venous dilation or reflux that must be present to meet the definition of a varicocele<sup>[5,12,13,36-45]</sup>. A widely accepted US criterion for the diagnosis of varicocele is the existence of veins larger than 2 mm in diameter, with 95% sensitivity<sup>[38]</sup>. In general, clinicians agree that clinically relevant varicoceles are more than 2.5-3 mm in diameter<sup>[33]</sup>. Multiple grading systems exist for classifying the US findings of varicocele; however, all have a low predictive value in terms of impairment of spermatogenesis, which is the main indication for any therapeutic plan<sup>[5,12,13,31,46,47]</sup>. The Sarteschi (Table 1) and Chiou *et al.*<sup>[47]</sup> (Table 2) classifications systems are among the most commonly used.

Advances in US and magnetic resonance imaging (MRI) provide the potential to expand the role of imaging beyond that of visual confirmation and characterization of varicoceles. The ability to identify the early signs of testicular dysfunction based on imaging findings may have implications for the selection of patients for varicocele repair.

## US IN THE EVALUATION OF INTRATESTICULAR MICROCIRCULATION IN TESTES WITH VARICOCELE

The testis gets its arterial supply mainly from the testicular artery (TA) supplemented with the cremasteric artery and the deferential artery, all coursing through the deep inguinal canal to enter the spermatic cord<sup>[48-51]</sup>. TA penetrates the tunica albuginea along the posterior surface of the testis and divides into capsular arteries. These capsular branches then give rise to the centripetal arteries which carry blood from the capsular surface, centrally towards the mediastinum along the testicular septa. Branches of the centripetal arteries then course backward towards the capsular surface, known as recurrent rami. In approximately 50% of testes, the transtesticular artery can also be seen passing directly from the testicular artery at the mediastinum into the parenchyma<sup>[48-51]</sup>. Testicular perfusion can be evaluated with color Doppler (CD), power Doppler, and spectral

**Table 2** Chiou *et al.*<sup>[47]</sup> classification (total score of  $\geq 4$  defined as varicocele)

Characteristics	Grade
Maximum vein diameter (mm)	
< 2.5	0
2.5-2.9	1
3-3.9	2
$\geq 4$	3
Plexus/sum of diameter of veins	
No plexus identified	0
Plexus (+) with sum diameter < 3 mm	1
Plexus (+) with sum diameter 3-5.9 mm	2
Plexus (+) with sum diameter $\geq 6$ mm	3
Change of flow velocity on Valsalva maneuver	
< 2 cm/s or duration < 1 s	0
2-4.9	1
5-9.9	2
$\geq 10$	3
Total score	0-9

Doppler US. The spectral waveform of the intratesticular arteries characteristically has a low-resistance pattern, with a mean resistive index (RI) in adults and postpubertal boys of 0.62 (range, 0.48-0.75)<sup>[48]</sup>.

Several clinical studies have assessed the effects of varicocele on testicular blood flow by US<sup>[49,50-56]</sup>. In an early study, Ross *et al.*<sup>[52]</sup> compared the testicular blood flow in 248 patients with varicocele and 34 fertile volunteers with color Doppler ultrasonography (CDUS) and reported no significant differences<sup>[52]</sup>. A similar result was reported by Grasso Leanza *et al.*<sup>[53]</sup>. In this study, the peak systolic velocity (PSV) of the testicular arteries was evaluated in men with varicocele and healthy subjects with normal or impaired spermatogenesis using CDUS. No significant difference was found in relation to the presence or degree of varicocele<sup>[53]</sup>.

However, in subsequent studies, CDUS proved to be sensitive in assessing alterations in intratesticular circulation in testes with clinical varicocele<sup>[37,49,54-56]</sup>. A significant decrease in testicular arterial blood flow and an increase in RI and PSV in testes with clinical varicocele were reported<sup>[37,49,54-56]</sup>. Semiz *et al.*<sup>[37]</sup> concluded that spectral Doppler parameters might be used as a noninvasive method to assess the hemodynamic changes and testicular microcirculation in cases of clinical varicocele<sup>[37]</sup>. The PSV, end-diastolic velocity (EDV), RI and pulsatility index (PI) from capsular and intratesticular arteries in 50 men with clinical varicocele were measured and correlated with semen analysis parameters, including count, motility, volume and morphology. PSV significantly correlated with sperm count in men with unilateral and bilateral varicocele. No significant correlation between EDV, RI, PI and semen analysis results was found<sup>[37]</sup>. Unsal *et al.*<sup>[54]</sup> evaluated the effects of clinical varicocele on testicular microcirculation comparing PSV, EDV, RI and PI from capsular and intratesticular arteries in 15 men with left clinical varicocele and 34 controls<sup>[54]</sup>. The authors found

a significantly greater RI and PI of capsular branches of the left testes (RI =  $0.68 \pm 0.04$ ; PI =  $1.22 \pm 0.15$ ) compared to the control group (RI =  $0.64 \pm 0.06$ ; PI =  $1.07 \pm 0.18$ )<sup>[54]</sup>.

Biagiotti *et al.*<sup>[55]</sup> reported that spectral Doppler traces from the TA can be used to differentiate the various causes of impaired spermatogenesis<sup>[55]</sup>. The RI and PSV proved the most reliable indicators for routine clinical use to identify infertile men in this study, whereas EDV, FSH and TV were not. Specifically, men with varicoceles or, varicoceles and male accessory glands inflammation or fertile men with varicoceles had the highest PSV and RI<sup>[55]</sup>.

In cases of subclinical varicocele, no significant changes in intratesticular perfusion are probably seen on CDUS<sup>[50]</sup>. Akcar *et al.*<sup>[50]</sup> assessed the testicular volume (TV) and the RI from centripetal intratesticular arteries in 27 men with left varicocele, 96% of which were subclinical. The authors found that subclinical varicocele is not associated with testicular atrophy and does not affect the intratesticular arterial resistance<sup>[50]</sup>.

Testicular contrast harmonic imaging has been proposed as an adjuvant diagnostic tool in the assessment of the effects of varicocele on intratesticular microcirculation<sup>[57]</sup>. Caretta *et al.*<sup>[57]</sup> in a study of 90 patients with left varicocele, associated with either normozoospermia or oligospermia calculated contrast material arrival time in the arteriolar circulation (wash-in), time to peak arterial circulation, arrival time in the venular circulation (washout) and mean transit time in each testis after intravenous administration of contrast agent containing phospholipid stabilized microbubbles filled with sulfur hexafluoride. All parameters were significantly higher in patients with varicocele plus normozoospermia or oligospermia compared to controls, although they did not correlate with varicocele grading. A negative linear correlation between total sperm count and left mean transit time was found in patients with varicocele. In the multivariate analysis, left mean transit time was the only independent predicting parameter of oligospermia in this study<sup>[57]</sup>.

Tissue elastography (TE) is a relatively new imaging technique that measures the stiffness of tissue<sup>[58-60]</sup>. TE has been reported as a useful diagnostic tool, further enhancing the characterization of focal testicular lesions<sup>[58-60]</sup>. Acoustic radiation force impulse (ARFI) elastography represents one of the main types of elastography currently in use, involving the estimation of shear wave speed. In a prospective controlled study of 30 men with clinical varicocele and 30 controls, Dede *et al.*<sup>[61]</sup> concluded that ARFI elastography may be used to assess the early damage of testicular structure by varicocele<sup>[61]</sup>. Mean elastography results were significantly different between the two groups and significantly lower in testes with varicoceles. Significant negative correlations between FSH and testis elasticity was also reported. Additionally, a negative correlation was determined between varicocele grade and elasticity

of testes<sup>[61]</sup>.

## ROLE OF MRI

Although US represents the primary imaging modality in the assessment of scrotal diseases, MRI has recently emerged as an important supplemental diagnostic tool, used both as a problem-solving technique in patients with inconclusive US findings and as a primary imaging modality<sup>[62-64]</sup>. Recently, functional MRI techniques, including diffusion-weighted imaging (DWI), dynamic contrast-enhanced (DCE) MRI and MR spectroscopy have added important diagnostic information to the interpretation of testicular diseases<sup>[65-75]</sup>.

DWI, with the calculation of apparent diffusion coefficient (ADC), is an evolving technique that can be used to improve tissue characterization if interpreted in combination with the findings of conventional MR sequences. DWI applications in scrotal pathology include characterization of intratesticular lesions, diagnosis of testicular torsion and detection and localization of nonpalpable undescended testes<sup>[65-67]</sup>. Karakas *et al.*<sup>[72]</sup> in a preliminary study of 25 men with varicocele and 25 healthy volunteers recommended the potential role of DWI for the early detection and the determination of the degree of testicular damage due to varicocele<sup>[72]</sup>. The authors found lower ADC both in the ipsilateral and contralateral testicular parenchyma of patients with varicocele, compared to that of healthy volunteers. A significant negative correlation between the mean ADC and venous diameter was also found<sup>[72]</sup>. Decreased ADC of the ipsilateral testis in patients with varicocele might be associated with hypoxia and fibrosis. Decreased ADC of the contralateral testis might be related to hormonal and autoimmune factors and heat stress<sup>[72]</sup>.

DCE-MRI evaluates the kinetics of the distribution of the paramagnetic contrast medium in the microvessels and the interstitial spaces of the tissues used. The technique has been useful in the characterization of scrotal lesions and the discrimination of various causes of acute scrotal pain<sup>[68,69,73-75]</sup>. Normal testes enhance slowly, moderately and homogeneously with a linear increase in signal intensity during the entire dynamic period (type I curve)<sup>[68,69]</sup>. This pattern of enhancement is probably related to an intact "blood-testis" barrier. Minor disruptions of the blood-testis barrier could be associated with alterations of testicular perfusion in testes with varicocele and could be detected using DCE-MRI<sup>[73]</sup>.

Although MRI is not routinely used in the assessment of testes with varicocele, large prospective studies evaluating functional MRI data might validate the possible role of this technique in the investigation of harmful effects on spermatogenesis.

## TREATMENT

There are numerous surgical and non-surgical techniques for treating clinically significant varicocele, although

there is no consensus on which might be considered the treatment of choice<sup>[4,5,7,8,11,25,76-78]</sup>. Microsurgical varicocelectomy is the most recommended type of therapy and is associated with fewer complications and lower recurrence rates, compared to the other techniques<sup>[4,11]</sup>.

Varicocele embolization represents a technically feasible, minimally invasive and outpatient treatment option for men with varicocele, with high success rates. A major advantage of embolization over surgery is the ability to simultaneously perform intra-operative venography<sup>[79-83]</sup>. Postoperative recurrence of varicocele has been mainly attributed to the persistence of collaterals or anomalous veins missed during surgical ligation<sup>[84-86]</sup>. Better anatomic delineation on pre-embolization venography enables the identification of these veins, therefore reducing the possibility of future recurrences<sup>[79-86]</sup>. Embolization may be suggested for patients with recurrence, although no strong evidence to recommend the ideal treatment for recurrent varicocele exists<sup>[79-86]</sup>.

The diagnosis and treatment of varicoceles are embraced by the American Society for Reproductive Medicine (ASRM), American Urological Association (AUA) and European Urological Association, and the recommendations are presented in Table 3<sup>[8,76-78]</sup>. If varicocele repair is decided, it is advisable to include both sides, if a clinically palpable varicocele is present bilaterally. For now, the available data indicate no benefit for subclinical varicocele treatment<sup>[11]</sup>.

Another controversial topic in urology is the effects of varicocele treatment on male infertility<sup>[11]</sup>. Several studies indicated that varicocele repair improves semen parameters, including sperm density, count, concentration, motility and morphology and the percentage of progressively motile sperm in most treated men with clinical varicocele and abnormal semen parameters<sup>[4,5,9]</sup>. In addition to the improvement in semen parameters, varicocele repair may allow a couple with severely impaired semen parameters to have less invasive treatment. Men with severe oligospermia who would otherwise require *in vitro* fertilization/intra cytoplasmic sperm injection (IVF-ICSI) to conceive may have adequate improvement in semen analysis to allow intrauterine insemination instead of IVF-ICSI, and those with oligospermia may have sufficient improvement in semen parameters to allow natural conception in some cases. Surgical varicocele repair also proved useful in alleviating OS-associated infertility and improving sperm nuclear DNA integrity. Temporal changes in the testicular histology after varicocelectomy, including maturation of the germ cells, with the absence of meiotic abnormalities and normalization of the number of Leydig cells, have been reported<sup>[8]</sup>.

The debate about the role of varicocele repair in male infertility mainly lies on its actual positive effect on improving natural fertility. Several studies attempting to investigate this issue have yielded equivocal results. However, most of the existing data agree that varicocele repair increases natural pregnancy rates and mitigates



**Table 3 Summary of recommendations for the diagnosis and treatment of varicoceles**

	ASRM/SMRU	AUA	EAU
Guideline title	Report on varicocele and infertility: A committee opinion	The optimal evaluation of the infertile male: AUA best practice statement	Guidelines on male infertility
Infertile male evaluation	Medical and reproductive history, physical examination and at least two semen analyses	Complete medical history, physical examination by a urologist or other specialist in male reproduction and at least two semen analyses	Medical history and physical examination, including semen analysis: One semen analysis is sufficient if normal, two will be performed if the first one is abnormal based on WHO 2010 criteria
Optimal method to detect varicocele	Physical examination; varicoceles graded, 1 to 3	Physical examination; varicoceles graded, 1 to 3	Physical examination; varicoceles graded, 1 to 3
Role of scrotal US	For inconclusive physical examination	Indicated in those patients in whom physical examination is difficult or inadequate or a testicular mass is suspected	Used to confirm presence of varicocele identified on physical examination
Indications for treatment of varicocele	If the male partner of a couple attempting to conceive has a varicocele, treatment should be considered if most or all the following are met: clinically palpable varicocele; abnormal semen parameters; known infertility; female partner has normal fertility or a potentially treatable cause of infertility; time to conception is not a concern. An adult male who is not currently attempting to achieve conception but has a palpable varicocele, abnormal semen analyses and a desire for future fertility, and/or pain related to the varicocele is also a candidate for varicocele repair	Not stated	Varicocele repair may be effective in men with abnormal semen analysis, a clinical varicocele and otherwise unexplained infertility of duration > 2 yr
Contraindications to treatment	Patients with either normal semen analysis, isolated teratozoospermia, or a subclinical varicocele; and, if IVF or IVF-ICSI is otherwise required for the treatment of a female factor infertility	Not stated	
Method of treatment	There are two types of varicocele management, surgical repair and percutaneous embolization. Multiple types exist within each category. None of these has been proven superior to the others in its ability to improve fertility, although there are differences in recurrence rates with microsurgical subinguinal varicocelectomy having the lowest recurrence rates	Not stated	Reviews all types of treatment within guidelines and provides complication and recurrence rates of each, without specific recommendations

ASRM: American Society of Reproductive Medicine; SMRU: Society of Male Reproduction and Urology; AUA: American Urological Association; EAU: European Association of Urology; WHO: World Health Organization; IVF: *In vitro* fertilization; ICSI: Intracytoplasmic sperm injection.

the need for multiple assisted reproductive technology cycles<sup>[87-89]</sup>. Recently, there is increased evidence that clinically significant varicocele may influence testosterone production, and some researchers advocate varicocele repair in cases of decreased testosterone levels, including patients with non-obstructive azoospermia<sup>[90-92]</sup>.

## US ASSESSMENT OF TESTICULAR BLOOD FLOW AFTER VARICOCELE REPAIR

Several groups have assessed the effects of varicocelectomy on testicular arterial blood flow by CDUS<sup>[51,93-98]</sup>. Sun *et al*<sup>[93]</sup> used CDUS to assess the changes in testicular perfusion following laparoscopic varicocele clipping in 14 children and reported no significant change<sup>[93]</sup>. However, the authors evaluated only the

magnitude of arterial perfusion, not using any arterial flow parameters<sup>[93]</sup>. Student *et al*<sup>[94]</sup> reported no major changes in RI after laparoscopic varicocelectomy in comparing cases with spermatic artery ligation to those with spermatic artery preservation<sup>[94]</sup>. Tanriverdi *et al*<sup>[96]</sup> compared microsurgery and high ligation varicocelectomy by evaluating intratesticular arterial flow 7 d after surgery and reported no significant difference between the preoperative and postoperative RI in both groups<sup>[96]</sup>. A similar study comparing two laparoscopic surgical methods of varicocelectomy at 3 mo follow-up demonstrated that mean RI in the group of patients with spermatic artery ligation was comparable to the group of spermatic artery preservation.

However, subsequent studies reported a correlation between CDUS parameters and the effects of varicocele repair<sup>[51,97,98]</sup>. Balci *et al*<sup>[97]</sup> assessed the long-term effects of varicocele repair on intratesticular arterial RI in 26 infertile men with left varicocele, undergoing



subinguinal varicocelectomy. CDUS was performed before and 6 mo after the operation, and spectral Doppler indexes were measured in the intratesticular arteries and correlated with semen analysis results. RI, PI and EDV decreased significantly after surgery, but no significant change was observed in PSV. Surgery resulted in a significant increase in total sperm count, motility, morphology, and total motile sperm count, although no significant correlation was found between sperm parameters and RI<sup>[97]</sup>. CDUS was performed by Tarhan *et al.*<sup>[98]</sup> in 30 men with left clinical varicocele who underwent a microsurgical inguinal varicocelectomy before, 3 and 6 mo after surgery<sup>[98]</sup>. Spectral Doppler parameters, including PSV, EDV, RI and PI, were measured from testicular, capsular, and intratesticular arteries and were correlated with preoperative and postoperative semen analysis results. A significant improvement in both testicular blood supply and sperm parameters was found. Specifically, PSV and EDV in the left TA increased, whereas RI and PI in the left capsular and intratesticular arteries decreased significantly after surgery, both reflecting an increase in testicular arterial blood flow. Regarding semen analysis, significant increases in sperm concentration, morphology percentage, and total motile sperm concentration were seen 3 mo after surgery<sup>[98]</sup>. Recently, Zhang *et al.*<sup>[51]</sup> evaluated the effects of laparoscopic varicocelectomy (LV) and microsurgical subinguinal varicocelectomy (MV) on testicular microcirculation using CDUS and concluded that the RI and the PI of ipsilateral capsular artery (CA) and intratesticular artery (ITA) probably represent important indexes for the prognosis after varicocelectomy<sup>[51]</sup>. Specifically, the authors found a significant decrease in the mean values of PSV, PI and RI of CA and ITA after LV and MV, but no significant change in EDV. In comparing the two groups, the RI and PI of left CA and ITA in the third month and of ITA in the sixth month postoperatively in the MV group were significantly lower than those in the LV group. Both types of surgery resulted in a significant increase in the sperm density, morphology and total motile sperm count. Moreover, the PI and RI of ipsilateral CA and ITA seemed negatively correlated with sperm quality<sup>[51]</sup>.

## CONCLUSION

Varicocele is a common medical condition entangled with many controversies. Determining which patients are negatively affected by varicocele would help clinicians better select those men who will benefit the most from therapy. Functional imaging techniques, including US and MRI, might provide early indications of testicular dysfunction in testes with varicocele. Large prospective studies are needed to validate the potential role of non-invasive imaging, including US and MRI, in the assessment of the functional status of the testis in men with varicocele, thereby helping to differentiate causal from incidental varicocele.

## REFERENCES

- 1 **Simpson WL**, Rausch DR. Imaging of male infertility: pictorial review. *AJR Am J Roentgenol* 2009; **192**: S98-107 (Quiz S108-11) [PMID: 19458104 DOI: 10.2214/AJR.07.7109]
- 2 **Ammar T**, Sidhu PS, Wilkins CJ. Male infertility: the role of imaging in diagnosis and management. *Br J Radiol* 2012; **85** Spec No 1: S59-S68 [PMID: 22763036 DOI: 10.1259/bjr/31818161]
- 3 **Donkol RH**. Imaging in male-factor obstructive infertility. *World J Radiol* 2010; **2**: 172-179 [PMID: 21161032 DOI: 10.4329/wjr.v2.i5.172]
- 4 **Sofikitis N**, Stavrou S, Skouros S, Dimitriadis F, Tsounapi P, Takenaka A. Mysteries facts and fiction in varicocele pathophysiology and treatment. *European Urology Supplements* 2014; **13**: 89-99 [DOI: 10.1016/j.eursup.2014.07.002]
- 5 **Valentino M**, Bertolotto M, Derchi L, Pavlica P. Children and adults varicocele: diagnostic issues and therapeutical strategies. *J Ultrasound* 2014; **17**: 185-193 [PMID: 25177391 DOI: 10.1007/s40477-014-0088-3]
- 6 **Chiba K**, Ramasamy R, Lamb DJ, Lipshultz LI. The varicocele: diagnostic dilemmas, therapeutic challenges and future perspectives. *Asian J Androl* 2016; **18**: 276-281 [PMID: 26698233 DOI: 10.4103/1008-682X.167724]
- 7 **Esteves SC**, Agarwal A. Afterword to varicocele and male infertility: current concepts and future perspectives. *Asian J Androl* 2016; **18**: 319-322 [PMID: 26780876 DOI: 10.4103/1008-682X.172820]
- 8 **Shridharani A**, Owen RC, Elkelany OO, Kim ED. The significance of clinical practice guidelines on adult varicocele detection and management. *Asian J Androl* 2016; **18**: 269-275 [PMID: 26806081 DOI: 10.4103/1008-682X.172641]
- 9 **Tiseo BC**, Esteves SC, Cocuzza MS. Summary evidence on the effects of varicocele treatment to improve natural fertility in subfertile men. *Asian J Androl* 2016; **18**: 239-245 [PMID: 26806080 DOI: 10.4103/1008-682X.172639]
- 10 **Will MA**, Swain J, Fode M, Sonksen J, Christman GM, Ohl D. The great debate: varicocele treatment and impact on fertility. *Fertil Steril* 2011; **95**: 841-852 [PMID: 21272869 DOI: 10.1016/j.fertnstert.2011.01.002]
- 11 **Baazeem A**, Belzile E, Ciampi A, Dohle G, Jarvi K, Salonia A, Weidner W, Zini A. Varicocele and male factor infertility treatment: a new meta-analysis and review of the role of varicocele repair. *Eur Urol* 2011; **60**: 796-808 [PMID: 21733620 DOI: 10.1016/j.eururo.2011.06.018]
- 12 **Iosa G**, Lazzarini D. Hemodynamic classification of varicoceles in men: our experience. *J Ultrasound* 2013; **16**: 57-63 [PMID: 24294344 DOI: 10.1007/s40477-013-0016-y]
- 13 **Pauroso S**, Di Leo N, Fulle I, Di Segni M, Alessi S, Maggini E. Varicocele: Ultrasonographic assessment in daily clinical practice. *J Ultrasound* 2011; **14**: 199-204 [PMID: 23396816 DOI: 10.1016/j.jus.2011.08.001]
- 14 **Alsaikhan B**, Alrabeeh K, Delouya G, Zini A. Epidemiology of varicocele. *Asian J Androl* 2016; **18**: 179-181 [PMID: 26763551 DOI: 10.4103/1008-682X.172640]
- 15 **Gulleroglu K**, Gulleroglu B, Baskin E. Nutcracker syndrome. *World J Nephrol* 2014; **3**: 277-281 [PMID: 25374822 DOI: 10.5527/wjn.v3.i4.277]
- 16 **Nielsen ME**, Zderic S, Freedland SJ, Jarow JP. Insight on pathogenesis of varicoceles: relationship of varicocele and body mass index. *Urology* 2006; **68**: 392-396 [PMID: 16904459 DOI: 10.1016/j.urology.2006.02.005]
- 17 **Gökçe A**, Davarci M, Yalçinkaya FR, Güven EO, Kaya YS, Helvacı MR, Balbay MD. Hereditary behavior of varicocele. *J Androl* 2010; **31**: 288-290 [PMID: 19834129 DOI: 10.2164/jandrol.109.008698]
- 18 **Cho CL**, Esteves SC, Agarwal A. Novel insights into the pathophysiology of varicocele and its association with reactive oxygen species and sperm DNA fragmentation. *Asian J Androl* 2016; **18**: 186-193 [PMID: 26732105 DOI: 10.4103/1008-682X.170441]

- 19 **Gat Y**, Bachar GN, Everaert K, Levinger U, Gornish M. Induction of spermatogenesis in azoospermic men after internal spermatic vein embolization for the treatment of varicocele. *Hum Reprod* 2005; **20**: 1013-1017 [PMID: 15618245 DOI: 10.1093/humrep/deh706]
- 20 **Sofikitis N**, Dritsas K, Miyagawa I, Koutselinis A. Anatomical characteristics of the left testicular venous system in man. *Arch Androl* 1993; **30**: 79-85 [PMID: 8470944 DOI: 10.3109/01485019308987738]
- 21 **Sofikitis N**, Miyagawa I. Experimental models for the study of varicocele: a selected review. *Jpn J Fertil Steril* 1993; **38**: 168-177
- 22 The influence of varicocele on parameters of fertility in a large group of men presenting to infertility clinics. World Health Organization. *Fertil Steril* 1992; **57**: 1289-1293 [PMID: 1601152 DOI: 10.1016/S0015-0282(16)55089-4]
- 23 **Agarwal A**, Sharma R, Harlev A, Esteves SC. Effect of varicocele on semen characteristics according to the new 2010 World Health Organization criteria: a systematic review and meta-analysis. *Asian J Androl* 2016; **18**: 163-170 [PMID: 26780872 DOI: 10.4103/1008-682X.172638]
- 24 **Dubin L**, Amelar RD. Varicocele size and results of varicocelectomy in selected subfertile men with varicocele. *Fertil Steril* 1970; **21**: 606-609 [PMID: 5433164]
- 25 **Shiraishi K**, Matsuyama H, Takiyama H. Pathophysiology of varicocele in male infertility in the era of assisted reproductive technology. *Int J Urol* 2012; **19**: 538-550 [PMID: 22417329 DOI: 10.1111/j.1442-2042.2012.02982.x]
- 26 **Agarwal A**, Prabakaran S, Allamaneni SS. Relationship between oxidative stress, varicocele and infertility: a meta-analysis. *Reprod Biomed Online* 2006; **12**: 630-633 [PMID: 16790111 DOI: 10.1016/S1472-6483(10)61190-X]
- 27 **Wang YJ**, Zhang RQ, Lin YJ, Zhang RG, Zhang WL. Relationship between varicocele and sperm DNA damage and the effect of varicocele repair: a meta-analysis. *Reprod Biomed Online* 2012; **25**: 307-314 [PMID: 22809864 DOI: 10.1016/j.rbmo.2012.05.002]
- 28 **Sofikitis N**, Miyagawa I, Zavos PM, Inaga S, Iino A, Toda T, Harada T, Mio Y, Terakawa N. Acrosin profiles of human spermatozoa recovered from the new Sperm Prep II filtration column. *Tohoku J Exp Med* 1992; **166**: 451-457 [PMID: 1502691 DOI: 10.1620/tjem.166.451]
- 29 **Sofikitis N**, Takahashi C, Nakamura I, Hirakawa S, Miyagawa I. Surgical repair of secondary right varicocele in rats with primary left varicocele: effects on fertility, testicular temperature, spermatogenesis, and sperm maturation. *Arch Androl* 1992; **28**: 43-52 [PMID: 1550427 DOI: 10.3109/01485019208987679]
- 30 **Oztürk H**, Tander B, Aydın A, Okumus Z, Cetinkursun S. The effects of chemical sympathectomy on testicular injury in varicocele. *BJU Int* 2001; **87**: 232-234 [PMID: 11167648 DOI: 10.1046/j.1464-410x.2001.01987.x]
- 31 **Camargo M**, Intasqui P, Bertolla RP. Proteomic profile of seminal plasma in adolescents and adults with treated and untreated varicocele. *Asian J Androl* 2016; **18**: 194-201 [PMID: 26643563 DOI: 10.4103/1008-682X.168788]
- 32 **Agarwal A**, Sharma R, Samanta L, Durairajanayagam D, Sabanegh E. Proteomic signatures of infertile men with clinical varicocele and their validation studies reveal mitochondrial dysfunction leading to infertility. *Asian J Androl* 2016; **18**: 282-291 [PMID: 26732106 DOI: 10.4103/1008-682X.170445]
- 33 **Belay RE**, Huang GO, Shen JK, Ko EY. Diagnosis of clinical and subclinical varicocele: how has it evolved? *Asian J Androl* 2016; **18**: 182-185 [PMID: 26780869 DOI: 10.4103/1008-682X.169991]
- 34 **Freund J**, Handelsman DJ, Bautovich GJ, Conway AJ, Morris JG. Detection of varicocele by radionuclide blood-pool scanning. *Radiology* 1980; **137**: 227-230 [PMID: 7422850 DOI: 10.1148/radiology.137.1.7422850]
- 35 **Paz A**, Melloul M. Comparison of radionuclide scrotal blood-pool index versus gonadal venography in the diagnosis of varicocele. *J Nucl Med* 1998; **39**: 1069-1074 [PMID: 9627346 DOI: 10.1097/00005392-199901000-00129]
- 36 **Kim YS**, Kim SK, Cho IC, Min SK. Efficacy of scrotal Doppler ultrasonography with the Valsalva maneuver, standing position, and resting-Valsalva ratio for varicocele diagnosis. *Korean J Urol* 2015; **56**: 144-149 [PMID: 25685302 DOI: 10.4111/kju.2015.56.2.144]
- 37 **Semiz I**, Tokgöz O, Tokgoz H, Voyvoda N, Serifoglu I, Erdem Z. The investigation of correlation between semen analysis parameters and intraparenchymal testicular spectral Doppler indices in patients with clinical varicocele. *Ultrasound Q* 2014; **30**: 33-40 [PMID: 24901777 DOI: 10.1097/RUQ.0000000000000055]
- 38 **Gonda RL**, Karo JJ, Forte RA, O'Donnell KT. Diagnosis of subclinical varicocele in infertility. *AJR Am J Roentgenol* 1987; **148**: 71-75 [PMID: 3024475 DOI: 10.2214/ajr.148.1.71]
- 39 **Aydos K**, Baltaci S, Salih M, Anafarta K, Bedük Y, Gülsoy U. Use of color Doppler sonography in the evaluation of varicoceles. *Eur Urol* 1993; **24**: 221-225 [PMID: 8375443]
- 40 **Cina A**, Minnetti M, Pirroni T, Vittoria Spampinato M, Canadè A, Oliva G, Ribatti D, Bonomo L. Sonographic quantitative evaluation of scrotal veins in healthy subjects: normative values and implications for the diagnosis of varicocele. *Eur Urol* 2006; **50**: 345-350 [PMID: 16542771 DOI: 10.1016/j.eururo.2006.02.055]
- 41 **Kocakoc E**, Serhatlioglu S, Kiris A, Bozgeyik Z, Ozdemir H, Bodakci MN. Color Doppler sonographic evaluation of interrelations between diameter, reflux and flow volume of testicular veins in varicocele. *Eur J Radiol* 2003; **47**: 251-256 [PMID: 12927671 DOI: 10.1016/S0720-048X(02)00182-1]
- 42 **Lee J**, Binsaleh S, Lo K, Jarvi K. Varicoceles: the diagnostic dilemma. *J Androl* 2008; **29**: 143-146 [PMID: 18077824 DOI: 10.2164/jandrol.107.003467]
- 43 **Pilatz A**, Altinkilic B, Köhler E, Marconi M, Weidner W. Color Doppler ultrasound imaging in varicoceles: is the venous diameter sufficient for predicting clinical and subclinical varicocele? *World J Urol* 2011; **29**: 645-650 [PMID: 21607575 DOI: 10.1007/s00345-011-0701-4]
- 44 **Stahl P**, Schlegel PN. Standardization and documentation of varicocele evaluation. *Curr Opin Urol* 2011; **21**: 500-505 [PMID: 21926627 DOI: 10.1097/MOU.0b013e32834b8698]
- 45 **Eskew LA**, Watson NE, Wolfman N, Bechtold R, Scharling E, Jarow JP. Ultrasonographic diagnosis of varicoceles. *Fertil Steril* 1993; **60**: 693-697 [PMID: 8405527 DOI: 10.1016/S0090-4295(97)00452-4]
- 46 **Sarteschi LM**, Liguori G, Trombetta C. Varicocele. In: Sarteschi LM, Menchini-Fabris GF. *Ecografia andrologica*. Athena Srl: Modena, 2003: 139-155
- 47 **Chiou RK**, Anderson JC, Wobig RK, Rosinsky DE, Matamoros A, Chen WS, Taylor RJ. Color Doppler ultrasound criteria to diagnose varicoceles: correlation of a new scoring system with physical examination. *Urology* 1997; **50**: 953-956 [PMID: 9426729 DOI: 10.1016/S0090-4295(97)00452-4]
- 48 **Dogra VS**, Gottlieb RH, Oka M, Rubens DJ. Sonography of the scrotum. *Radiology* 2003; **227**: 18-36 [PMID: 12616012 DOI: 10.1148/radiol.2271001744]
- 49 **Schurich M**, Aigner F, Frauscher F, Pallwein L. The role of ultrasound in assessment of male fertility. *Eur J Obstet Gynecol Reprod Biol* 2009; **144** Suppl 1: S192-S198 [PMID: 19303691 DOI: 10.1016/j.ejogrb.2009.02.034]
- 50 **Akcar N**, Turgut M, Adapinar B, Ozkan IR. Intratesticular arterial resistance and testicular volume in infertile men with subclinical varicocele. *J Clin Ultrasound* 2004; **32**: 389-393 [PMID: 15372446 DOI: 10.1002/jcu.20059]
- 51 **Zhang M**, Du L, Liu Z, Qi H, Chu Q. The effects of varicocelectomy on testicular arterial blood flow: laparoscopic surgery versus microsurgery. *Urol J* 2014; **11**: 1900-1906 [PMID: 25361712]
- 52 **Ross JA**, Watson NE, Jarow JP. The effect of varicoceles on testicular blood flow in man. *Urology* 1994; **44**: 535-539 [PMID: 7941192 DOI: 10.106/S0090-4295(94)80053-7]
- 53 **Grasso Leanza F**, Pepe P, Panella P, Pepe F. Volocimetric evaluation of spermatic vessels with echo color doppler in patients with idiopathic varicocele. *Minerva Urol Nefrol* 1997; **49**: 179-182 [PMID: 9557498]
- 54 **Unsal A**, Turgut AT, Taşkın F, Koşar U, Karaman CZ. Resistance and pulsatility index increase in capsular branches of testicular artery: indicator of impaired testicular microcirculation in

- varicocele? *J Clin Ultrasound* 2007; **35**: 191-195 [PMID: 17366558 DOI: 10.1002/jcu.20331]
- 55 **Biagiotti G**, Cavallini G, Modenini F, Vitali G, Gianaroli L. Spermatogenesis and spectral echo-colour Doppler traces from the main testicular artery. *BJU Int* 2002; **90**: 903-908 [PMID: 12460354 DOI: 10.1046/j.1464-410X.2002.03033.x]
  - 56 **Gordon SJ**, Campbell S, Bhardwa J, Nargund VH. Spermatogenesis and spectral echo-colour Doppler traces from the main testicular artery. *BJU Int* 2003; **91**: 897-898 [PMID: 12780864 DOI: 10.1046/j.1464-410X.2003.t01-3-04246.x]
  - 57 **Caretta N**, Palego P, Schipilliti M, Torino M, Pati M, Ferlin A, Foresta C. Testicular contrast harmonic imaging to evaluate intratesticular perfusion alterations in patients with varicocele. *J Urol* 2010; **183**: 263-269 [PMID: 19942233 DOI: 10.1016/j.juro.2009.08.140]
  - 58 **Huang DY**, Sidhu PS. Focal testicular lesions: colour Doppler ultrasound, contrast-enhanced ultrasound and tissue elastography as adjuvants to the diagnosis. *Br J Radiol* 2012; **85** Spec No 1: S41-S53 [PMID: 22674702 DOI: 10.1259/bjr/30029741]
  - 59 **Aigner F**, De Zordo T, Pallwein-Pretner L, Junker D, Schäfer G, Pichler R, Leonhartsberger N, Pinggera G, Dogra VS, Frauscher F. Real-time sonoelastography for the evaluation of testicular lesions. *Radiology* 2012; **263**: 584-589 [PMID: 22396607 DOI: 10.1148/radiol.12111732]
  - 60 **Goddi A**, Sacchi A, Magistretti G, Almolla J, Salvatore M. Real-time tissue elastography for testicular lesion assessment. *Eur Radiol* 2012; **22**: 721-730 [PMID: 22028111 DOI: 10.1007/s00330-011-2312-2]
  - 61 **Dede O**, Teke M, Daggullu M, Utangaç M, Baş O, Penbegül N. Elastography to assess the effect of varicoceles on testes: a prospective controlled study. *Andrologia* 2016; **48**: 257-261 [PMID: 26011193 DOI: 10.1111/and.12440]
  - 62 **Tsili AC**, Giannakis D, Sylakos A, Ntorkou A, Sofikitis N, Argyropoulou MI. MR imaging of scrotum. *Magn Reson Imaging Clin N Am* 2014; **22**: 217-38, vi [PMID: 24792679 DOI: 10.1016/j.mric.2014.01.007]
  - 63 **Aganovic L**, Cassidy F. Imaging of the scrotum. *Radiol Clin North Am* 2012; **50**: 1145-1165 [PMID: 23122043 DOI: 10.1016/j.rcl.2012.08.003]
  - 64 **Cassidy FH**, Ishioka KM, McMahon CJ, Chu P, Sakamoto K, Lee KS, Aganovic L. MR imaging of scrotal tumors and pseudotumors. *Radiographics* 2010; **30**: 665-683 [PMID: 20462987 DOI: 10.1148/rg.303095049]
  - 65 **Tsili AC**, Argyropoulou MI, Giannakis D, Tsampalas S, Sofikitis N, Tsampoulas K. Diffusion-weighted MR imaging of normal and abnormal scrotum: preliminary results. *Asian J Androl* 2012; **14**: 649-654 [PMID: 22367182 DOI: 10.1038/aja.2011.172]
  - 66 **Maki D**, Watanabe Y, Nagayama M, Ishimori T, Okumura A, Amoh Y, Nakashita S, Terai A, Dodo Y. Diffusion-weighted magnetic resonance imaging in the detection of testicular torsion: feasibility study. *J Magn Reson Imaging* 2011; **34**: 1137-1142 [PMID: 21928380 DOI: 10.1002/jmri.22698]
  - 67 **Kantarci M**, Doganay S, Yalcin A, Aksoy Y, Yilmaz-Cankaya B, Salman B. Diagnostic performance of diffusion-weighted MRI in the detection of nonpalpable undescended testes: comparison with conventional MRI and surgical findings. *AJR Am J Roentgenol* 2010; **195**: W268-W273 [PMID: 20858788 DOI: 10.2214/AJR.10.4221]
  - 68 **Tsili AC**, Argyropoulou MI, Astrakas LG, Ntoulia EA, Giannakis D, Sofikitis N, Tsampoulas K. Dynamic contrast-enhanced subtraction MRI for characterizing intratesticular mass lesions. *AJR Am J Roentgenol* 2013; **200**: 578-585 [PMID: 23436847 DOI: 10.2214/AJR.12.9064]
  - 69 **Watanabe Y**, Dohke M, Ohkubo K, Ishimori T, Amoh Y, Okumura A, Oda K, Hayashi T, Dodo Y, Arai Y. Scrotal disorders: evaluation of testicular enhancement patterns at dynamic contrast-enhanced subtraction MR imaging. *Radiology* 2000; **217**: 219-227 [PMID: 11012448 DOI: 10.1148/radiology.217.1.r00oc41219]
  - 70 **Aaronson DS**, Iman R, Walsh TJ, Kurhanewicz J, Turek PJ. A novel application of 1H magnetic resonance spectroscopy: non-invasive identification of spermatogenesis in men with non-obstructive azoospermia. *Hum Reprod* 2010; **25**: 847-852 [PMID: 20124393 DOI: 10.1093/humrep/dep475]
  - 71 **Tsili AC**, Astrakas LG, Ntorkou A, Giannakis D, Stavrou S, Maliakas V, Sofikitis N, Argyropoulou MI. MR Spectra of Normal Adult Testes and Variations with Age: Preliminary Observations. *Eur Radiol* 2016; **26**: 2261-2267 [PMID: 26474986 DOI: 10.1007/s00330-015-4055-y]
  - 72 **Karakas E**, Karakas O, Cullu N, Badem OF, Boyacı FN, Gulum M, Cece H. Diffusion-weighted MRI of the testes in patients with varicocele: a preliminary study. *AJR Am J Roentgenol* 2014; **202**: 324-328 [PMID: 24450672 DOI: 10.2214/AJR.13.10594]
  - 73 **Choyke PL**. Dynamic contrast-enhanced MR imaging of the scrotum: reality check. *Radiology* 2000; **217**: 14-15 [PMID: 11012418 DOI: 10.1148/radiology.217.1.r00oc4414]
  - 74 **Terai A**, Yoshimura K, Ichioke K, Ueda N, Utsunomiya N, Kohei N, Arai Y, Watanabe Y. Dynamic contrast-enhanced subtraction magnetic resonance imaging in diagnostics of testicular torsion. *Urology* 2006; **67**: 1278-1282 [PMID: 16765192 DOI: 10.1016/j.urology.2005.12.021]
  - 75 **Watanabe Y**, Nagayama M, Okumura A, Amoh Y, Suga T, Terai A, Dodo Y. MR imaging of testicular torsion: features of testicular hemorrhagic necrosis and clinical outcomes. *J Magn Reson Imaging* 2007; **26**: 100-108 [PMID: 17659558 DOI: 10.1002/jmri.20946]
  - 76 **Practice Committee of the American Society for Reproductive Medicine; Society for Male Reproduction and Urology**. Report on varicocele and infertility: a committee opinion. *Fertil Steril* 2014; **102**: 1556-1560 [PMID: 25458620 DOI: 10.1016/j.fertnstert.2014.10.007]
  - 77 **American Urological Association Education and Research, Inc.** Report on Varicocele and Infertility: An AUA Best Practice Policy and ASRM Practice Committee Report. Linthicum, MD: American Urological Association, Inc.; Birmingham, AL: American Society for Reproductive Medicine; 2001. Available from: URL: <http://www.auanet.org/common/pdf/education/clinical-guidance/Varicocele-Archive.pdf>
  - 78 **Jungwirth A**, Giwercman A, Tournaye H, Diemer T, Kopa Z, Dohle G, Krausz C. European Association of Urology guidelines on Male Infertility: the 2012 update. *Eur Urol* 2012; **62**: 324-332 [PMID: 22591628 DOI: 10.1016/j.eururo.2012.04.048]
  - 79 **Halpern J**, Mittal S, Pereira K, Bhatia S, Ramasamy R. Percutaneous embolization of varicocele: technique, indications, relative contraindications, and complications. *Asian J Androl* 2016; **18**: 234-238 [PMID: 26658060 DOI: 10.4103/1008-682X.169985]
  - 80 **Nabi G**, Asterlings S, Greene DR, Marsh RL. Percutaneous embolization of varicoceles: outcomes and correlation of semen improvement with pregnancy. *Urology* 2004; **63**: 359-363 [PMID: 14972491 DOI: 10.1016/j.urology.2003.09.026]
  - 81 **Sze DY**, Kao JS, Frisoli JK, McCallum SW, Kennedy WA, Razavi MK. Persistent and recurrent postsurgical varicoceles: venographic anatomy and treatment with N-butyl cyanoacrylate embolization. *J Vasc Interv Radiol* 2008; **19**: 539-545 [PMID: 18375298 DOI: 10.1016/j.jvir.2007.11.009]
  - 82 **Rais-Bahrami S**, Montag S, George AK, Rastinehad AR, Palmer LS, Siegel DN. Angiographic findings of primary versus salvage varicoceles treated with selective gonadal vein embolization: an explanation for surgical treatment failure. *J Endourol* 2012; **26**: 556-560 [PMID: 22077657 DOI: 10.1089/end.2011.0387]
  - 83 **Jargiello T**, Drelich-Zbroja A, Falkowski A, Sojka M, Pyra K, Szczerbo-Trojanowska M. Endovascular transcatheter embolization of recurrent postsurgical varicocele: anatomic reasons for surgical failure. *Acta Radiol* 2015; **56**: 63-69 [PMID: 24413222 DOI: 10.1177/0284185113519624]
  - 84 **Rotker K**, Sigman M. Recurrent varicocele. *Asian J Androl* 2016; **18**: 229-233 [PMID: 26806078 DOI: 10.4103/1008-682X.171578]
  - 85 **Cayan S**, Shavakhabov S, Kadioğlu A. Treatment of palpable varicocele in infertile men: a meta-analysis to define the best technique. *J Androl* 2016; **30**: 33-40 [PMID: 18772487 DOI: 10.2164/jandrol.108.005967]
  - 86 **Cayan S**, Kadioğlu TC, Tefekli A, Kadioğlu A, Tellaloglu S. Comparison of results and complications of high ligation surgery and microsurgical high inguinal varicocelectomy in the treatment of varicocele. *Urology* 2000; **55**: 750-754 [PMID: 10792094 DOI: 10.1016/j.juro.2000.05.007]

- 10.2164/jandrol.112.016444]
- 87 **Chiles KA**, Schlegel PN. Cost-effectiveness of varicocele surgery in the era of assisted reproductive technology. *Asian J Androl* 2016; **18**: 259-261 [PMID: 26732113 DOI: 10.4103/1008-682X.172644]
  - 88 **Esteves SC**, Roque M, Agarwal A. Outcome of assisted reproductive technology in men with treated and untreated varicocele: systematic review and meta-analysis. *Asian J Androl* 2016; **18**: 254-258 [PMID: 26510504 DOI: 10.4103/1008-682X.163269]
  - 89 **Pathak P**, Chandrashekar A, Hakky TS, Pastuszak AW. Varicocele management in the era of in vitro fertilization/intracytoplasmic sperm injection. *Asian J Androl* 2016; **18**: 343-348 [PMID: 27030086]
  - 90 **Schlegel PN**, Goldstein M. Alternate indications for varicocele repair: non-obstructive azoospermia, pain, androgen deficiency and progressive testicular dysfunction. *Fertil Steril* 2011; **96**: 1288-1293 [PMID: 22130099 DOI: 10.1016/j.fertnstert.2011.10.033]
  - 91 **Esteves SC**, Miyaoka R, Roque M, Agarwal A. Outcome of varicocele repair in men with nonobstructive azoospermia: systematic review and meta-analysis. *Asian J Androl* 2016; **18**: 246-253 [PMID: 26680033 DOI: 10.4103/1008-682X.169562]
  - 92 **Dabaja AA**, Goldstein M. When is a varicocele repair indicated: the dilemma of hypogonadism and erectile dysfunction? *Asian J Androl* 2016; **18**: 213-216 [PMID: 26696437 DOI: 10.4103/1008-682X.169560]
  - 93 **Sun N**, Cheung TT, Khong PL, Chan KL, Tam PK. Varicocele: Laparoscopic clipping and color Doppler follow-up. *J Pediatr Surg* 2001; **36**: 1704-1707 [PMID: 11685706 DOI: 10.1053/jpsu.2001.27967]
  - 94 **Student V**, Zátura F, Scheinar J, Vrtal R, Vrána J. Testicle hemodynamics in patients after laparoscopic varicocelectomy evaluated using color Doppler sonography. *Eur Urol* 1998; **33**: 91-93 [PMID: 9471047]
  - 95 **Tarhan S**, Gümüş B, Gündüz I, Ayyıldız V, Gökten C. Effect of varicocele on testicular artery blood flow in men--color Doppler investigation. *Scand J Urol Nephrol* 2003; **37**: 38-42 [PMID: 12745742 DOI: 10.1080/00365590310008677]
  - 96 **Tanriverdi O**, Miroglu C, Horasanli K, Altay B, Caliskan KC, Gumus E. Testicular blood flow measurements and mean resistive index values after microsurgical and high ligation varicocelectomy. *Urology* 2006; **67**: 1262-1265 [PMID: 16765187 DOI: 10.1016/j.urol.2005.12.033]
  - 97 **Balci A**, Karazincir S, Gorur S, Sumbas H, Egilmez E, Inandi T. Long-term effect of varicocele repair on intratesticular arterial resistance index. *J Clin Ultrasound* 2008; **36**: 148-152 [PMID: 18088054 DOI: 10.1002/jcu.20439]
  - 98 **Tarhan S**, Ucer O, Sahin MO, Gumus B. Long-term effect of microsurgical inguinal varicocelectomy on testicular blood flow. *J Androl* 2011; **32**: 33-39 [PMID: 20671143 DOI: 10.2164/jandrol.109.009977]

**P- Reviewer:** Chen SS, Rais-Bahrami S, Seo JT **S- Editor:** Qiu S  
**L- Editor:** A **E- Editor:** Wu HL





## Magnetic resonance enterography in Crohn's disease: How we do it and common imaging findings

Annalisa Mantarro, Paola Scalise, Elisa Guidi, Emanuele Neri

Annalisa Mantarro, Paola Scalise, Elisa Guidi, Emanuele Neri, Department of Translational Research and New Technologies in Medicine and Surgery, Diagnostic Radiology, 56126 Pisa, Italy

**Author contributions:** Mantarro A wrote the paper; Scalise P performed research; Guidi E analysed data; Neri E designed research.

**Conflict-of-interest statement:** No potential conflicts of interest and no financial support.

**Open-Access:** This article is an open-access article which was selected by an in-house editor and fully peer-reviewed by external reviewers. It is distributed in accordance with the Creative Commons Attribution Non Commercial (CC BY-NC 4.0) license, which permits others to distribute, remix, adapt, build upon this work non-commercially, and license their derivative works on different terms, provided the original work is properly cited and the use is non-commercial. See: <http://creativecommons.org/licenses/by-nc/4.0/>

**Manuscript source:** Invited manuscript

**Correspondence to:** Emanuele Neri, MD, Professor of Radiology at the University of Pisa, Department of Translational Research and New Technologies in Medicine and Surgery, Diagnostic Radiology, Radiodiagnostica 3 Ospedale S, Chiara - Edificio 18, Via Roma 67, 56126 Pisa, Italy. [emanuele.neri@med.unipi.it](mailto:emanuele.neri@med.unipi.it)  
Telephone: +39-050-992509  
Fax: +39-050-551461

Received: April 30, 2016

Peer-review started: May 4, 2016

First decision: July 20, 2016

Revised: October 22, 2016

Accepted: December 13, 2016

Article in press: December 14, 2016

Published online: February 28, 2017

### Abstract

Crohn's disease (CD) is a chronic inflammatory disease

of the gastrointestinal tract, with unpredictable clinical course by phases of relapses alternating with other of quiescence. The etiology is multifactorial and is still not completely known; globally the westernization of lifestyle is causing an increasing incidence of CD, with peak age of 20-30 years. The diagnostic workup begins with the evaluation of the clinical history, physical examination and laboratory tests. However, the clinical assessment is subjected to interobserver variability and, occasionally, the symptoms of acute and chronic inflammation may be indistinguishable. In this regard, the role of magnetic resonance (MR) enterography is crucial to determine the extension, the disease activity and the presence of any complications without ionizing radiations, making this method very suitable for young population affected by CD. The purpose of this review article is to illustrate the MR enterography technique and the most relevant imaging findings of CD, allowing the detection of small bowel involvement and the assessment of disease activity.

**Key words:** Crohn's disease; Disease activity; Magnetic resonance sequences; Small bowel; Magnetic resonance enterography

© **The Author(s) 2017.** Published by Baishideng Publishing Group Inc. All rights reserved.

**Core tip:** Magnetic resonance (MR) enterography represents a non-invasive technique for Crohn's disease (CD) diagnosis, allowing morphological and functional evaluation of the small bowel loops. For all these reasons, MR enterography is assuming a prominent role as first-choice radiological examination in patients affected by CD. In this setting, the purpose of this review article is to illustrate the MR enterography technique and the most relevant imaging findings of CD, in order to discriminate among the various subtypes of CD (active, fistulizing/perforating or chronic subtype) and to assess disease activity.



Mantarro A, Scalise P, Guidi E, Neri E. Magnetic resonance enterography in Crohn's disease: How we do it and common imaging findings. *World J Radiol* 2017; 9(2): 46-54 Available from: URL: <http://www.wjgnet.com/1949-8470/full/v9/i2/46.htm> DOI: <http://dx.doi.org/10.4329/wjrr.v9.i2.46>

## INTRODUCTION

Crohn's disease (CD) is a type of chronic inflammatory bowel disease, characterized by typical fluctuating course with relapses alternating with periods of remission<sup>[1]</sup>. The incidence of CD is increasing worldwide, but the highest has been reported in Northern Europe, United Kingdom, and North America, occurring 20%-30% more frequently in women, with age of onset during young adulthood and, in a small subset of patients, between the 60 and 80 years of age<sup>[2]</sup>. Nowadays, the etiopathogenesis is not completely known; however the development of CD depends on several factors (immunological, genetic, and environmental, such as diet or smoking), which lead to a dysregulated immune response to commensal flora or common antigens, in genetically susceptible hosts<sup>[3,4]</sup>. Usually, CD may manifest with increased frequency of bowel movements, diarrhoea, abdominal pain and weight loss; while symptoms like asthenia, anorexia, nausea, vomiting, fever and extra-intestinal manifestations (*i.e.*, arthritis, uveitis, episcleritis, skin rashes, erythema nodosum, pyoderma gangrenosum) occur in about a quarter of patients<sup>[5]</sup>.

Moreover, CD may affect any portion of the gastrointestinal tract from mouth to anus, mainly involving the ileocaecal region (about one half of all cases), following by the ileum and colon (30% and 20% of patients, respectively)<sup>[6]</sup>. Both the transmural chronic inflammation and the discontinuous involvement ("skip lesions") of affected bowel loops, alternating inflamed and uninvolved segments, are typical features of CD<sup>[7]</sup>. During the active phase of inflammatory response, the enteric mucosa appears as irregular due to neutrophils and mononuclear cell infiltration, alternating ulceration and edema ("cobblestoning" pattern), associated with cryptitis, crypt microabscesses, and sometimes non-caseating granulomas. When the inflammation becomes chronic, the superficial aphthoid ulcers can penetrate into the bowel wall resulting in deep ulcerations, sinus tracts or fistula formation, thus extending into mesentery, lymph nodes and adjacent structures (*i.e.*, other bowel loops, bladder, uterus, vagina or skin).

Moreover, the chronic inflammatory response promotes smooth muscle cell proliferation, collagen accumulation, wall thickening, stenosis and fibrosis of the affected bowel segments with mesenteric fibro-fatty proliferation<sup>[8,9]</sup>.

Given this context, the management and staging of patients with CD requires the correct determination of inflammatory lesion location, extension, activity and

severity, in order to choose appropriate therapeutic strategies<sup>[10,11]</sup>. Since the clinical presentation of acute and chronic inflammation may be overlapped, the cross-sectional imaging techniques are useful for distinguishing them and preventing the development of potential complications. Among imaging modalities, magnetic resonance (MR) enterography provides the advantages of high-tissue-contrast evaluation with optimal detection of fluid and submucosal edema, multiplanar capability, multiparametric assessment and functional informations (motility, perfusion, diffusion) without ionizing radiations, making this method very suitable for young population affected by CD<sup>[12]</sup>.

The purpose of this article is to review MR enterography technique and the most relevant imaging findings of CD, in order to provide an overview of the current state-of-art of MR imaging in CD, highlighting the recent MR innovations that allow a better evaluation of disease activity.

## TECHNIQUE

MR enterography requires fast imaging techniques, luminal distension and 6-h fasting before the procedure<sup>[11]</sup>. In this regard, an adequate colonic distension is mandatory to better identify wall thickening and parietal enhancement on the post-contrastographic images. The oral contrast agents used to obtain a well-distended lumen are classified based on their effects on T1 and T2-weighted images. The positive contrast agents (diluted gadolinium, some fruit juices or milk) yield the advantage of high intraluminal signal due to their high T2, but they may interfere with the detection of mucosal enhancement in T1-weighted sequences after gadolinium administration due to T1 shortening effect. By contrast, the use of negative contrast agents, as superparamagnetic iron oxide, determines a low intraluminal signal (low T2 and T1) and allows a better evaluation of the bowel walls<sup>[13]</sup>. However the widest accepted contrast agents are the biphasic ones (methylcellulose, mannitol, polyethylene glycol), characterized by hyperosmolar effect, that promotes luminal distention. Furthermore, they permit the assessment of wall thickening thanks to high signal intensity on T2-weighted sequences (positive effect), in which the bowel walls appear as hypointense, while the lumen is hyperintense. On T1-weighted images after gadolinium administration, these biphasic contrast agents maximize the depiction of wall enhancement by means of low intraluminal signal (negative effect)<sup>[14]</sup>. As above mentioned the biphasic contrast agent are more frequently preferred for MR enterography in CD. The patients are instructed to ingest about 1.5-2 L of water solution with biphasic contrast agent 45 min preceding the procedure<sup>[15]</sup>. The patient is positioned in prone decubitus in order to increase bowel loop separation and decrease both the peristalsis and the acquired abdominal volume in MR sequences, consequently

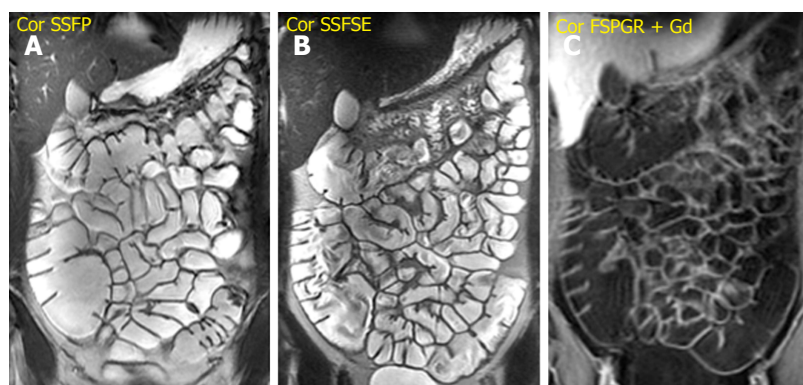


**Figure 1** Assessment of small bowel anatomy, disease localization and segmental extension. A: Steady-state free precession (SSFP); B: T2-weighted single shot fast spin echo (SSFSE) sequence; C: Gadolinium-enhanced fat-suppressed 3D spoiled gradient-echo (FSPGR) sequence.

reducing blurring and bowel motility artifacts. The supine position is required for noncompliant patients with abdominal stomas or entero-cutaneous fistulas. Moreover, before T2-weighted sequences and contrast medium injection, endovenous administration of 20 mg of hyoscine butylbromide is recommended to further reduce bowel peristalsis<sup>[16]</sup>. MR enterography is performed using phased-array coils to improve signal-to-noise ratio and spatial resolution, simultaneously minimizing the acquisition time with faster sequences and parallel imaging.

The MR study protocol consists of the following sequences.

#### **Steady-state free precession sequence - (FIESTA, General Electric; True-FISP, Siemens)**

It is a very fast sequence thanks to a short repetition and echo time, providing high-contrast MR images dependent on T2\*/T1 ratio. It allows motion-free images, ensuring a good visualization of the small bowel, mesentery, vascularization and lymphadenopathy in coronal and axial view. Furthermore, this sequence may provide cine assessment of the bowel loops, facilitating the discrimination between fibrotic stricture and functional stenosis. However, the images suffer from magnetic susceptibility artifacts, caused by the presence of gas or ferromagnetic materials, and chemical shift artifacts resulting in a "black boundary" effect around structures, which may hamper a correct definition of bowel wall thickening<sup>[17]</sup>.

#### **T2-weighted SSFSE (Single Shot Fast Spin Echo, General Electric) or HASTE (Half-fourier Acquisition Single-shot Turbo spin-Echo, Siemens)**

It allows to obtain high-contrast resolution MR images in coronal and axial planes for the depiction of wall thickening, fold pattern changes, ulceration, intramural bowel edema and extraluminal fluid collections (particularly with fat-suppressed images). It is a fast sequence with a long echo train, which utilizes the partial Fourier encoding of K-space data for reducing the acquisition time, nevertheless decreasing signal-to-noise ratio of MR

images. It is not sensitive to magnetic susceptibility or chemical shift artifacts, allowing an optimal evaluation of wall thickening. However, this sequence is sensitive to intraluminal flow voids, blurring and bowel motility artifacts; in this regard, the endovenous administration of spasmolytic agent is recommended to reduce bowel peristalsis<sup>[13]</sup>.

#### **Gadolinium-enhanced fat-suppressed 3D spoiled gradient-echo sequence**

It is performed after the intravenous injection of 0.1-0.2 mmol/kg of gadopentetate dimeglumine (Gd-DTPA) with a delay time of 40-80 s; the acquisition of arterial phase after 25 s is optional. It is very useful to evaluate bowel wall enhancement, which is highlighted by endoluminal low-signal intensity caused by positive contrast agent administration. Moreover, it provides relevant information about vasculature, lymph nodes, fistulas or abscesses. Frequently the sequence is performed in the coronal plane; axial acquisitions may be useful for evaluating the pathological and thickened bowel loops<sup>[18]</sup> (Figure 1).

#### **Diffusion-weighted imaging sequence**

Diffusion-weighted imaging sequence in the axial plane has been proposed to better identify the inflamed bowel loops in active phase<sup>[16]</sup>.

#### **MR enterography advantages**

Several studies have compared the accuracy of different non-invasive diagnostic methods in the assessment of CD.

In this setting, MR enterography is more effective than ultrasound (US), particularly in the evaluation of the entire gastrointestinal tract, perianal region and complications; although US permits a rapid and accurate examination of the terminal ileum<sup>[19]</sup>.

Moreover, Lee *et al*<sup>[20]</sup> have demonstrated that the effectiveness of MR enterography is comparable to that of CT enterography, with the advantage of not using ionizing radiations, making this modality ideal in imaging the youth.

## MR ENTEROGRAPHY INDICATIONS

The clinical indications of MR enterography include the following conditions: (1) assesment of small bowel anatomy, disease localization and segmental extension; (2) morphological evaluation (bowel wall, mesentery, vascular supply and lymph nodes); (3) dynamic evaluation (disease activity and neoangiogenesis); (4) classification of CD into three subtypes based on inflammatory activity, including active inflammatory, fistulizing/perforating and fibrostenosing categories; (5) follow-up of patients with diagnosed CD; (6) exclusion of CD diagnosis in symptomatic patients; (7) suspected disease relapse, stricturing disease and/or extraluminal complications; (8) monitoring therapeutic response or failure; and (9) planning of surgical intervention<sup>[17]</sup>.

The assessment of CD subtypes is required by clinicians for the therapeutic planning, through the detection of linear and aphthoid ulcers, wall edema, skip lesions, fistulas, abscess or strictures; and their correlation with clinical data<sup>[21]</sup>. Frequently, acute and chronic changes may coexist in the same bowel segment with a wide variety of intestinal and extra-intestinal abnormalities. In this context, the bowel wall lesions characterizing active disease are managed medically, whereas fibrotic strictures with bowel obstruction are frequently treated with surgical intervention<sup>[22]</sup>.

### Active inflammatory subtype

The typical pathological findings of active CD comprehend: Aphthoid and deep ulceration, wall thickening (greater than 4 mm), intramural and mesenteric edema, stratified enhancement pattern of bowel wall, increased mesenteric vascularity, reactive lymphadenopathy<sup>[13]</sup>.

**Ulcers:** The aphthoid ulcers, typical findings of CD in the early stages, can only be detected through an adequate luminal distension and high-resolution MR imaging, they appear as a nidus of high signal intensity in T2-weighted images, surrounded by a rim of moderate signal intensity<sup>[23]</sup>. Advanced inflammation may produce other changes, such as deep and transmural (linear) ulcerations. The typical "cobblestone" mucosal appearance result from confluent (longitudinal and transverse) ulcerations combined with bulging of the edematous mucosa<sup>[12]</sup>.

**Fold thickening:** The SSFSE sequence allows to identify fold thickening and distortion caused by mucosal ulceration<sup>[24]</sup>.

**Wall thickening:** It is easily identified on steady-state free precession (SSFP), T2-weighted (SSFSE) and fat-suppressed 3D spoiled gradient-echo (FSPGR) (after Gd-DTPA administration) sequences, previous adequate distension of the small bowel loops. Nevertheless, the SSFP sequence hampers the correct definition of wall thickening, because of the chemical shift artefact. For this reason, the measurement of wall thickness

should be performed in SSFSE images. The degree of wall thickening correlates with both the presence of inflammation and the degree of disease activity. Particularly, a wall thickening greater than 3 mm is indicative of inflammation, while a thickening ranging from 5 to 10 mm is suggestive of CD<sup>[25]</sup>.

**Intramural edema:** This is a typical sign of active inflammation resulting in submucosal thickening, which appears as hyperintensity on T2-weighted (SSFSE) images with fat saturation<sup>[26]</sup>.

**Mesenteric changes:** In some cases of advanced inflammation, the mesentery may be edematous around the inflamed intestinal loops. Typically, the mesenteric edema is associated with both submucosal edema and stratified enhancement of the bowel wall; all these findings are suggestive of active inflammation. The mesenteric fibro-fatty proliferation (or fat-wrapping) represents another sign of advanced CD with consolidated transmural inflammation. It can be defined as an increase of mesenteric fat, which can determine mass effect with consequent anatomical displacement of the mesenteric vessels or the adjacent abdominal viscera, increasing the separation among the bowel loops. Moreover, the vascular engorgement produces an increased mesenteric vascularity ("comb sign"), resulting in hyperenhancement of mesenteric vessels supplying inflamed bowel loops<sup>[16,21]</sup> (Figure 2).

**Stratified enhancement pattern:** The bowel wall enhancement, evaluated after Gd-DTPA intravenous administration, represents the parameter that most closely correlates to both the degree of inflammation and clinical indices of disease activity. The mucosal hyperemia of the affected loops is represented by hyperenhancement, which is significantly higher than normal loops; it decreases decrease in response to therapy. The typical stratified enhancement pattern ("target sign") is produced by mucosal and muscle/serosa increased enhancement with intermediate hypointensity of edematous submucosa<sup>[27]</sup> (Figure 3).

**Reactive mesenteric lymphadenopathy:** Hyperenhancement, enlargement, and edema of lymph nodes can be present in active disease, but they are not specific of CD. These findings are easily identified with SSFP and FSPGR (after Gd-DTPA administration) sequences<sup>[28]</sup>.

### Fistulizing/perforating subtype

It is characterized by the presence of deep penetrating ulcers, which can lead to the creation of sinus tract, fistulas and/or abscesses. The sinus tracts appear as hyperintense blind-ending tracts on T2-weighted images, that arise from bowel wall without ever reaching the surface of another structure (Figure 4). By contrast, fistulas originate from deep transmural ulcers, which communicate with adjacent epithelial



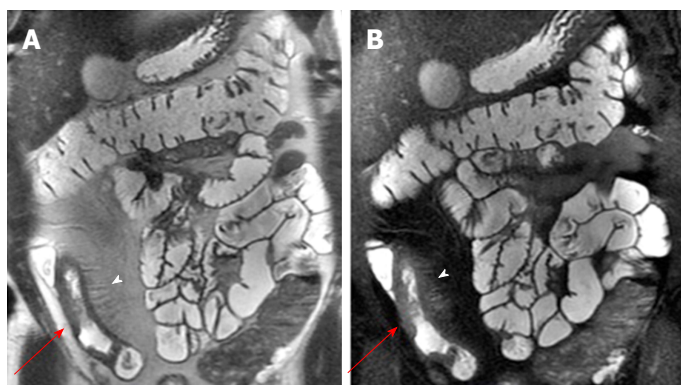


**Figure 2 Wall thickening and mesenteric changes.** SSFSE (A) and gadolinium-enhanced FSPGR (B) sequences show wall thickening (red arrows) of terminal ileum with comb signs (arrowhead) and mesenteric fat proliferation. SSFSE: Single shot fast spin echo; FSPGR: Fat-suppressed 3D spoiled gradient-echo.

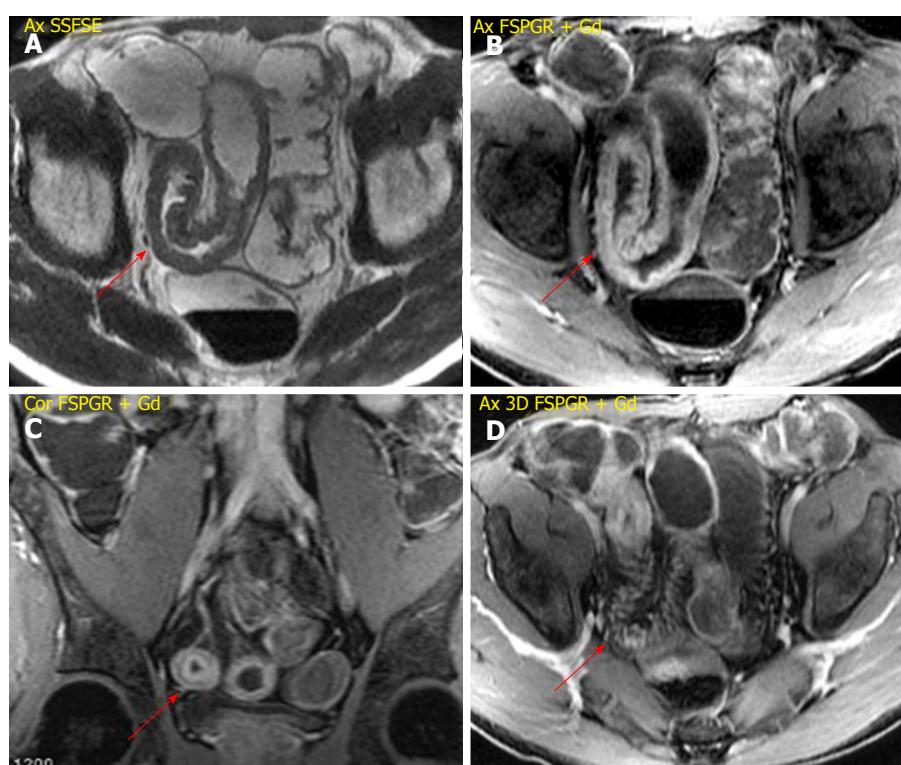


**Figure 3 Active inflammation.** A: Wall thickening (10 mm) of terminal ileum extending for about 18 cm detected on SSFSE sequence; B: Gadolinium-enhanced FSPGR sequence shows the stratified enhancement pattern characterized by mucosal and muscle/serosa increased enhancement with intermediate hypointensity of edematous submucosa; C: Coronal FSPGR sequence revealing typical "target sign" due to stratified enhancement of bowel wall; D: Mesenteric fat thickening and vascular engorgement of vasa recta (comb sign) displayed on gadolinium-enhanced image. SSFSE: Single shot fast spin echo; FSPGR: Fat-suppressed 3D spoiled gradient-echo.

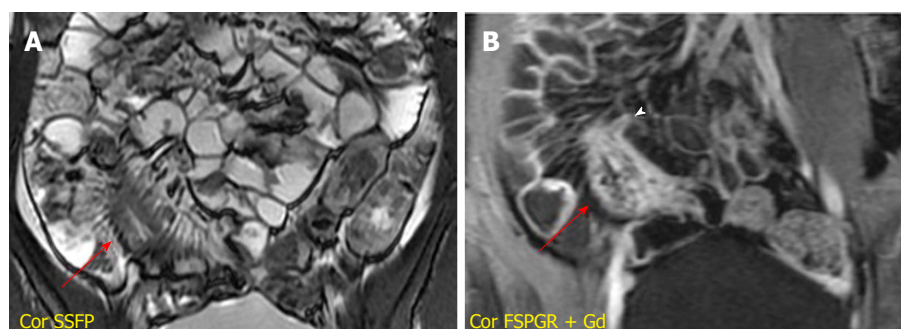


**Figure 4 Subacute and stenotic disease with sinus tract.** A: SSFP sequence showing wall thickening (11 mm; red arrow) of terminal ileum with comb sign and mesenteric fat thickening; B: Post-gadolinium image reveals diffuse enhancement of the stenotic bowel loop and sinus tract (arrowhead), which is a blind-ending tract arising from the bowel wall. SSFP: Steady-state free precession; FSPGR: Fat-suppressed 3D spoiled gradient-echo.

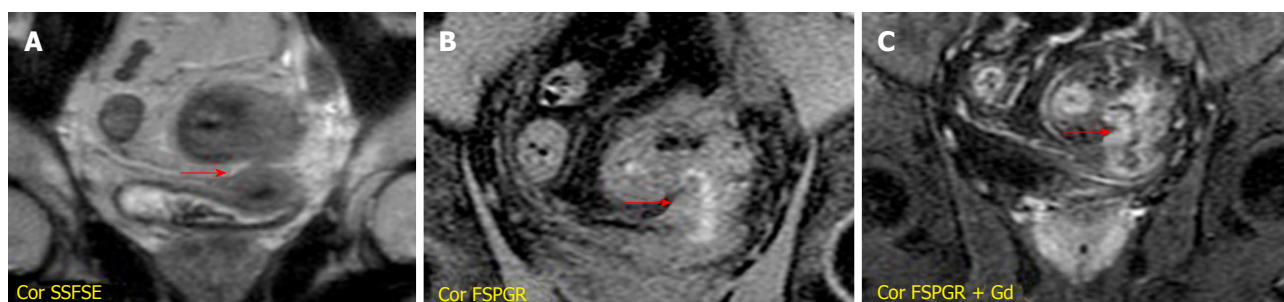


**Figure 5 Entero-vesical fistula.** A: Coronal SSFSE sequence detects wall thickening of the sigmoid colon with entero-vesical fistula (red arrow); B: FSPGR without gadolinium administration highlights the entero-vesical fistula, which appears hyperintense due to colonic content; C: Entero-vesical fistula appears as hyperintense transmurals in post-gadolinium sequence. SSFSE: Single shot fast spin echo; FSPGR: Fat-suppressed 3D spoiled gradient-echo.

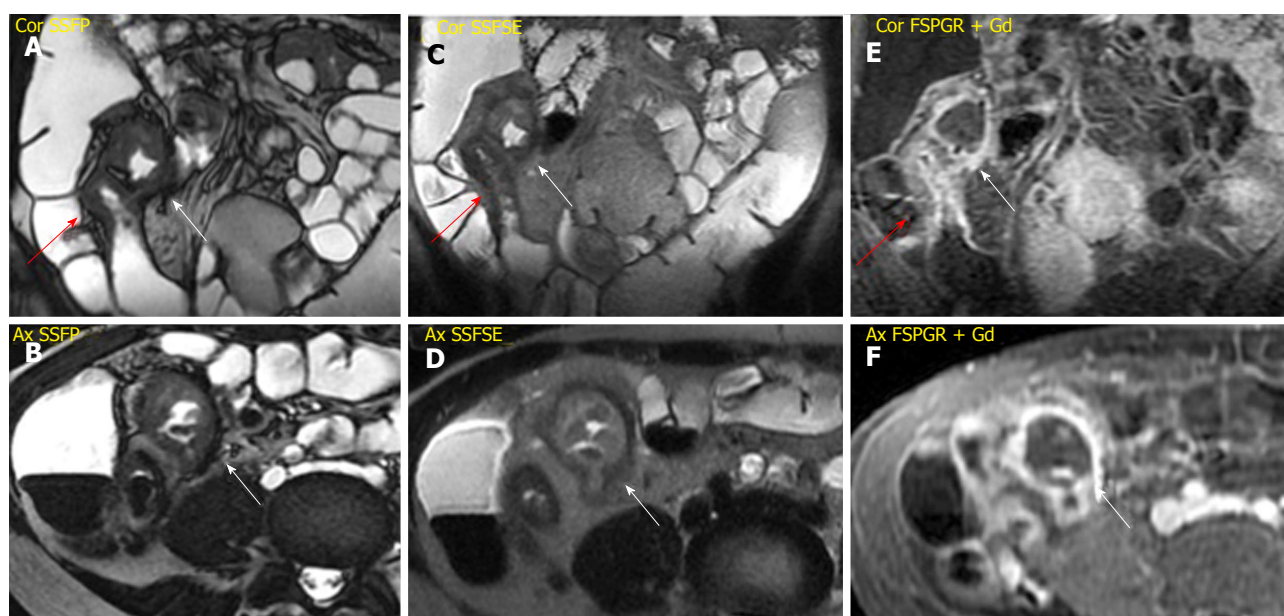


**Figure 6 Peri-ileal abscess.** A-D: SSFP and SSFSE sequences display wall thickening of the terminal ileum associated (red arrow) with contiguous encapsulated collection of pus and inhomogeneous content (abscess, white arrow); E and F: FSPGR sequence shows mucosal enhancement with hypointense deep layers of the bowel wall (fibrotic disease), associated with enhancing peripheral rim of the capsulated collection (abscess, white arrow). SSFP: Steady-state free precession; SSFSE: Single shot fast spin echo; FSPGR: Fat-suppressed 3D spoiled gradient-echo.

surfaces (bowel loops or other organs), appearing as hyperintense transmural lines on FSPGR (after Gd-DTPA administration) sequences<sup>[29,30]</sup>. The fistulas can penetrate into contiguous bowel loops (enteroenteric or enterocolic fistulas) or into other structures (*i.e.*, bladder, uterus, vagina or skin); however, their identification in the earliest phase is very difficult due to low spatial resolution and partial volume averaging of MR images (Figure 5). An accurate high-resolution MR study associated with the use of multiplanar imaging can help to reveal the presence of fistulas. The desmoplastic reaction in the mesenteric tissue contributes to produce stellate appearance of fistulas, with spiculated margins<sup>[31]</sup>.

Other locoregional complications of CD comprehend the development of phlegmon and abscesses. The penetrating process may lead to a localized inflammatory reaction resulting into phlegmon formation, which is an inflammatory mass with mild/moderate increase signal on T2-weighted and post-gadolinium sequences<sup>[32]</sup>. An

abscess is an encapsulated collection of pus, which has MR characteristics similar to those of fluid collections (hyperintense on T2-weighted and hypointense on T1-weighted images), but with inhomogeneous content because of solid and gaseous components, delimited by an enhancing peripheral rim<sup>[13]</sup> (Figure 6).

#### **Fibrostenotic subtype**

The chronic inflammation of the bowel wall tends to progress towards fibrostenotic and irreversible complications (bowel strictures and obstruction), as consequence of prolonged intestinal injury<sup>[33]</sup>. During chronic disease, the deposition of submucosal fat is promoted resulting in stratified appearance on T2-weighted images. This finding may be distinguished by submucosal edema on T2-weighted images thanks to fat saturation, which reduces the signal of fat in chronic disease<sup>[34]</sup>. Moreover, the bowel wall enhancement differs from the stratified pattern, typical of active



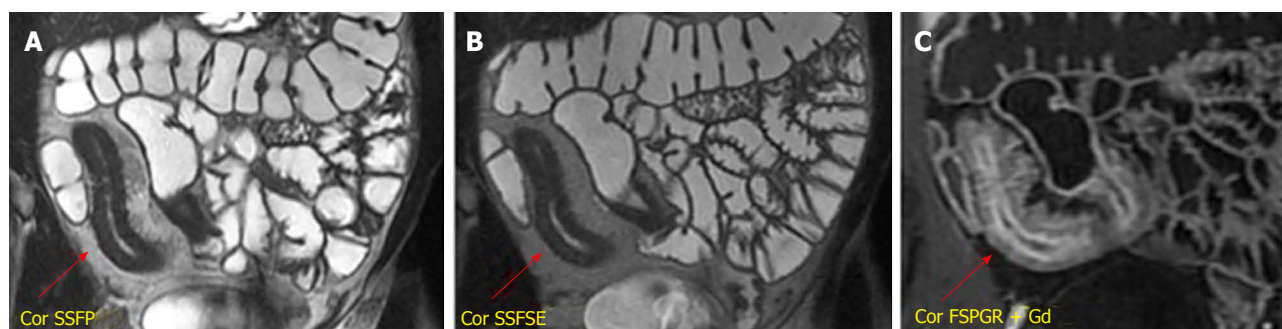


**Figure 7 Chronic disease.** A and B: Coronal SSFP and SSFSE sequences detect wall thickening (10 mm, red arrows) of neo-terminal ileum, after ileo-cecal resection, extending for about 19 cm; C: Coronal FSPGR sequence shows mucosal enhancement with hypointensity of the deep layers indicating the fibrotic disease. SSFP: Steady-state free precession; SSFSE: Single shot fast spin echo; FSPGR: Fat-suppressed 3D spoiled gradient-echo.

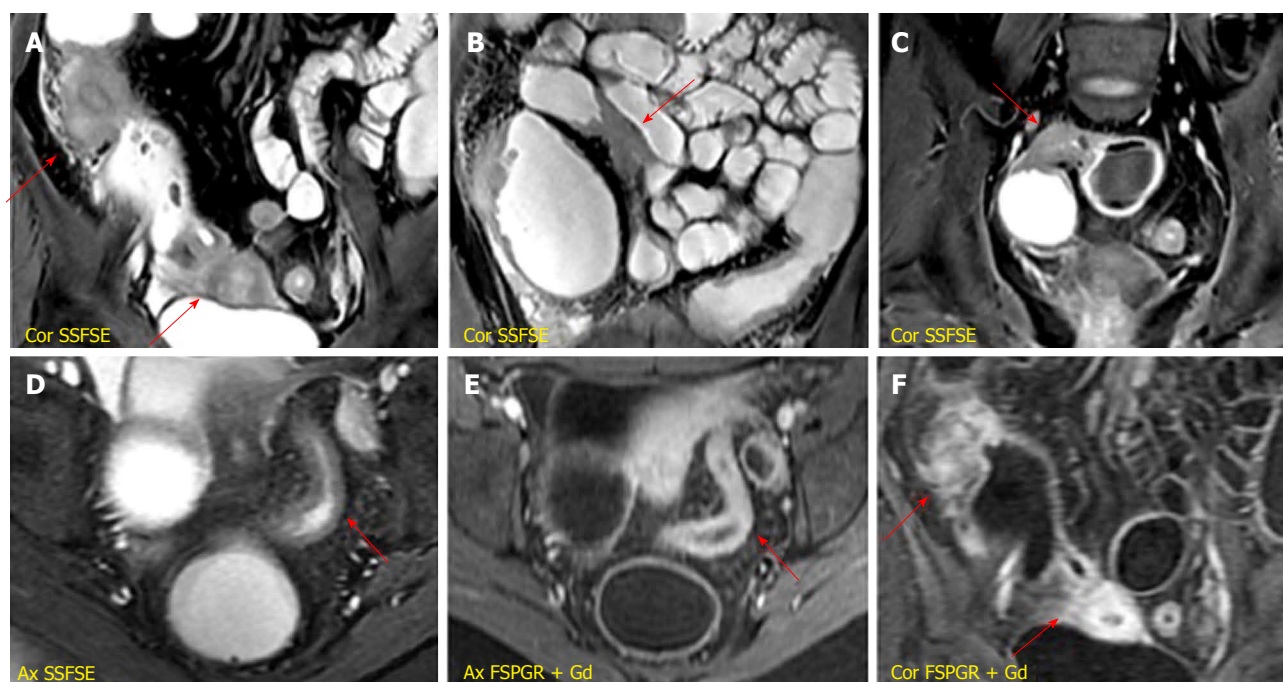


**Figure 8 Fibrostenotic disease.** A-C: Multiple fibrotic strictures of the small bowel alternating with prestenotic dilated tracts detected on SSFSE sequences; D: Wall thickening of the sigmoid colon producing luminal narrowing displayed on SSFSE image; E and F: Post-gadolinium sequences reveal a diffuse and homogeneous enhancement in sigmoid colon (E) and small bowel (F) suggestive of subacute inflammation. SSFSE: Single shot fast spin echo; FSPGR: Fat-suppressed 3D spoiled gradient-echo.

disease. On this ground, the thickened and fibrotic bowel wall shows diffuse and homogeneous enhancement during subacute transmural inflammation, while the moderate mucosal enhancement with hypointensity of the deep layers suggests fibrotic disease<sup>[35]</sup> (Figure 7). In chronic disease, fibrosis may lead to stricture formation with high risk of small bowel obstruction of the affected segment, and consequent prestenotic dilatation (Figure 8). The fibrotic stricture appears as fixed luminal narrowing without any high signal intensity on T2-weighted images; by contrast the inflamed stricture, in acute disease, shows submucosal edema with the typical stratified enhancement pattern. It is important to identify the presence of fibrotic strictures because they are not responsive to medical therapy, but require prompt surgical approach to avoid complications such as

bowel obstruction<sup>[12,36]</sup>. Furthermore, MR enterography is useful for detecting asymmetric bowel fibrosis on the mesenteric border with apparent dilatation (pseudodiverticula) on the antimesenteric side, and rare complications such as small bowel adenocarcinoma<sup>[37]</sup>.

### Reading and reporting MR enterography

The recommended reading strategy for MR enterography examinations should integrate previous morphological evaluation, followed by functional assessment of the small bowel loops. The clinical information received and the specific diagnostic query are crucial for the radiologist, in order to better adapt the examination technique to the specific patient conditions.

According to the RSNA reporting initiative, consisting of a library of report templates, the MR entero-

graphy report should include these criteria: (1) clinical indication; (2) description of imaging technique and quality; (3) small bowel findings (*i.e.*, distension, peristalsis, bowel wall thickening, post-contrast findings, fistulas and/or abscess, lymph nodes); (4) collateral findings in abdominal organs; and (5) final impression indicating location and activity of disease, complications and extra-enteric findings<sup>[38]</sup>.

## CONCLUSION

MR enterography is now considered a well-established imaging technique for small bowel evaluation. It plays an increasingly important role as non-invasive and effective method to evaluate the small-bowel involvement and the possible intestinal and extra-intestinal complications, in patients affected by CD.

Nevertheless, MR enterography examination should be tailored both to the patient and diagnostic query, in order to guide the clinical management.

## REFERENCES

- Ananthakrishnan AN. Epidemiology and risk factors for IBD. *Nat Rev Gastroenterol Hepatol* 2015; **12**: 205-217 [PMID: 25732745 DOI: 10.1038/nrgastro.2015.34]
- Cosnes J, Gower-Rousseau C, Seksik P, Cortot A. Epidemiology and natural history of inflammatory bowel diseases. *Gastroenterology* 2011; **140**: 1785-1794 [PMID: 21530745 DOI: 10.1053/j.gastro.2011.01.055]
- Baumgart DC, Sandborn WJ. Crohn's disease. *Lancet* 2012; **380**: 1590-1605 [PMID: 22914295 DOI: 10.1016/S0140-6736(12)60026-9]
- Sartor RB. Mechanisms of disease: pathogenesis of Crohn's disease and ulcerative colitis. *Nat Clin Pract Gastroenterol Hepatol* 2006; **3**: 390-407 [PMID: 16819502 DOI: 10.1038/ncpgasthep0528]
- Di Sabatino A, Rovedatti L, Vidali F, Macdonald TT, Corazza GR. Recent advances in understanding Crohn's disease. *Intern Emerg Med* 2013; **8**: 101-113 [PMID: 21553239 DOI: 10.1007/s11739-011-0599-2]
- Hart A, Ng SC. Crohn's disease. *Medicine* 2011; **39**: 229-236 [DOI: 10.1016/j.mpmed.2011.01.004]
- Laass MW, Roggenbuck D, Conrad K. Diagnosis and classification of Crohn's disease. *Autoimmun Rev* 2014; **13**: 467-471 [PMID: 24424189 DOI: 10.1016/j.autrev.2014.01.029]
- Alzoghaibi MA. Neutrophil expression and infiltration into Crohn's intestine. *Saudi J Gastroenterol* 2005; **11**: 63-72 [PMID: 19861848 DOI: 10.4103/1319-3767.33322]
- Randall CW, Vizuite JA, Martinez N, Alvarez JJ, Garapati KV, Malakouti M, Taboada CM. From historical perspectives to modern therapy: a review of current and future biological treatments for Crohn's disease. *Therap Adv Gastroenterol* 2015; **8**: 143-159 [PMID: 25949527 DOI: 10.1177/1756283X15576462]
- Wilkins T, Jarvis K, Patel J. Diagnosis and management of Crohn's disease. *Am Fam Physician* 2011; **84**: 1365-1375 [PMID: 22230271]
- Panes J, Bouhnik Y, Reinisch W, Stoker J, Taylor SA, Baumgart DC, Danese S, Halligan S, Marincak B, Matos C, Peyrin-Biroulet L, Rimola J, Rogler G, van Assche G, Ardizzone S, Ba-Salamah A, Bali MA, Bellini D, Biancone L, Castiglione F, Ehehalt R, Grassi R, Kucharzik T, Maccioni F, Maconi G, Magro F, Martin-Comin J, Morana G, Pendsé D, Sebastian S, Signore A, Tolan D, Tielbeek JA, Weishaupt D, Wiarda B, Laghi A. Imaging techniques for assessment of inflammatory bowel disease: joint ECCO and ESGAR evidence-based consensus guidelines. *J Crohns Colitis* 2013; **7**: 556-585 [PMID: 23583097 DOI: 10.1016/j.crohns.2013.02.020]
- Leyendecker JR, Bloomfield RS, DiSantis DJ, Waters GS, Mott R, Bechtold RE. MR enterography in the management of patients with Crohn disease. *Radiographics* 2009; **29**: 1827-1846 [PMID: 19959524 DOI: 10.1148/rg.296095510]
- Tolan DJ, Greenhalgh R, Zealley IA, Halligan S, Taylor SA. MR enterographic manifestations of small bowel Crohn disease. *Radiographics* 2010; **30**: 367-384 [PMID: 20228323 DOI: 10.1148/rg.302095028]
- Laghi A, Paolantonio P, Iafrate F, Borrelli O, Dito L, Tomei E, Cucchiara S, Passariello R. MR of the small bowel with a biphasic oral contrast agent (polyethylene glycol): technical aspects and findings in patients affected by Crohn's disease. *Radiol Med* 2003; **106**: 18-27 [PMID: 12951547]
- Kuehle CA, Ajaj W, Ladd SC, Massing S, Barkhausen J, Lauenstein TC. Hydro-MRI of the small bowel: effect of contrast volume, timing of contrast administration, and data acquisition on bowel distention. *AJR Am J Roentgenol* 2006; **187**: W375-W385 [PMID: 16985108 DOI: 10.2214/AJR.05.1079]
- Griffin N, Grant LA, Anderson S, Irving P, Sanderson J. Small bowel MR enterography: problem solving in Crohn's disease. *Insights Imaging* 2012; **3**: 251-263 [PMID: 22696087 DOI: 10.1007/s13244-012-0154-3]
- Furukawa A, Saotome T, Yamasaki M, Maeda K, Nitta N, Takahashi M, Tsujikawa T, Fujiyama Y, Murata K, Sakamoto T. Cross-sectional imaging in Crohn disease. *Radiographics* 2004; **24**: 689-702 [PMID: 15143222 DOI: 10.1148/rg.243035120]
- Gourtsoyiannis N, Papanikolaou N, Grammatikakis J, Maris T, Prassopoulos P. MR enteroclysis protocol optimization: comparison between 3D FLASH with fat saturation after intravenous gadolinium injection and true FISP sequences. *Eur Radiol* 2001; **11**: 908-913 [PMID: 11419161 DOI: 10.1007/s003300000805]
- Stasi C, Falchini M, Milani S. Imaging modalities for the noninvasive assessment of fibrosis in Crohn's disease. *ScientificWorldJournal* 2012; **2012**: 450151 [PMID: 22654607 DOI: 10.1100/2012/450151]
- Lee SS, Kim AY, Yang SK, Chung JW, Kim SY, Park SH, Ha HK. Crohn disease of the small bowel: comparison of CT enterography, MR enterography, and small-bowel follow-through as diagnostic techniques. *Radiology* 2009; **251**: 751-761 [PMID: 19276325 DOI: 10.1148/radiol.2513081184]
- Fidler JL, Guimaraes L, Einstein DM. MR imaging of the small bowel. *Radiographics* 2009; **29**: 1811-1825 [PMID: 19959523 DOI: 10.1148/rg.296095507]
- Maglinte DD, Gourtsoyiannis N, Rex D, Howard TJ, Kelvin FM. Classification of small bowel Crohn's subtypes based on multimodality imaging. *Radiol Clin North Am* 2003; **41**: 285-303 [PMID: 12659339 DOI: 10.1016/S0033-8389(02)00117-3]
- Sinha R, Rajiah P, Murphy P, Hawker P, Sanders S. Utility of high-resolution MR imaging in demonstrating transmural pathologic changes in Crohn disease. *Radiographics* 2009; **29**: 1847-1867 [PMID: 19959525 DOI: 10.1148/rg.296095503]
- Sinha R, Verma R, Verma S, Rajesh A. MR enterography of Crohn disease: part 2, imaging and pathologic findings. *AJR Am J Roentgenol* 2011; **197**: 80-85 [PMID: 21701014 DOI: 10.2214/AJR.11.6740]
- Sempere GA, Martinez Sanjuan V, Medina Chulia E, Benages A, Tome Toyosato A, Canelles P, Bulto A, Quiles F, Puchades I, Cuquerella J, Celma J, Orti E. MRI evaluation of inflammatory activity in Crohn's disease. *AJR Am J Roentgenol* 2005; **184**: 1829-1835 [PMID: 15908538 DOI: 10.2214/ajr.184.6.01841829]
- Yoon K, Chang KT, Lee HJ. MRI for Crohn's Disease: Present and Future. *Biomed Res Int* 2015; **2015**: 786802 [PMID: 26413543 DOI: 10.1155/2015/786802]
- Del Vescovo R, Sansoni I, Caviglia R, Ribolsi M, Perrone G, Leoncini E, Grasso RF, Cicala M, Zobel BB. Dynamic contrast enhanced magnetic resonance imaging of the terminal ileum: differentiation of activity of Crohn's disease. *Abdom Imaging* 2008; **33**: 417-424 [PMID: 17639383 DOI: 10.1007/s00261-007-9267-4]
- Prassopoulos P, Papanikolaou N, Grammatikakis J, Rousomoustakaki M, Maris T, Gourtsoyiannis N. MR enteroclysis imaging of Crohn disease. *Radiographics* 2001; **21** Spec No: S161-S172 [PMID: 11598255 DOI: 10.1148/radiographics.21.suppl.1.g01oc02s161]
- Scharl M, Rogler G. Pathophysiology of fistula formation in Crohn's

- disease. *World J Gastrointest Pathophysiol* 2014; **5**: 205-212 [PMID: 25133023 DOI: 10.4291/wjgp.v5.i3.205]
- 30 **Maccioni F**, Bruni A, Viscido A, Colaiacomo MC, Cocco A, Montesani C, Caprilli R, Marini M. MR imaging in patients with Crohn disease: value of T2- versus T1-weighted gadolinium-enhanced MR sequences with use of an oral superparamagnetic contrast agent. *Radiology* 2006; **238**: 517-530 [PMID: 16371574 DOI: 10.1148/radiol.2381040244]
  - 31 **Herrmann KA**, Michaely HJ, Zech CJ, Seiderer J, Reiser MF, Schoenberg SO. Internal fistulas in Crohn disease: magnetic resonance enteroclysis. *Abdom Imaging* 2006; **31**: 675-687 [PMID: 16447079 DOI: 10.1007/s00261-005-0400-y]
  - 32 **Cullen G**, Vaughn B, Ahmed A, Peppercorn MA, Smith MP, Moss AC, Cheifetz AS. Abdominal phlegmons in Crohn's disease: outcomes following antitumor necrosis factor therapy. *Inflamm Bowel Dis* 2012; **18**: 691-696 [PMID: 21648022 DOI: 10.1002/ibd.21783]
  - 33 **Latella G**, Di Gregorio J, Flati V, Rieder F, Lawrance IC. Mechanisms of initiation and progression of intestinal fibrosis in IBD. *Scand J Gastroenterol* 2015; **50**: 53-65 [PMID: 25523556 DOI: 10.3109/00365521.2014.968863]
  - 34 **Maccioni F**, Viscido A, Broglia L, Marrollo M, Masciangelo R, Caprilli R, Rossi P. Evaluation of Crohn disease activity with magnetic resonance imaging. *Abdom Imaging* 2000; **25**: 219-228 [PMID: 10823437 DOI: 10.1007/s002610000004]
  - 35 **Punwani S**, Rodriguez-Justo M, Bainbridge A, Greenhalgh R, De Vita E, Bloom S, Cohen R, Windsor A, Obichere A, Hansmann A, Novelli M, Halligan S, Taylor SA. Mural inflammation in Crohn disease: location-matched histologic validation of MR imaging features. *Radiology* 2009; **252**: 712-720 [PMID: 19635832 DOI: 10.1148/radiol.2523082167]
  - 36 **Rimola J**, Planell N, Rodríguez S, Delgado S, Ordás I, Ramírez-Morros A, Ayuso C, Aceituno M, Ricart E, Jauregui-Amezaga A, Panés J, Cuatrecasas M. Characterization of inflammation and fibrosis in Crohn's disease lesions by magnetic resonance imaging. *Am J Gastroenterol* 2015; **110**: 432-440 [PMID: 25623654 DOI: 10.1038/ajg.2014.424]
  - 37 **Cahill C**, Gordon PH, Petrucci A, Boutros M. Small bowel adenocarcinoma and Crohn's disease: any further ahead than 50 years ago? *World J Gastroenterol* 2014; **20**: 11486-11495 [PMID: 25206256 DOI: 10.3748/wjg.v20.i33.11486]
  - 38 MR Enterography Template. [accessed 2016 Apr 23]. Available from: URL: <http://www.radreport.org/template/0000051>

**P- Reviewer:** Anzola LK, Giudici F **S- Editor:** Gong ZM  
**L- Editor:** A **E- Editor:** Wu HL



Basic Study

## Radiology education in Europe: Analysis of results from 22 European countries

Bhavya Rehani, Yi C Zhang, Madan M Rehani, András Palkó, Lawrence Lau, Miriam N Mikhail Lette, William P Dillon

Bhavya Rehani, Yi C Zhang, William P Dillon, Department of Radiology and Biomedical Imaging, University of California, San Francisco, CA 94110, United States

Madan M Rehani, Department of Radiology, Massachusetts General Hospital, Harvard Medical School, Boston, MA 02115, United States

András Palkó, Department of Radiology, University of Szeged, H-6720 Szeged, Hungary

Lawrence Lau, Consultant Radiologist, Melbourne, 3103 Victoria, Australia

Miriam N Mikhail Lette, Consultant Diagnostic Radiologist, RAD-AID International, 1110 Geneva, Switzerland

**Author contributions:** Rehani B, Zhang YC and Dillon WP made substantial contributions to conception and design of the study and acquisition of data, and the remaining authors made substantial contributions to acquisition of data, or analysis and interpretation of data; all authors made substantial contributions to drafting the article or making critical revisions related to important intellectual content of the manuscript; all authors gave final approval of the version of the article to be published.

**Institutional review board statement:** The University of California San Francisco IRB does not consider this project as human subject research.

**Conflict-of-interest statement:** Bhavya Rehani is the recipient of a RSNA Education Scholar grant for development of RISEMed.org. All other authors have no conflict of interest to disclose.

**Data sharing statement:** Technical appendix, statistical code, and dataset available from the corresponding author at [bhavya.rehani@ucsf.edu](mailto:bhavya.rehani@ucsf.edu). Consent was not obtained but the potential benefits of sharing these data outweigh the potential harms because the data does not contain any personal information. The data only pertains to radiology education infrastructure on a national level.

**Open-Access:** This article is an open-access article which was

selected by an in-house editor and fully peer-reviewed by external reviewers. It is distributed in accordance with the Creative Commons Attribution Non Commercial (CC BY-NC 4.0) license, which permits others to distribute, remix, adapt, build upon this work non-commercially, and license their derivative works on different terms, provided the original work is properly cited and the use is non-commercial. See: <http://creativecommons.org/licenses/by-nc/4.0/>

**Manuscript source:** Unsolicited manuscript

**Correspondence to:** Bhavya Rehani, MD, Assistant Professor, Department of Radiology and Biomedical Imaging, University of California, 1001 Potrero Ave, San Francisco, CA 94110, United States. [bhavya.rehani@ucsf.edu](mailto:bhavya.rehani@ucsf.edu)  
**Telephone:** +1-415-2068024  
**Fax:** +1-415-4760616

**Received:** July 30, 2016

**Peer-review started:** July 31, 2016

**First decision:** September 2, 2016

**Revised:** October 25, 2016

**Accepted:** December 1, 2016

**Article in press:** December 2, 2016

**Published online:** February 28, 2017

## Abstract

### AIM

To assess the state of radiology education across Europe by means of a survey study.

### METHODS

A comprehensive 23-item radiology survey was distributed *via* email to the International Society of Radiology members, national radiological societies, radiologists and medical physicists. Reminders to complete the survey were sent and the results were analyzed over a period of 4 mo (January-April 2016). Survey questions include length of medical school and residency training;



availability of fellowship and subspecialty training; number of residency programs in each country; accreditation pathways; research training; and medical physics education. Descriptive statistics were used to analyze and summarize data.

## RESULTS

Radiology residency training ranges from 2-6 years with a median of 5 years, and follows 1 year of internship training in 55% (12 out of 22) European countries. Subspecialty fellowship training is offered in 55% (12 out of 22) European countries. Availability for specialization training by national societies is limited to eight countries. For nearly all respondents, less than fifty percent of radiologists travel abroad for specialization. Nine of 22 (41%) European countries have research requirements during residency. The types of certifying exam show variation where 64% (14 out of 22) European countries require both written and oral boards, 23% (5 out of 22) require oral examinations only, and 5% (1 out of 22) require written examinations only. A degree in medical physics is offered in 59% (13 out of 22) European countries and is predominantly taught by medical physicists. Nearly all respondents report that formal examinations in medical physics are required.

## CONCLUSION

Comparative learning experiences across the continent will help guide the development of comprehensive yet pragmatic infrastructures for radiology education and collaborations in radiology education worldwide.

**Key words:** Radiology education; European radiology survey; Radiology training; Residency; Radiology research

© **The Author(s) 2017.** Published by Baishideng Publishing Group Inc. All rights reserved.

**Core tip:** The authors report survey results of radiology education across 22 European countries with respect to length of training, subspecialty fellowship availability, research opportunities, and national certification and credentialing. Given the diversity in training requirements and its impact on cross-border training recognition, our results provide important insights to understand radiology education and its potential on portability across different countries in Europe.

Rehani B, Zhang YC, Rehani MM, Palkó A, Lau L, Lette MNM, Dillon WP. Radiology education in Europe: Analysis of results from 22 European countries. *World J Radiol* 2017; 9(2): 55-62 Available from: URL: <http://www.wjgnet.com/1949-8470/full/v9/i2/55.htm> DOI: <http://dx.doi.org/10.4329/wjr.v9.i2.55>

## INTRODUCTION

Radiology provides cutting-edge imaging information that guides clinical decision-making. As our under-

standing of disease processes has grown more complex, radiology itself has branched into increasingly subspecialized fields. The number of distinct subspecialties in the broader scope of the discipline has significant implications for radiology teaching. Radiology training programs around the world face a challenging task in both teaching a common knowledge base across all the imaging modalities and in imparting deep subspecialty knowledge within each specialty domain.

A paucity of literature exists regarding the radiology education infrastructure worldwide<sup>[1]</sup>. This gap in the literature can be challenging for radiologists who would like to collaborate, contribute and learn from differences, similarities and challenges in radiology education systems outside their country. Highlighting the variations in residency training may encourage exchange of best practices and experiences to better prepare trainees for an ever-evolving practice environment. There is a wide range of training infrastructure and assessment methods across the globe with respect to pre-clinical qualifications, radiology residency structure, on-call requirements, access to teaching, and certifying national or board examinations<sup>[2]</sup>.

The goal of this paper is to understand the radiology education infrastructure across the European continent, share common practices and explore different perspectives to better prepare the next generation of radiologists leaders.

## MATERIALS AND METHODS

### Medical school, internship, radiology residency

A comprehensive radiology survey (Table 1) was created to analyze the state of Radiology education worldwide. Each survey consisted of questions assessing medical school, radiology residency, internship, fellowships and subspecialties, medical physics, research, and accreditation, along with supplemental questions specifically targeted to their specific audience.

### Subspecialty training

Apart from the overall infrastructure of radiology residency and subspecialty training, we also inquired about the number of radiology residency programs in the country, availability and type of subspecialty fellowship programs and the percentage of radiologists who have to travel outside the country for further training. We surveyed fellowship availability in the following subspecialties: Neuroradiology, Interventional Radiology, Musculoskeletal Radiology, Chest Radiology, Abdominal Radiology, Interventional Neuroradiology, Nuclear Medicine, Ultrasound, Breast Imaging, Cardiovascular Imaging, and Pediatric Radiology.

### National or university based board certifying exam and research

The type of national or university based board certifying exam was questioned. Research requirements to finish



**Table 1** List of survey questions

Survey questions	
A	How long is medical school in your country excluding internship?
B	Is internship required in your country?
C	How long is the radiology residency/post-graduate training in your country including internship in number of years?
D	Please provide the number of radiology residency programs in your country (rough estimate if exact figure is not known)
E	Is subspecialty radiology fellowship training available in your country?
F	Which subspecialty fellowship trainings are available in your country?
G	What percentage of radiology residents travel outside your country for subspecialized radiology training?
H	Approximately how many radiologists are there in your country?
I	If subspecialty training is not present in your country, are week- or month-long courses for advanced training and credentialing in a particular subspecialty available from your national societies?
J	Are there research requirements for radiology residents/trainees to finish training?
K	If there is a research requirement to finish training, please explain. Otherwise, please skip this question
L	What kind of national certifying exam or university based exam is required for residents to be certified in radiology?
M	How many MRI scanners are available in your country?
N	What percentage of radiology/medical imaging procedures is done by non-radiologists?
O	Is there a degree option like MSc in medical physics in your country?
P	Who teaches medical physics to radiology residents in your country?
Q	Are radiology residents formally examined for medical physics?

**Table 2** Medical school, internship, and residency responses

Country	Length of medical school (excluding internship)	Internship requirement	Length of radiology residency (internship included)	Number of radiology residency programs
Armenia	6	No	2	1-5
Austria	6	Yes	6	6-10
Bulgaria	6	No	4	1-5
Croatia	6	Yes	5	6-10
Denmark	6	Yes	5	41-50
Estonia	5	No	4	1-5
Greece	6	No	5	11-20
Hungary	6	No	5	6-10
Italy	6	Yes	4	31-40
Lithuania	5	No	5	1-5
Malta	5	Yes	5	1-5
Norway	6	No	5	--
Poland	6	Yes	5	41-50
Portugal	6	Yes	5	> 80
Romania	5	Yes	4	21-30
Serbia	6	Yes	4	> 80
Slovakia	6	No	5	6-10
Slovenia	6	Yes	5	1-5
Spain	6	No	4	> 80
Sweden	6	Yes	7	51-100
Switzerland	6	No	5	21-30
United Kingdom	5	Yes	5	41-50

residency training were assessed.

### Medical physics

Availability of masters programs in medical physics, medical physicists for education, and national radiation safety programs was queried.

The 23-item survey was distributed *via* email to the International Society of Radiology members, national radiological societies, radiologists and medical physicists. Reminders to complete the survey were sent and the results were analyzed over a period of 4 mo (January-April 2016).

To check the accuracy of information submitted we contacted radiologists, representatives of national radiology and neuroradiology societies by email who validated the responses and answered specific discordant questions. Descriptive statistics were used to analyze and summarize data.

## RESULTS

### Medical school, internship, radiology residency (Table 2)

We gathered data for 22 European countries based upon responses from national radiological society representatives or radiologists (Figure 1). Seventy-seven percent (17 out of 22) respondents report six-year medical school training. Radiology residency training ranges from 2-6 years with a median of 5 years, and follows 1 year of internship training in 55% (12 out of 22) European countries.

### Subspecialty training (Table 3)

Subspecialty fellowship training is offered in 55% (12 out of 22) European countries. Within those countries, interventional radiology fellowship is the most common subspecialty followed by neuroradiology, pediatrics, and nuclear medicine fellowships. Switzerland offers the greatest variety of fellowship opportunities including neuroradiology, interventional, neuro-interventional, musculoskeletal, nuclear medicine, and pediatrics training. In contrast, Austria, Estonia and Sweden offer only one fellowship subspecialty. Availability for specialization training by national societies is limited to eight countries. For nearly all respondents, less than fifty percent of radiologists travel abroad for specialization.

### Research opportunities (Table 4)

Nine of 22 (41%) European countries have research requirements during residency, which range from 1-mo to 9-mo research blocks, or at least one publication



Figure 1 Survey responses representing countries (place markers) across the European continent.

during residency with an open time frame of research commitment.

#### **National or university based board certifying exam (Table 4)**

The types of certifying exam show variation where 64% (14 out of 22) European countries require both written and oral boards, 23% (5 out of 22) require oral examinations only, and 5% (1 out of 22) require written examinations only.

#### **Medical physics education (Table 5)**

A degree in medical physics is offered in 59% (13 out of 22) European countries and is predominantly taught by medical physicists. Nearly all respondents report that formal examinations in medical physics are required.

## **DISCUSSION**

Europe is the third most populous continent after Asia and Africa with a wide diversity of cultures and languages. Similarly, there is diversity in radiology education systems. Although medical school training is six years long in the majority of European countries included in our study, there are differences in clinical

internship requirement and length of residency training, which may vary by up to two years<sup>[3]</sup>. Given the diversity in training requirements and its impact on cross-border training recognition, our results provide important insights to understand radiology education and its potential on portability across different countries in Europe.

While some countries have greater than eighty radiology residency programs, others like Armenia, Bulgaria, Estonia, Lithuania, Malta and Slovenia have only one to five radiology residency programs in the entire country. It is unclear if the number of residency programs is sufficient, given the size and population of these countries.

Fellowship training is available in 50% of the respondent countries in our study. The countries that offer at least one fellowship include Austria, Croatia, Estonia, Greece, Hungary, Romania, Serbia, Slovakia, Sweden, Switzerland, and United Kingdom. The most common fellowship offered is interventional radiology. Ultrasound fellowship is only available in one respondent country (Croatia), while none of the respondent countries have chest radiology fellowships.

Compared to the 2004 EAR Education Survey<sup>[3]</sup>, there has been an increase in both the number of

**Table 3** Subspecialty fellowship responses

Country	Subspecialty	Types of available subspecialties											Percent radiologists traveling abroad for specialization	Approx. number of radiologists	Specialization training by national society
		Neuro	IR	MSK	Chest	Abd	Neuro-IR	NM	US	Breast	CV	Ped			
Armenia	N												< 50%	201-400	Y
Austria	Y	Y											< 50%	> 400	Y
Bulgaria	N												< 50%	Difficult to estimate	N
Croatia	Y	Y	Y						Y				< 50%	201-400	N
Denmark	N												< 50%	> 400	N
Estonia	Y		Y										< 50%	--	N
Greece	Y		Y	Y		Y						Y	< 50%	--	--
Hungary	Y	Y	Y				Y			Y		Y	< 50%	> 400	Y
Italy	N												< 50%	> 400	Y
Lithuania	N												< 50%	201-400	Y
Malta	N												> 50%	< 50	Y
Norway	---												< 50%	> 400	--
Poland	N												< 50%	> 400	N
Portugal	N												< 50%	> 400	N
Romania	Y	Y				Y		Y					< 50%	> 400	N
Serbia	Y		Y			Y							< 50%	101-200	N
Slovakia	Y		Y							Y	Y	Y	--	> 400	N
Slovenia	N												< 50%	101-200	N
Spain	N												< 50%	> 400	N
Sweden	Y							Y					0%	--	--
Switzerland	Y	Y	Y	Y			Y	Y				Y	< 50%	> 400	--
United Kingdom	Y	Y	Y				Y	Y					< 50%	> 400	N

Neuro: Neuroradiology; IR: Interventional radiology; MSK: Musculoskeletal radiology; Chest: Chest radiology; Abd: Abdominal radiology; Neuro-IR: Interventional neuroradiology; NM: Nuclear medicine; US: Ultrasound; Breast: Breast imaging; CV: Cardiovascular imaging; Ped: Pediatric radiology; Y: Yes; N: No.

countries that offer fellowship training as well as in the variety of available subspecialties. For example, fellowship training in Switzerland now encompasses interventional radiology (IR), musculoskeletal (MSK), Neurointerventional, and Nuclear Medicine. Similarly, Slovakia increased fellowship training to include Interventional Radiology, Breast, Cardiovascular, and Pediatrics. Estonia, Greece, Hungary, and Romania are additional examples of countries that expanded subspecialty training.

Given rapid innovation across many imaging modalities, increasing exposure to fellowship training is fast becoming a priority to ensure that residents learn up-to-date subspecialty knowledge worldwide. Our results show that less than 50% of radiologists travel outside their respective countries for training. It has been discussed that practicing radiologists understandably face the challenge of meeting clinical demands while maintaining teaching responsibilities<sup>[4]</sup>. Individual didactic teaching sessions may not be feasible in a high-volume work environment<sup>[5]</sup>.

This creates a potential role for interactive e-learning teaching modules<sup>[6-9]</sup> and virtual education<sup>[10]</sup> to supplement education in a particular subspecialty for self-motivated learners. Accessible electronic modules have served as useful extensions to radiology teaching<sup>[11,12]</sup>. The European Society of Radiology (ESR) offers accre-

dated electronic modules categorized by subspecialty content with optional self assessments<sup>[13]</sup>. The ESR has also implemented and continuously updated the European Training Curriculum, a subspecialty-specific framework organized by training level that enhances the quality of radiology education throughout Europe<sup>[14]</sup>.

The European Society of Radiology offers courses to help prepare trainees for the European Diploma in Radiology (EDiR)<sup>[15]</sup>. The EDiR, a certificate of excellence, helps standardize radiology training in the setting of varied certification methods across Europe as demonstrated in our survey results.

Basic and translational research exposure form a significant component of radiology education and should be made widely available<sup>[16]</sup>. Residents can make considerable contributions to the field because they have a unique perspective on the day-to-day practice from an "in-the-trenches" point of view, ranging from image interpretation to workflow management and on-call demands. Residents also have first hand experiences with different technology platforms and thus can bring new ideas that drive innovation in radiology. In our surveyed European countries, fewer than half of European countries have dedicated research blocks during residency. Challenges in promoting research include limited finances, lack of incentives for researchers, issues of career planning, and gender

**Table 4** Certification and research responses

Country	Research requirement for residency	If yes, describe research requirement	Type of certifying exam required	Number of MRI scanners	Percentage of radiology procedures by non-radiologists
Armenia	No	---	Oral	6-10	---
Austria	Yes	9-mo research	Written and oral	> 100	15%-20%
Bulgaria	No	---	Oral	10-50	> 20%
Croatia	Yes	Indexed publication	Written and oral	10-50	---
Denmark	Yes	1-mo research	Oral	10-50	0%-5%
Estonia	No	---	Oral	---	---
Greece	Yes	---	Written and oral	---	---
Hungary	No	---	Written and oral	5-10	---
Italy	Yes	At least one research project	Written and oral	> 100	0%-5%
Lithuania	Yes	Research presentation	Written and oral	10-50	---
Malta	No	---	Written and oral	6-10	---
Norway	---	---	---	> 100	---
Poland	No	---	Written and oral	> 100	15%-20%
Portugal	No	---	Oral	51-100	> 20%
Romania	No	---	Written and oral	< 5	---
Serbia	No	---	Written and oral	10-50	5%-10%
Slovakia	No	---	Written and oral	10-50	---
Slovenia	Yes	At least one publication during residency	Written and oral	10-50	10%-15%
Spain	No	---	Written	> 100	10%-15%
Sweden	Yes	---	---	---	---
Switzerland	No	---	Written and oral	51-100	> 20%
United Kingdom	Yes	Basic research competency	Written and oral	> 100	> 20%

**Table 5** Medical physics responses

Country	Medical physics degree	Medical physics taught by	Formal examination of medical physics
Armenia	Yes	Radiologist	Yes, there is a question paper combined with another subject Only oral test
Austria	No	Radiologist	Only written test
Bulgaria	No	Radiologist	Yes, there is a separate question paper on this subject Radiologists review the answer sheets for medical physics portion
Croatia	No	Radiologist	Radiologists review the answer sheets for medical physics part Radiologists conduct oral exam in medical physics and radiation safety
Denmark	Yes	Medical physicist	Yes, there is a separate question paper on this subject Only written test Radiologists review the answer sheets for medical physics portion
Estonia	Yes	---	---
Greece	Yes	Medical physicist	Only oral test
Hungary	Yes	Medical physicist	There is both oral and written test
Italy	No	Medical physicist	Only oral test
Lithuania	No	Medical physicist	Yes, there is a separate question paper on this subject Yes, there is a question paper combined with another subject
Malta	Yes	Medical physicist	Yes, there is a question paper combined with another subject Only written test
Norway	No	Medical physicist	Yes, there is a question paper combined with another subject
Poland	Yes	Radiologist	Only written test
Portugal	No	Other	---
Romania	No	Medical physicist	Yes there is a question paper along combined with another subject Radiologists review the answer sheets for medical physics part
Serbia	Yes	Medical physicist	Yes, there is a separate question paper on this subject Yes, there is a question paper combined with another subject
Slovakia	Yes	Medical physicist	Yes, there is a question paper combined with another subject There is both oral and written test
Slovenia	No	Medical physicist	Radiologists review the answer sheets for medical physics portion
Spain	Yes	Medical physicist	Only written test
Sweden	Yes	Medical physicist	Yes, there is a separate question paper on this subject
Switzerland	Yes	Medical physicist	Yes, there is a separate question paper on this subject Only written test
United Kingdom	Yes	Medical physicist	Radiologists review the answer sheets for medical physics portion Yes, there is a separate question paper on this subject Radiologists review the answer sheets for medical physics portion



issues<sup>[16]</sup>. This also seems to be a challenge worldwide and increased emphasis on research during residency has been encouraged<sup>[17-19]</sup>. Increasing time and mentorship resources for research will help establish radiology innovation early in the career pathway. Radiologists around the world could assist in mentoring trainees in research outside their programs to encourage future world leaders in radiology.

Medical physics and radiation safety is particularly important given the reported radiation injuries due to imaging<sup>[20-22]</sup>. The ESR recently noted an increase in inappropriate exposure to ionizing radiation along with significant variations in dosimetry for the same examination<sup>[23]</sup>. To reduce patient exposure to unnecessary radiation, the ESR plans to implement individual patient dose tracking, mobile dose information for physicians, and radiation protection training with certification<sup>[23]</sup>. Nearly all survey respondents reported that formal examination in medical physics is required in Europe. In addition, 70% had medical physics training from medical physicist rather than a radiologist. Medical physics degree programs are also offered by majority of respondent European countries.

Each European country included in our study offers a unique perspective on radiology education based on what is feasible for resident teaching, subspecialty training, and research. Comparative learning experiences across the continent will help guide the development of comprehensive yet pragmatic infrastructures for radiology education and collaborations in radiology education worldwide.

Limitations of our study include a sample size of twenty out of a total of forty-eight European countries. As such, our data may not be representative of the radiologic education landscape across all of Europe. In addition, our survey response rate indicates that our results represent only a fraction of all countries in Europe, likely due to the approach in questionnaire distribution and collection. Our survey channels through the International Society of Radiology also may have introduced bias in selecting for countries that are its participating members.

Future research may involve potential collaboration with the European Society of Radiology to gain insight into the radiology infrastructure across a greater number of European countries. E-learning modules may help augment the variety of fellowship training and increase resident engagement with real time communication and feedback. Innovative technology platforms that offer indexed and searchable didactic content will contribute to a sustainable solution for international radiology education.

## ACKNOWLEDGMENTS

We would like to profoundly thank International Society of Radiology for collaboration and radiologists in Europe who participated in this survey.

## COMMENTS

### Background

The status of radiology education in Europe, particularly in specialty fellowship training and research, merits an in-depth study in order to gain an understanding of challenges and potential collaborations among the regional training programs.

### Research frontiers

Recent advances in technology platforms for web-based applications and mobile tools have enabled trainees to gain access to specialty training that may supplement availability of radiology education at their home institutions.

### Innovations and breakthroughs

This study demonstrates that subspecialty fellowship training is offered in approximately half of European countries and the availability for specialization training by national societies is limited to eight countries. Other differences in board certifications and medical physics curricula differ among the regional training programs. The European Training Curriculum serves as a reference for the establishment and revision of national training programs and sets the basis for the European Diploma in Radiology exam.

### Applications

Practical applications of this study include the use of country-specific training availability data to augment radiology education and in providing access to online teaching curricula to supplement radiology education.

### Peer-review

This is a well-written paper regarding radiology education in Europe.

## REFERENCES

- 1 **Di Marco L**, Conway WF, Chapin R. Radiology Resident Education in France from Medical School Through Board Certification. *J Am Coll Radiol* 2015; **12**: 1097-1102 [PMID: 26435123 DOI: 10.1016/j.jacr.2015.06.030]
- 2 **Willatt JM**, Mason AC. Comparison of radiology residency programs in ten countries. *Eur Radiol* 2006; **16**: 437-444 [PMID: 15702337 DOI: 10.1007/s00330-004-2635-3]
- 3 **European Society of Radiology**. Radiological Training Programmes in Europe: EAR Education Survey - Analysis of Results. 2004 EAR Education Committee. [accessed 2016 May 8]. Available from: URL: [https://www.myesr.org/html/img/pool/ESR\\_brochure\\_05.pdf](https://www.myesr.org/html/img/pool/ESR_brochure_05.pdf)
- 4 **Gunderman RB**, Kang YP, Fraley RE, Williamson KB. Teaching the teachers. *Radiology* 2002; **222**: 599-603 [PMID: 11867772 DOI: 10.1148/radiol.2223010825]
- 5 **Cohen MD**, Gunderman RB. Academic radiology: sustaining the mission. *Radiology* 2002; **224**: 1-4 [PMID: 12091654 DOI: 10.1148/radiol.2241011741]
- 6 **Colucci PG**, Kostandy P, Shrauner WR, Arleo E, Fuortes M, Griffin AS, Huang YH, Juluru K, Tsiouris AJ. Development and utilization of a web-based application as a robust radiology teaching tool (radstax) for medical student anatomy teaching. *Acad Radiol* 2015; **22**: 247-255 [PMID: 25964956]
- 7 **Carriero A**, Bonomo L, Calliada F, Campioni P, Colosimo C, Cotroneo A, Cova M, Ettorre GC, Fugazzola C, Garlaschi G, Macarini L, Mascalchi M, Meloni GB, Midiri M, Mucelli RP, Rossi C, Sironi S, Torricelli P, Beomonte BZ, Zompatori M, Zuiani C. E-learning in radiology: an Italian multicentre experience. *Eur J Radiol* 2012; **81**: 3936-3941 [PMID: 22902406 DOI: 10.1016/j.ejrad.2012.07.007]
- 8 **Pinto A**, Brunese L, Pinto F, Acampora C, Romano L. E-learning and education in radiology. *Eur J Radiol* 2011; **78**: 368-371 [PMID: 21255951 DOI: 10.1016/j.ejrad.2010.12.029]
- 9 **Zafar S**, Safdar S, Zafar AN. Evaluation of use of e-Learning in undergraduate radiology education: a review. *Eur J Radiol* 2014; **83**: 2277-2287 [PMID: 25242658 DOI: 10.1016/j.ejrad.2014.08.017]
- 10 **RISE**: Real-time International Student Education. [accessed 2016 June 27]. Available from: URL: <http://www.risemed.org>

- 11 **Farkhondeh A**, Geist JR. Evaluation of Web-Based Interactive Instruction in Intraoral and Panoramic Radiographic Anatomy. *J Mich Dent Assoc* 2015; **97**: 34-38 [PMID: 26292503]
- 12 **Scherer A**, Kröpil P, Heusch P, Buchbender C, Sewerin P, Blondin D, Lanzman RS, Miese F, Ostendorf B, Bölke E, Mödder U, Antoch G. Case-based interactive PACS learning: introduction of a new concept for radiological education of students. *Radiologe* 2011; **51**: 969-970, 973-977 [PMID: 22033604 DOI: 10.1007/s00117-011-2241-8]
- 13 eLearning - Education on Demand. [accessed 2016 June 27]. Available from: URL: <https://cslide.ctimeetingtech.com/library/esr/home>
- 14 European Training Curriculum for Radiology. [accessed 2016 June 27]. Available from: URL: [http://www.myesr.org/cms/website.php?id=en/education\\_training/european\\_training\\_curriculum\\_for\\_radiology.htm](http://www.myesr.org/cms/website.php?id=en/education_training/european_training_curriculum_for_radiology.htm)
- 15 EDiR - European Diploma in Radiology. [accessed 2016 June 23]. Available from: URL: [http://www.myesr.org/cms/website.php?id=29634/en/education\\_training/elearning/european\\_diploma\\_in\\_radiology\\_edir.htm](http://www.myesr.org/cms/website.php?id=29634/en/education_training/elearning/european_diploma_in_radiology_edir.htm)
- 16 **European Society of Radiology (ESR)**. Research education in Europe: an opinion paper by the European Society of Radiology. *Insights Imaging* 2015; **6**: 157-162 [PMID: 25763995 DOI: 10.1007/s13244-015-0397-x]
- 17 **Alderson PO**, Bresolin LB, Becker GJ, Thrall JH, Dunnick NR, Hillman BJ, Lee JK, Nagy EC. Enhancing research in academic radiology departments: recommendations of the 2003 Consensus Conference. *J Am Coll Radiol* 2004; **1**: 591-596 [PMID: 17411658 DOI: 10.1016/j.jacr.2004.03.011]
- 18 **Barker CF**. Making imaging research a part of radiology resident training. *Acad Radiol* 2013; **20**: 135-136 [PMID: 23395241 DOI: 10.1016/j.acra.2012.11.003]
- 19 **Costello JR**, Mullins ME, Votaw JR, Karolyi DR, Kalb B, Gonzales P, Fornwalt B, Meltzer CC. Establishing a new radiology residency research track. *Acad Radiol* 2013; **20**: 243-248 [PMID: 23085410 DOI: 10.1016/j.acra.2012.08.011]
- 20 **Valk PE**, Dillon WP. Radiation injury of the brain. *AJNR Am J Neuroradiol* 1991; **12**: 45-62 [PMID: 7502957]
- 21 **Sodickson A**, Baeyens PF, Andriole KP, Prevedello LM, Nawfel RD, Hanson R, Khorasani R. Recurrent CT, cumulative radiation exposure, and associated radiation-induced cancer risks from CT of adults. *Radiology* 2009; **251**: 175-184 [PMID: 19332852 DOI: 10.1148/radiol.2511081296]
- 22 **Schonfeld SJ**, Lee C, Berrington de González A. Medical exposure to radiation and thyroid cancer. *Clin Oncol (R Coll Radiol)* 2011; **23**: 244-250 [PMID: 21296564 DOI: 10.1016/j.clon.2011.01.159]
- 23 **European Society of Radiology**. ESR statement on radiation protection: globalisation, personalised medicine and safety (the GPS approach). *Insights Imaging* 2013; **4**: 737-739 [PMID: 24092563 DOI: 10.1007/s13244-013-0287-z]

**P- Reviewer:** Boffano P, Gao BL, Pinto A, Quattrocchi CC, Wan YL  
**S- Editor:** Kong JX **L- Editor:** A **E- Editor:** Wu HL



## Basic Study

# Radiation dose enhancement in skin therapy with nanoparticle addition: A Monte Carlo study on kilovoltage photon and megavoltage electron beams

Xiao J Zheng, James C L Chow

Xiao J Zheng, Department of Physics, Ryerson University, Toronto, ON M5B 2K3, Canada

James C L Chow, Radiation Medicine Program, Princess Margaret Cancer Centre, Department of Radiation Oncology, University of Toronto, Toronto, ON M5G 2M9, Canada

**Author contributions:** Zheng XJ performed the Monte Carlo experiments and data analyses which were reviewed by Chow JCL; the figures of the manuscript were prepared by Zheng XJ and Chow JCL; Chow JCL designed the study and wrote the manuscript.

**Institutional review board statement:** This study does not involve any human or animal subject.

**Informed consent statement:** This study does not involve any human subject.

**Conflict-of-interest statement:** The authors declare no conflicts of interest regarding this manuscript.

**Open-Access:** This article is an open-access article which was selected by an in-house editor and fully peer-reviewed by external reviewers. It is distributed in accordance with the Creative Commons Attribution Non Commercial (CC BY-NC 4.0) license, which permits others to distribute, remix, adapt, build upon this work non-commercially, and license their derivative works on different terms, provided the original work is properly cited and the use is non-commercial. See: <http://creativecommons.org/licenses/by-nc/4.0/>

**Manuscript source:** Invited manuscript

**Correspondence to:** James C L Chow, PhD, Radiation Medicine Program, Princess Margaret Cancer Centre, Department of Radiation Oncology, University of Toronto, 610 University Avenue, Toronto, ON M5G 2M9, Canada. [james.chow@rmp.uhn.on.ca](mailto:james.chow@rmp.uhn.on.ca)  
Telephone: +1-416-9464501  
Fax: +1-416-9466566

Received: August 11, 2016

Peer-review started: August 11, 2016

First decision: September 28, 2016

Revised: October 24, 2016

Accepted: December 7, 2016

Article in press: December 9, 2016

Published online: February 28, 2017

## Abstract

### AIM

To investigate the dose enhancement due to the incorporation of nanoparticles in skin therapy using the kilovoltage (kV) photon and megavoltage (MV) electron beams. Monte Carlo simulations were used to predict the dose enhancement when different types and concentrations of nanoparticles were added to skin target layers of varying thickness.

### METHODS

Clinical kV photon beams (105 and 220 kVp) and MV electron beams (4 and 6 MeV), produced by a Gulmay D3225 orthovoltage unit and a Varian 21 EX linear accelerator, were simulated using the EGSnrc Monte Carlo code. Doses at skin target layers with thicknesses ranging from 0.5 to 5 mm for the photon beams and 0.5 to 10 mm for the electron beams were determined. The skin target layer was added with the Au, Pt, I, Ag and Fe<sub>2</sub>O<sub>3</sub> nanoparticles with concentrations ranging from 3 to 40 mg/mL. The dose enhancement ratio (DER), defined as the dose at the target layer with nanoparticle addition divided by the dose at the layer without nanoparticle addition, was calculated for each nanoparticle type, nanoparticle concentration and target layer thickness.

### RESULTS

It was found that among all nanoparticles, Au had the

highest DER (5.2-6.3) when irradiated with kV photon beams. Dependence of the DER on the target layer thickness was not significant for the 220 kVp photon beam but it was for 105 kVp beam for Au nanoparticle concentrations higher than 18 mg/mL. For other nanoparticles, the DER was dependent on the atomic number of the nanoparticle and energy spectrum of the photon beams. All nanoparticles showed an increase of DER with nanoparticle concentration during the photon beam irradiations regardless of thickness. For electron beams, the Au nanoparticles were found to have the highest DER (1.01-1.08) when the beam energy was equal to 4 MeV, but this was drastically lower than the DER values found using photon beams. The DER was also found affected by the depth of maximum dose of the electron beam and target thickness. For other nanoparticles with lower atomic number, DERs in the range of 0.99-1.02 were found using the 4 and 6 MeV electron beams.

### CONCLUSION

In nanoparticle-enhanced skin therapy, Au nanoparticle addition can achieve the highest dose enhancement with 105 kVp photon beams. Electron beams, while popular for skin therapy, did not produce as high dose enhancements as kV photon beams. Additionally, the DER is dependent on nanoparticle type, nanoparticle concentration, skin target thickness and energies of the photon and electron beams.

**Key words:** Skin therapy; Monte Carlo simulation; Nanoparticle; Dose enhancement; Photon and electron beams

© The Author(s) 2017. Published by Baishideng Publishing Group Inc. All rights reserved.

**Core tip:** This paper investigated the dose enhancement effect due to nanoparticle addition using the kilovoltage (kV) photon and megavoltage (MV) electron beams in skin therapy. Dose enhancements of skin layers with different thicknesses were studied with various nanoparticle types, nanoparticle concentrations, radiation beam types and beam energies using Monte Carlo simulation. From the results, it is found that kV photon beams can achieve much higher dose enhancements at the skin compared to MV electron beams. Moreover, gold nanoparticles, which had the highest atomic number in our study, provided the highest dose enhancement for nanoparticle-enhanced skin therapy.

Zheng XJ, Chow JCL. Radiation dose enhancement in skin therapy with nanoparticle addition: A Monte Carlo study on kilovoltage photon and megavoltage electron beams. *World J Radiol* 2017; 9(2): 63-71 Available from: URL: <http://www.wjgnet.com/1949-8470/full/v9/i2/63.htm> DOI: <http://dx.doi.org/10.4329/wjr.v9.i2.63>

## INTRODUCTION

In cancer treatment, chemotherapy and radiotherapy are two popular methods to control the tumour cell. Chemotherapy uses anticancer drugs at molecular, cellular and tissue levels through various mechanisms such as enhancing the double-strand break due to the conformation changes in chromatin and DNA, and inhibiting the DNA repair processes leading to the conversion of sublethal DNA damage<sup>[1-5]</sup>. In radiotherapy, on the other hand, it is necessary to provide conformal dose coverage at the target (tumour) while sparing the surrounding normal tissues. Target dose escalation is therefore desired to increase the tumour control probability, but at the same time decrease normal tissue complication probabilities for organs-at-risk (OARs). Under such circumstances, nanoparticle-enhanced radiotherapy is suggested for providing dose enhancement in the target<sup>[6-8]</sup>. There are two advantages of accumulating heavy-atom nanoparticles within the tumour. First, due to the increased compositional atomic number of tumours with nanoparticles, imaging contrast is increased due to the enhancement of photoelectric absorption when using a kilovoltage (kV) photon source (e.g., computed tomography)<sup>[9,10]</sup>. Such contrast enhancement can help the radiation staff to identify and outline the target during radiation treatment planning. Second, the increase in the photoelectric cross-section due to the addition of nanoparticles increases the dose absorption of the target<sup>[11,12]</sup>. This results in dose enhancement at the target and improved treatment outcome. Preclinical results of Au nanoparticle enhanced radiotherapy have proven that the addition of 1.9 nm Au nanoparticles to mammary cancer cells of mice can lead to a significant increase in survival rate of 86% compared to 20% with radiotherapy alone and 0% with Au nanoparticle addition alone<sup>[13]</sup>. For radiotherapy of EGFR-positive cancer, a facile synthetic method of indium-111 to Au nanoparticle was developed with high payload to enhance the delivery of radioactivity to the tumour<sup>[14]</sup>. Au nanoparticle was also studied as a drug-delivery platform in transient anti-angiogenic therapies to induce tumour vascular normalization and enhance the efficacy of the cytotoxic drugs<sup>[15]</sup>. Moreover, tumour radiosensitizations for breast and prostate with Au nanoparticle addition were studied both *in vitro* and *in vivo* based on the cell-line and small-animal model<sup>[16,17]</sup>.

Since dose enhancement is due to an increase in the photoelectric cross-section by raising the compositional atomic number through heavy-atom nanoparticle addition, such enhancement decreases when using megavoltage (MV) instead of kV range photon beams where Compton interactions dominate. Unlike preclinical models using kV photon beams, human radiotherapy requires MV energies for deep-seated targets. This is due to the considerable differences in size and thickness for humans compared to small animals and therefore higher penetrative MV photon beams are required<sup>[18]</sup>.



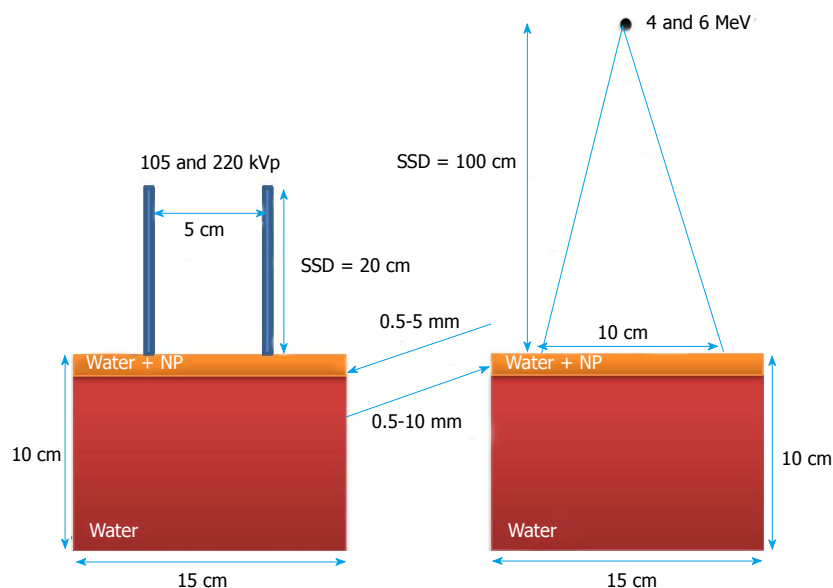


**Figure 1** Schematic diagrams (not-to-scale) showing the experimental setups of the kilovoltage photon beams (left) and megavoltage electron beams (right). The thicknesses of the skin target layer (water mixed with nanoparticles) ranged from 0.5-5 mm for the photon beams and 0.5-10 mm for the electron beams. SSD: Source-to-surface distance.

Dose enhancement using MV photon beams is lower than kV beams when treating deep-seated tumours in radiotherapy. In skin therapy, however, kV photon beams are used to treat superficial lesions as the target is located on the patient's surface. Therefore, sufficient dose enhancement at the target can be achieved using kV (e.g., 105 and 220 kVp) photon beams<sup>[19,20]</sup>. The aim of this study is to investigate the dose enhancement due to nanoparticle addition of various types, concentrations, beam energies for several skin target thicknesses. For dosimetric comparison, similar nanoparticle additions using electron beams were carried out because electron therapy is also popular in skin lesion treatment. In this study, lower electron beam energies of 4 and 6 MeV with relatively short electron paths were focused on as they were clinically used to treat superficial lesions<sup>[19]</sup>.

Monte Carlo simulations using EGSnrc<sup>[21]</sup> were used to calculate doses of the skin target using the macroscopic approach<sup>[22]</sup>. Heterogeneous phantoms were used with the clinical kV photon and MV electron beams from the orthovoltage unit and medical linear accelerator in this study, respectively. The dose enhancement ratio (DER), defined here as the ratio of the dose in the skin target with nanoparticle addition to the dose of target without nanoparticle addition, was determined with variations of the nanoparticle type, concentration and skin target thickness using the photon and electron beams.

## MATERIALS AND METHODS

### Calculation geometry

Figure 1 shows the calculation geometry used in the Monte Carlo simulations. A water phantom with dimensions of  $15 \times 15 \times 10 \text{ cm}^3$  was used in this study. The top skin target layers with thicknesses ranging from 0.5-5 mm for the photon beams and 0.5-10 mm for the electron beams. While varying the skin target thickness, the height of the phantom was

kept constant at 10 cm. For the target layer, different nanoparticles consisting of Au, Pt, I, Ag and  $\text{Fe}_2\text{O}_3$  with atomic numbers equal to 79, 78, 53, 47 and 23 were mixed with water for 5 concentrations (3, 7, 18, 30 and 40 mg/mL).

For the kV photon beam irradiations, the 105 and 220 kVp beams produced by a Gulmay D3225 orthovoltage unit were used. The photon beams were conformed by a standard circular applicator of 5 cm diameter with a source-to-surface distance (SSD) equal to 20 cm. In the electron beam irradiations, the 4 and 6 MeV electron beams produced by a Varian 21 EX linear accelerator were used with a  $10 \times 10 \text{ cm}^2$  standard square cutout in the bottom of a  $10 \times 10 \text{ cm}^2$  applicator (not shown in Figure 1). The SSD of the electron beam irradiation was set to 100 cm. It should be noted that both the photon and electron beam irradiations were based on typical clinical geometries for skin therapy.

### Monte Carlo simulation

The EGSnrc code developed by the National Research Council Canada was used in this study<sup>[21]</sup>. For the kV photon beams, the spectral shape in this code was improved by implementing the electron impact ionization model. In addition, the directional bremsstrahlung splitting approach was used to enhance the efficiency of energy transitions from the electron current to photons<sup>[23]</sup>.

Phase-space files of 105 and 220 kVp photon beams, produced by a Gulmay D3225 orthovoltage machine using a standard open circular applicator with diameter of 5 cm, were generated using the BEAMnrc code<sup>[24]</sup>. The SSD was set at 20 cm. The treatment head model in simulation included the X-ray tube, primary collimator, filter, ionization chamber and applicator with material and geometry information provided by the manufacturer. Phase-space files containing 36 million particles were generated including information on energy, orientation,

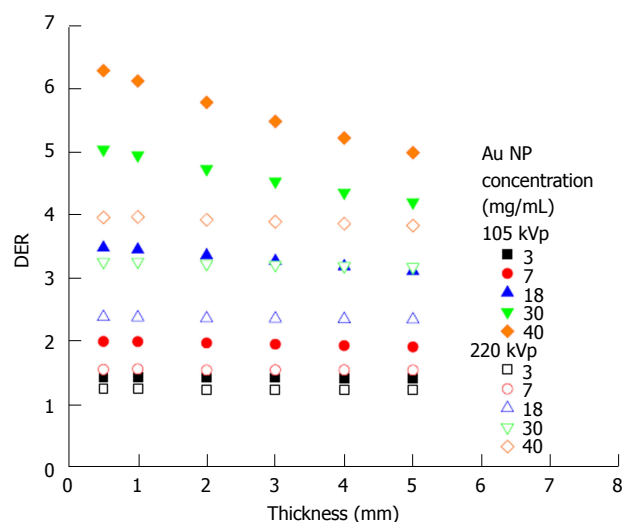


**Figure 2** Relationship between the dose enhancement ratio and skin target thickness with variation of Au nanoparticle concentration using the 105 and 220 kVp photon beams. DER: Dose enhancement ratio.

type, charge and position of particles crossing the scoring plane at the bottom of the applicator. The phase-space files were verified by comparing the percentage depth doses and beam profiles in water measured by a parallel-plate ionization chamber and water tank elsewhere<sup>[19]</sup>. For the 4 and 6 MeV electron beams produced by the Varian 21 EX linear accelerator, phase-space files were generated from BEAMnrc using a  $10 \times 10 \text{ cm}^2$  applicator with an SSD of 100 cm. Details of the geometries and materials of the treatment head were provided by the linear accelerator manufacturer, and the parameter reduced electron step transport algorithm II (PRESTA II) was used as the electron-step algorithm<sup>[25]</sup>. The phase-space files for the electron beams contained 55 million particles, and were verified elsewhere by comparing the percentage depth doses and beam profiles between the Monte Carlo and measurement results using radiographic film, ionization chamber and solid water phantom<sup>[19]</sup>.

The material data sets for different concentrations of nanoparticles were created using the EGSnrc-based PEGS4 code<sup>[21]</sup>. Data sets regarding particle interaction cross-sections for various concentrations (3, 7, 18, 30 and 40 mg/mL) of Au, Pt, I, Ag and  $\text{Fe}_2\text{O}_3$  nanoparticles mixed with water were generated. DOSXYZnrc was used to calculate the dose at the skin target layer irradiated by the photon and electron beams<sup>[26]</sup>. For the 105 and 220 kVp photon beams, 150 million histories were run for each calculation with the energy cut-off for the electron (ECUT) and photon (PCUT) transport set to 521 keV and 1 keV. The PRESTA II was used for the electron-step algorithm, and the spin effect, bound Compton scattering, Rayleigh scattering, atomic relaxation and electron impact ionization options were all used in the simulation. For the simulation using the electron beams, the ECUT, PCUT and ESTEPE were set to 521 keV, 10 keV and 25%, respectively<sup>[27]</sup>. Two hundred million histories were simulated in Monte

Carlo for the 4 and 6 MeV electron beams. Under these approaches, the relative dose error (statistical uncertainty as a fraction of dose in the voxel) was found to be around 1% according to the Monte Carlo output files<sup>[21]</sup>.

### DER

The doses determined from the skin target layer with different thicknesses, nanoparticle concentrations, and types using Monte Carlo simulations were used to calculate the DER, defined in this study as:

$$\text{DER} = \frac{\text{Dose with nanoparticle addition in the target layer}}{\text{Dose without nanoparticle addition in the target layer}} \quad (1)$$

It can be seen from Eq. (1) that due to the general dose enhancement effect from nanoparticle addition, the DER is typically close to or larger than one.

## RESULTS

The dependency of the DER on skin target thickness using Au nanoparticles with increasing concentration (3–40 mg/mL) and kV photon beams is shown in Figure 2. The target thickness ranged from 0.5 to 5 mm. For other nanoparticle materials, dependence of the DER on target thickness is shown in Figure 3 for nanoparticle concentrations equal to 7, 18 and 40 mg/mL using the 105 and 220 kVp photon beams. Figure 4 reveals the relationship between the DER and Au nanoparticle concentration for different target thicknesses. In addition, Figure 5 shows relationships between the DER and nanoparticle concentration for different nanoparticle types with target thicknesses equal to 0.5, 3 and 5 mm, respectively. For the 4 and 6 MeV electron beam irradiations, Figure 6 shows the dependence of the DER on the target thickness for the Au nanoparticles with different concentrations. Variations of the DER for the Au nanoparticles with different target thicknesses are shown in Figure 7 using 4 and 6 MeV electron beams, respectively. The relationship between the DER and nanoparticle concentration for different nanoparticle types are shown in Figure 8 with the target thickness equal to 2 mm.

## DISCUSSION

### Kilovoltage photon beams

#### Dependence of the DER on skin target thickness:

It can be seen from Figure 2 that the dependence of the DER on the skin target thickness was not significant, when the Au nanoparticle was added with concentrations ranging from 3 to 40 mg/mL using the 220 kVp photon beams. For the 105 kVp photon beams, however, the DER was found increasing with a decrease of target thickness when the nanoparticle concentration was higher than 18 mg/mL. This shows that the dose enhancement effect on the target thickness was more

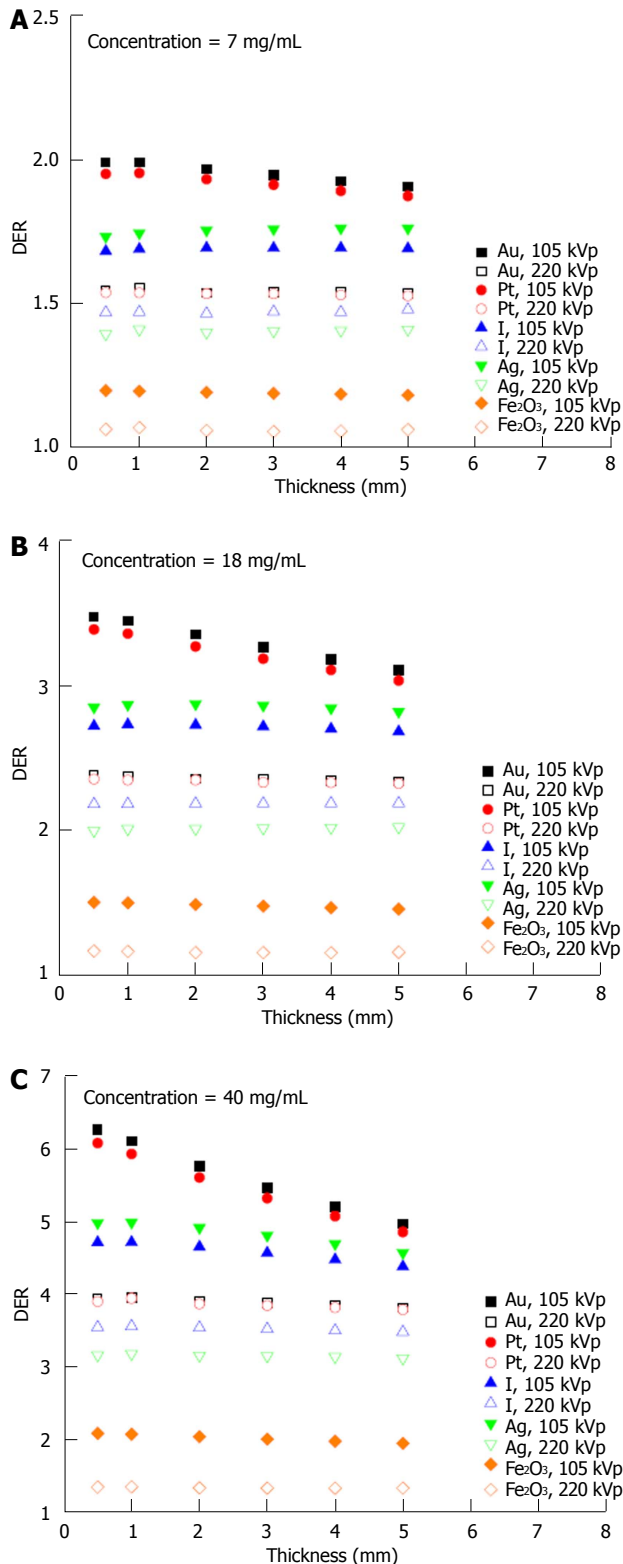


**Figure 3** Relationship between the dose enhancement ratio and skin target thickness with nanoparticle concentrations of (A) 7, (B) 18 and (C) 40 mg/mL using the Au, Pt, I, Ag and Fe<sub>2</sub>O<sub>3</sub> nanoparticles for the 105 and 220 kVp photon beams. DER: Dose enhancement ratio.

sensitive to lower energy photon beams and higher nanoparticle concentration.

For the dependence of the DER on skin target thickness for other nanoparticles, Figure 3 shows the

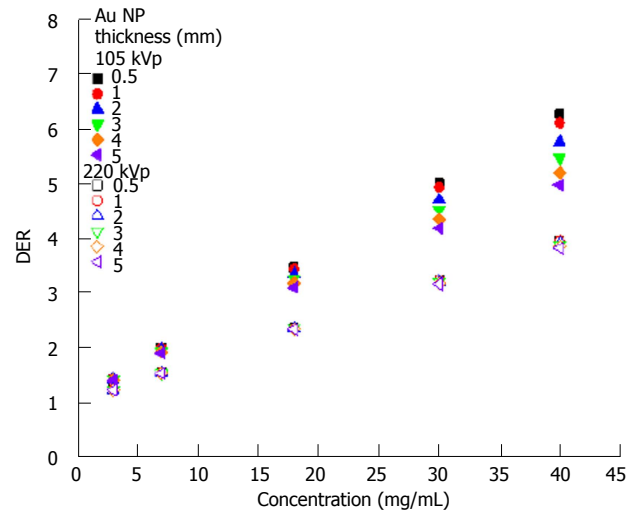


**Figure 4** Relationship between the dose enhancement ratio and Au nanoparticle concentration with variation of the skin target thickness using the 105 and 220 kVp photon beams. DER: Dose enhancement ratio.

relationship between the two for nanoparticle concentrations equal to 7, 18 and 40 mg/mL. In Figure 3, it is seen that the dose enhancement was generally affected by the atomic number of the nanoparticle and the quality of the kV photon beams. The DER for the Ag nanoparticles was slightly higher than for I for the 105 kVp photon beams. However, the atomic number of Ag (47) is smaller than I (53). This may be due to the energy spectrum of the polyenergetic 105 kVp photon beam produced by the orthovoltage machine<sup>[20]</sup>. In Figure 3, the Au nanoparticles are seen to have the highest DERs of 2, 3.5 and 6.3 when the nanoparticle concentration was 7, 18 and 40 mg/mL, respectively. A higher DER was found for higher nanoparticle concentrations and thinner target thicknesses due to the higher depth-dose gradient from the 105 kVp photon beams compared to 220 kVp<sup>[28]</sup>. Moreover, dependence of the DER on the target thickness was not significant for the Pt, I, Ag and Fe<sub>2</sub>O<sub>3</sub> nanoparticles using 220 kVp photon beams.

**Dependence of the DER on nanoparticle concentration:** In Figure 4, it can be seen that the DER increased with an increase of Au nanoparticle concentration from 3 to 40 mg/mL using the 105 and 220 kVp photon beams. For the 220 kVp photon beams, the increase of the DER in the nanoparticle concentration did not vary with the target thickness significantly. For the 105 kVp photon beams, however, the rate of change of the DER with nanoparticle concentration was found to increase with a decrease of target thickness. When the Au nanoparticle concentration increased from 3 to 40 mg/mL, the DER was found to increase from 1.4 to 6.3 when using 105 kVp photon beams, respectively.

The degree of DER variation on the nanoparticle concentration was found to be more significant when the atomic number of the nanoparticles increased, with the Au nanoparticles producing the highest DER

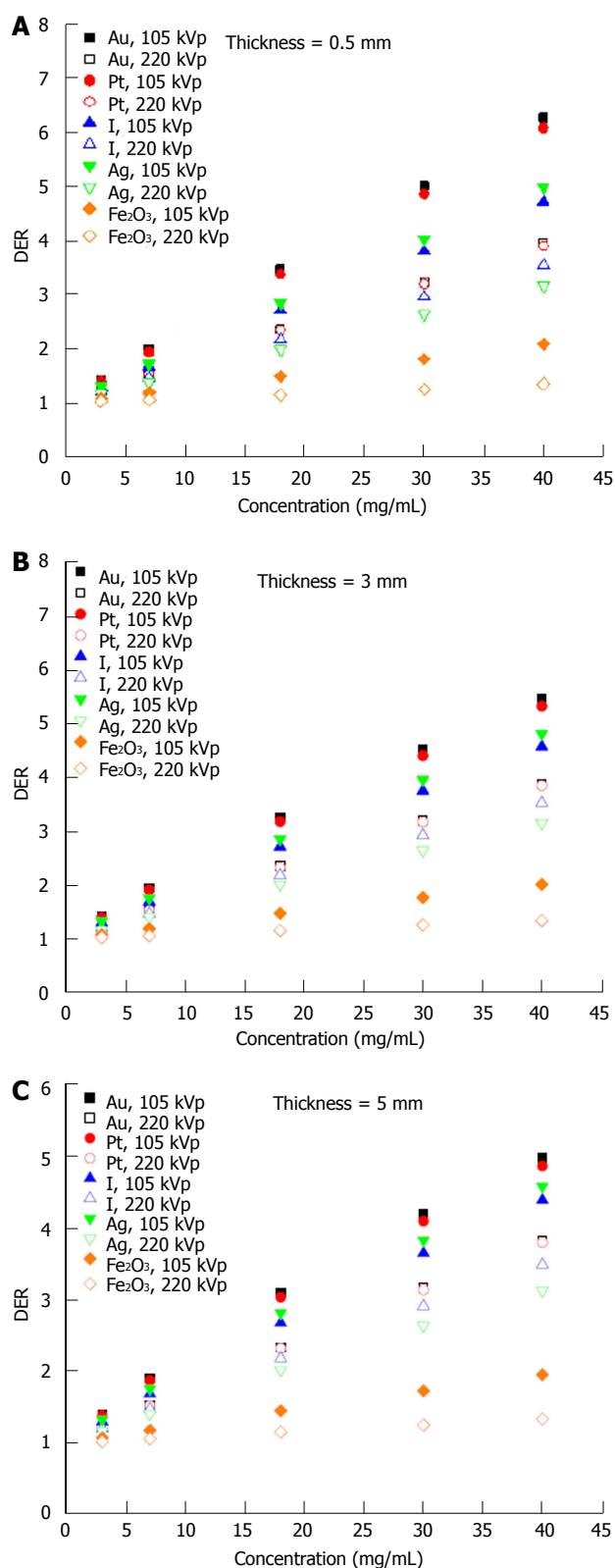


**Figure 5** Relationship between the dose enhancement ratio and nanoparticle concentration with skin target thickness equal to (A) 0.5, (B) 3 and (C) 5 mm using the Au, Pt, I, Ag and Fe<sub>2</sub>O<sub>3</sub> nanoparticles for the 105 and 220 kVp photon beams. DER: Dose enhancement ratio.

when using a 105 kVp photon beam. When the target thickness decreased from 5 mm to 0.5 mm (Figure 5), the DER increased for 105 kVp photon beams. In

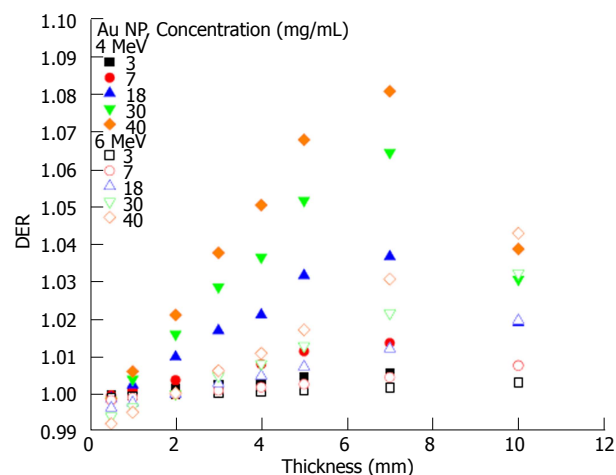


**Figure 6** Relationship between the dose enhancement ratio and skin target thickness with different Au nanoparticle concentrations using the 4 and 6 MeV electron beams. DER: Dose enhancement ratio.

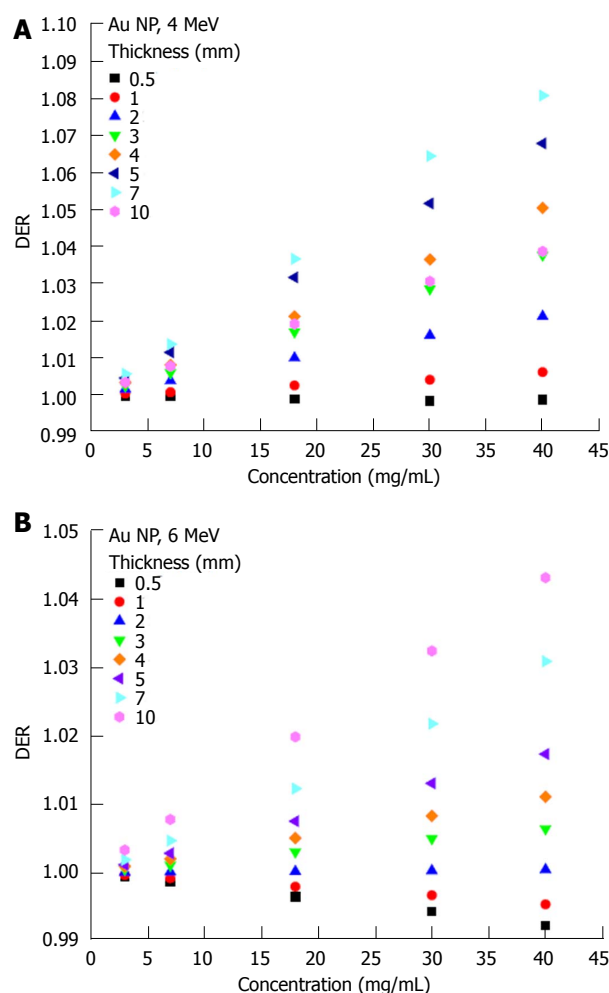


**Figure 7** Relationship between the dose enhancement ratio and Au nanoparticle concentration with variation of skin target thickness using the (A) 4 and (B) 6 MeV electron beams. DER: Dose enhancement ratio.

Figure 5, though it can be seen that the DER for the Fe<sub>2</sub>O<sub>3</sub> nanoparticles was only in the range of 1 to 2 in the concentration range of 3–40 mg/mL, DER of higher



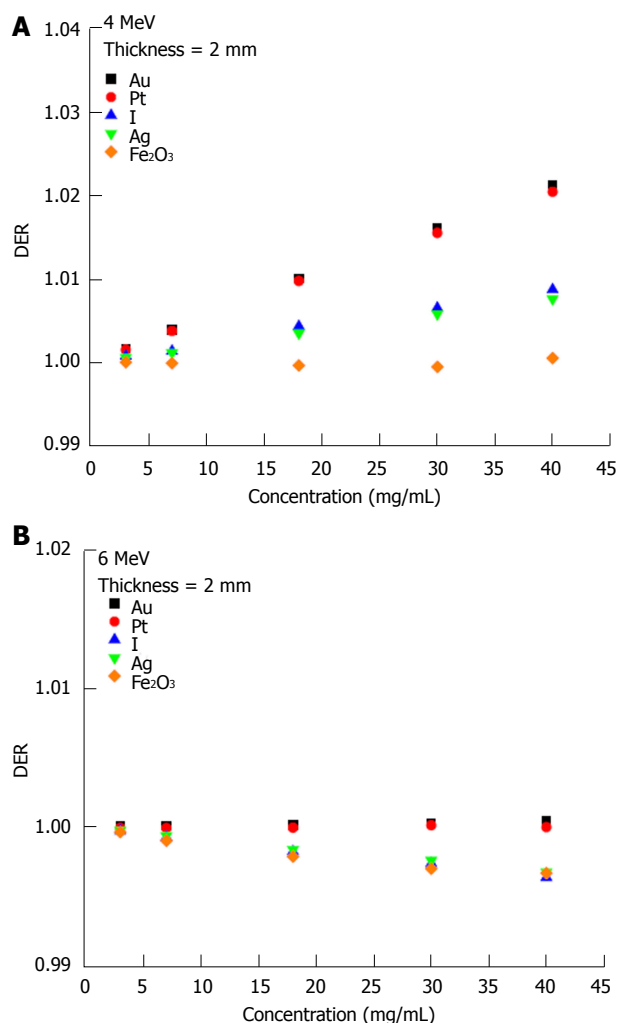


**Figure 8** Relationship between the dose enhancement ratio and nanoparticle concentrations of the Au, Pt, I, Ag and Fe<sub>2</sub>O<sub>3</sub> using the (A) 4 and (B) 6 MeV electron beams. The thickness of the target layer is equal to 2 mm. DER: Dose enhancement ratio.

than 5 can be achieved for the Au and Pt nanoparticles using the 105 kVp photon beams. It is found that dose enhancement was higher when using the lower energy 105 kVp photon beams, whenever the target thickness or nanoparticle concentration varied.

### Megavoltage electron beams

#### Dependence of the DER on skin target thickness:

For the Au nanoparticles, it can be seen in Figure 6 that variation of the DER on the skin target thickness became significant when the electron beam energy decreased from 6 to 4 MeV. However, when the nanoparticle concentration was equal to 40 mg/mL, the DER decreased when varying the target thickness from 7 to 10 mm. Such an effect can also be observed in Figure 7A. Typically, the DER was found to increase as the target thickness increased from 0.5 to 10 mm. Unlike the kV range photon beams, we can see in Figure 6 that the DER only varied between 0.99 and 1.1 for the Au nanoparticle, having the highest atomic number in this study. This is due to the fact that photoelectric effect,

which is dominant in the kV photon beam range, does not contribute to the energy absorption of the 4 and 6 MeV electron beams<sup>[11]</sup>.

#### Dependence of the DER on nanoparticle concentration:

Dependence of the DER on nanoparticle concentration was found to vary with the target thickness. For the 4 MeV electron beams, variation of the DER with Au nanoparticle concentration was not significant when the target thickness was small. For a nanoparticle concentration of 40 mg/mL in Figure 7A, it is seen that the DER increased when the target thickness increased from 0.5 mm to 7 mm. A decrease of DER was seen at a target thickness equal to 10 mm (also Figure 6). This is because the depth of maximum dose of the 4 MeV beam (7 mm) was smaller than the target thickness of 10 mm. For the 6 MeV electron beam with a deeper depth of maximum dose (15 mm), the highest DER can be found at the 10 mm target layer as shown in Figure 7B. Moreover, it is interesting to see that the DER was smaller than one when the target thickness was in the range of 0.5–2 mm for the 6 MeV electron beams. This shows that electron beams with higher energy (6 MeV) would not show dose enhancement (*i.e.*, DER ≤ 1) with Au nanoparticle addition when the target thickness was lower than 2 mm.

When the skin target thickness was equal to 2 mm, it can be seen from Figure 8 that only Au, Pt, I and Ag nanoparticles had slight dose enhancement using the 4 MeV electron beams (Figure 8A). The DER was found to be smaller than one when the 6 MeV electron beams were used (Figure 8B) with low atomic number nanoparticles (*e.g.*, Fe<sub>2</sub>O<sub>3</sub>) having the smallest DER in the range of nanoparticle concentration between 3 and 40 mg/mL.

In conclusion, different thicknesses of skin target layers with nanoparticle additions were irradiated by clinical kV photon and MV electron beams. The DER was calculated with variations of the target thickness, nanoparticle type, nanoparticle concentration and beam energy. It is found that with kV photon beams there was a higher DER than MV electron beams, with the Au nanoparticles having the highest DER compared to the other simulated materials (Pt, I, Ag and Fe<sub>2</sub>O<sub>3</sub>). For the kV photon beams, the 105 kVp beams showed higher dose enhancement than using a 220 kVp beam. It is therefore concluded that the kV photon beams and Au nanoparticles would be the most appropriate for use in nanoparticle-enhanced skin therapy. Moreover, higher nanoparticle concentration was shown to benefit dose enhancement.

### ACKNOWLEDGMENTS

The authors would like to thank Amada Tulk from Gulmay Medical to allow us to share the Monte Carlo input data from Dr T Knoos in the Lund University Hospital for the verification of the kV photon beams.

The authors would also like to thank Varti Vartanian and Mitch Spiegel of Varian Medical Systems for providing detailed information about the 21 EX linear accelerator, and Dr F Verhaegen of Maastricht Clinic for sharing his BEAMnrc input files for verification of the electron beam simulations. The authors would like to thank Dr D Markel of the Princess Margaret Cancer Centre/ University of Toronto for editing this manuscript.

## COMMENTS

### Background

This work studied the dose enhancement due to nanoparticle addition in skin therapy using the clinical kilovoltage photon and megavoltage electron beams.

### Research frontiers

The Monte Carlo results can guide the radiation staff which combination of nanoparticle type, nanoparticle concentration, beam type and beam energy should be used for different skin lesion thickness.

### Innovations and breakthroughs

This Monte Carlo study combined all practical nanoparticle types, nanoparticle concentrations, clinical radiation beams and beam energies in treating skin lesions.

### Applications

Nanoparticle-enhanced skin radiotherapy.

### Peer-review

This is a well-written paper.

## REFERENCES

- Ali I, Lone MN, Al-Othman ZA, Al-Warthan A, Sanagi MM. Heterocyclic Scaffolds: Centrality in Anticancer Drug Development. *Curr Drug Targets* 2015; **16**: 711-734 [PMID: 25751009 DOI: 10.2174/1389450116666150309115922]
- Ali I, Wani WA, Haque A, Saleem K. Glutamic acid and its derivatives: candidates for rational design of anticancer drugs. *Future Med Chem* 2013; **5**: 961-978 [PMID: 23682571 DOI: 10.4155/fmc.13.62]
- Ali I, Haque A, Saleem K, Hsieh MF. Curcumin-I Knoevenagel's condensates and their Schiff's bases as anticancer agents: synthesis, pharmacological and simulation studies. *Bioorg Med Chem* 2013; **21**: 3808-3820 [PMID: 23643901 DOI: 10.1016/j.bmc.2013.04.018]
- Ali I, Wani WA, Saleem K, Haque A. Platinum compounds: a hope for future cancer chemotherapy. *Anticancer Agents Med Chem* 2013; **13**: 296-306 [PMID: 22583420 DOI: 10.2174/1871520611313020016]
- Ali I. Nano anti-cancer drugs: pros and cons and future perspectives. *Curr Cancer Drug Targets* 2011; **11**: 131-134 [PMID: 21062238 DOI: 10.2174/156800911794328457]
- Her S, Jaffray DA, Allen C. Gold nanoparticles for applications in cancer radiotherapy: Mechanisms and recent advancements. *Adv Drug Deliv Rev* 2017; **109**: 84-101 [PMID: 26712711 DOI: 10.1016/j.addr.2015.12.012]
- Coulter JA, Butterworth KT, Jain S. Prostate cancer radiotherapy: potential applications of metal nanoparticles for imaging and therapy. *Br J Radiol* 2015; **88**: 20150256 [PMID: 26051659 DOI: 10.1259/bjr.20150256]
- Chow JCL. Characteristic of secondary electrons from irradiated gold nanoparticle in radiotherapy, 2015. Handbook of nanoparticle, Switzerland: Springer, 2015 [DOI: 10.1007/978-3-319-13188-7\_10-2]
- Cormode DP, Naha PC, Fayad ZA. Nanoparticle contrast agents for computed tomography: a focus on micelles. *Contrast Media Mol Imaging* 2014; **9**: 37-52 [PMID: 24470293 DOI: 10.1002/cmmi.1551]
- Chow JCL. Photon and electron interactions with gold nanoparticles: a Monte Carlo study on gold nanoparticle-enhanced radiotherapy. 2016 Nanobiomaterials in medical imaging: applications of nanobiomaterials, Amsterdam: Elsevier, 2016; in press [DOI: 10.1016/b978-0-323-41736-5.00002-9]
- Chow JC, Leung MK, Jaffray DA. Monte Carlo simulation on a gold nanoparticle irradiated by electron beams. *Phys Med Biol* 2012; **57**: 3323-3331 [PMID: 22572475 DOI: 10.1088/0031-9155/57/11/3323]
- Leung MK, Chow JC, Chithrani BD, Lee MJ, Oms B, Jaffray DA. Irradiation of gold nanoparticles by x-rays: Monte Carlo simulation of dose enhancements and the spatial properties of the secondary electrons production. *Med Phys* 2011; **38**: 624-631 [PMID: 21452700 DOI: 10.1118/1.3539623]
- Hainfeld JF, Slatkin DN, Smilowitz HM. The use of gold nanoparticles to enhance radiotherapy in mice. *Phys Med Biol* 2004; **49**: N309-N315 [PMID: 15509078]
- Song L, Falzone N, Vallis KA. EGF-coated gold nanoparticles provide an efficient nano-scale delivery system for the molecular radiotherapy of EGFR-positive cancer. *Int J Radiat Biol* 2016; **92**: 716-723 [PMID: 26999580 DOI: 10.3109/09553002.2016.1145360]
- Li W, Zhao X, Du B, Li X, Liu S, Yang XY, Ding H, Yang W, Pan F, Wu X, Qin L, Pan Y. Gold Nanoparticle-Mediated Targeted Delivery of Recombinant Human Endostatin Normalizes Tumour Vasculature and Improves Cancer Therapy. *Sci Rep* 2016; **6**: 30619 [PMID: 27470938 DOI: 10.1038/srep30619]
- Chattopadhyay N, Cai Z, Kwon YL, Lechtman E, Pignol JP, Reilly RM. Molecularly targeted gold nanoparticles enhance the radiation response of breast cancer cells and tumor xenografts to X-radiation. *Breast Cancer Res Treat* 2013; **137**: 81-91 [PMID: 23160926 DOI: 10.1007/s10549-012-2338-4]
- Butterworth KT, Nicol JR, Ghita M, Rosa S, Chaudhary P, McGarry CK, McCarthy HO, Jimenez-Sanchez G, Bazzi R, Roux S, Tillement O, Coulter JA, Prise KM. Preclinical evaluation of gold-DTTPA nanoparticles as theranostic agents in prostate cancer radiotherapy. *Nanomedicine (Lond)* 2016; **11**: 2035-2047 [PMID: 27463088 DOI: 10.2217/nnm-2016-0062]
- Chow JC, Leung MK, Lindsay PE, Jaffray DA. Dosimetric variation due to the photon beam energy in the small-animal irradiation: a Monte Carlo study. *Med Phys* 2010; **37**: 5322-5329 [PMID: 21089767 DOI: 10.1118/1.3488979]
- Chow JC, Jiang R. Bone and mucosal dosimetry in skin radiation therapy: a Monte Carlo study using kilovoltage photon and megavoltage electron beams. *Phys Med Biol* 2012; **57**: 3885-3899 [PMID: 22642985 DOI: 10.1088/0031-9155/57/12/3885]
- Chow JC, Owringi AM. Surface dose reduction from bone interface in kilovoltage X-ray radiation therapy: a Monte Carlo study of photon spectra. *J Appl Clin Med Phys* 2012; **13**: 3911 [PMID: 22955657 DOI: 10.1120/jacmp.v13i5.3911]
- Kawrakow I, Rogers DWO. The EGSnrc code system: Monte Carlo simulation of electron and photon transport, technique report PIRS-701. National Research Council of Canada: Ottawa, Canada
- Cho SH. Estimation of tumour dose enhancement due to gold nanoparticles during typical radiation treatments: a preliminary Monte Carlo study. *Phys Med Biol* 2005; **50**: N163-N173 [PMID: 16030374 DOI: 10.1088/0031-9155/50/15/N01]
- Knoos T, Rosenschold P, Wieslander E. Modelling of an orthovoltage x-ray therapy unit with the EGSnrc Monte Carlo package. *J Phys Conf Ser* 2007; **74**: 012009 [DOI: 10.1088/1742-6596/74/1/012009]
- Rogers DWO, Walters B, Kawrakow I. BEAMnrc user manual. NRC Report PIRS-0509: Ottawa, Canada: NRCC, 2006
- Bielajew AF, Rogers DWO. PRESTA: The parameter reduced electron-step transport algorithm for electron Monte Carlo transport. *Nucl Instrum Methods B* 1986; **18**: 165-171, 174-181 [DOI: 10.1016/S0168-583X(86)80027-1]
- Ma CM, Reckwerdt P, Holmes M, Rogers DWO, Geiser B. DOSXYZ user manual. NRC Report PIRS 509b, Ottawa, Canada: NRCC, 1995

- 27 **Chow JC**, Owraangi AM. Solid water as phantom material for dosimetry of electron backscatter using low-energy electron beams: a Monte Carlo evaluation. *Med Phys* 2009; **36**: 1587-1594 [PMID: 19544774 DOI: 10.1118/1.3110107]
- 28 **Chow JC**, Grigorov GN. Effect of the bone heterogeneity on the dose prescription in orthovoltage radiotherapy: A Monte Carlo study. *Rep Pract Oncol Radiother* 2011; **17**: 38-43 [PMID: 24376995 DOI: 10.1016/j.rpor.2011.09.001]

**P-Reviewer:** Cerwenka HR, Loomba RS, Moskowitz SI  
**S-Editor:** Qiu S **L-Editor:** A **E-Editor:** Wu HL



## Retrospective Study

# Magnetic resonance imaging in the assessment of brain involvement in alcoholic and nonalcoholic Wernicke's encephalopathy

Gianvincenzo Sparacia, Andrea Anastasi, Claudia Speciale, Francesco Agnello, Aurelia Banco

Gianvincenzo Sparacia, Andrea Anastasi, Claudia Speciale, Francesco Agnello, Aurelia Banco, Department of Radiology, University of Palermo, 90127 Palermo, Italy

**Author contributions:** Sparacia G contributed to guarantor of integrity of entire study, study design, text editing, literature research; Anastasi A, Speciale C and Agnello F contributed to imaging data collecting, drafting the article, literature research; Banco A contributed to imaging data collecting.

**Institutional review board statement:** This was a retrospective study approved by the Institutional Review Board of the University of Palermo, Department of Radiology, Palermo, Italy.

**Informed consent statement:** All patients had given written consent for this retrospective study.

**Conflict-of-interest statement:** All authors have no conflict-of-interest.

**Data sharing statement:** Participants gave informed consent for data sharing and the presented data are anonymized to avoid the risk of identification. No additional data are available.

**Open-Access:** This article is an open-access article which was selected by an in-house editor and fully peer-reviewed by external reviewers. It is distributed in accordance with the Creative Commons Attribution Non Commercial (CC BY-NC 4.0) license, which permits others to distribute, remix, adapt, build upon this work non-commercially, and license their derivative works on different terms, provided the original work is properly cited and the use is non-commercial. See: <http://creativecommons.org/licenses/by-nc/4.0/>

**Manuscript source:** Unsolicited manuscript

**Correspondence to:** Gianvincenzo Sparacia, MD, Department of Radiology, University of Palermo, Via del Vespro 127, 90127 Palermo, Italy. [sparacia@yahoo.com](mailto:sparacia@yahoo.com)  
Telephone: +39-091-6552385  
Fax: +39-091-6552302

Received: August 24, 2016  
Peer-review started: August 26, 2016  
First decision: October 8, 2016  
Revised: December 6, 2016  
Accepted: December 27, 2016  
Article in press: December 28, 2016  
Published online: February 28, 2017

## Abstract

### AIM

To present the typical and atypical magnetic resonance (MR) imaging findings of alcoholic and non-alcoholic Wernicke's encephalopathy.

### METHODS

This study included 7 patients with Wernicke's encephalopathy (2 men, 5 women; mean age, 52.3 years) that underwent brain MR examination between January 2012 and March 2016 in a single institution. Three patients were alcoholics and 4 patients were non-alcoholics. MR protocol included a T2-weighted sequence, a fluid attenuation inversion recovery (FLAIR) sequence, a diffusion-weighted sequence ( $b = 0$  and  $1000 \text{ s/mm}^2$ ), and a contrast-enhanced MR sequence. All MR images were retrospectively reviewed at baseline and follow-up by two radiologists.

### RESULTS

All patients with Wernicke's encephalopathy had bilateral areas showing high signal intensity on both T2-weighted and FLAIR MR images in the typical sites (*i.e.*, the periaqueductal region and the tectal plate). Signal intensity abnormalities in the atypical sites (*i.e.*, the cerebellum and the cerebellar vermis) were seen in 4 patients, all of which had no history of alcohol abuse. Six patients had areas with restricted diffusion



in the typical and atypical sites. Four patients had areas showing contrast-enhancement in the typical and atypical sites. Follow-up MR imaging within 6 mo after therapy (intravenous administration of thiamine) was performed in 4 patients, and demonstrated a complete resolution of all the signal intensities abnormalities previously seen in all patients.

### CONCLUSION

MR imaging is valuable in the diagnosis of Wernicke's encephalopathy particularly in patients presenting with atypical clinical symptoms, or with no history of alcohol abuse.

**Key words:** Brain; Magnetic resonance imaging; Neurodegenerative disorder; Wernicke's encephalopathy

© The Author(s) 2017. Published by Baishideng Publishing Group Inc. All rights reserved.

**Core tip:** The purpose of this study was to describe the typical and atypical magnetic resonance (MR) imaging findings of alcoholic and nonalcoholic Wernicke's encephalopathy. Bilateral increased T2-weighted and fluid attenuation inversion recovery MR signal intensity in the typical areas were seen in all patients. Signal-intensity alterations in atypical sites were seen only in nonalcoholic patients. This study demonstrated that MR imaging was useful in supporting the diagnosis of Wernicke's encephalopathy.

Sparacia G, Anastasi A, Speciale C, Agnello F, Banco A. Magnetic resonance imaging in the assessment of brain involvement in alcoholic and nonalcoholic Wernicke's encephalopathy. *World J Radiol* 2017; 9(2): 72-78 Available from: URL: <http://www.wjgnet.com/1949-8470/full/v9/i2/72.htm> DOI: <http://dx.doi.org/10.4329/wjor.v9.i2.72>

## INTRODUCTION

Wernicke's encephalopathy (WE) is a neurologic disease caused by thiamine (vitamin B1) deficiency<sup>[1]</sup>. Thiamine is involved in sustainment of the osmotic gradients of cell membranes and in the maintenance of membrane integrity. A thiamine deficiency could lead intra and extra cellular edema, as due to an inability of cell membranes to maintain osmotic gradient.

Thiamine deficiency is a consequence of inadequate dietary intake and of impaired absorption of the vitamin. Alcohol abuse is the most common cause of WE, other causes could be gastrointestinal surgery, hyperemesis gravidarum, anorexia nervosa and protracted parenteral therapy. Usually nonalcoholic WE is more difficult to diagnose. In previous study only 20% or less of patients with nonalcoholic WE were diagnosed premortem<sup>[1]</sup>.

However, in industrialized countries, 90% of the cases of thiamine deficiency are associated with alcohol abuse<sup>[2]</sup>. Alcohol chronic abuse can cause a thiamine

deficiency directly and indirectly with inadequate dietary intake, impaired intestinal absorption and poor intracellular use of thiamine.

The typical clinical presentation of WE is characterized by a triad of symptoms: Ocular manifestations (like nystagmus, bilateral lateral rectus palsies, ophthalmoplegia and conjugate gaze palsies), ataxia and global confusion. In the clinical practice, this typical triad occurs in only 13%-18% of all patients with WE<sup>[3-5]</sup>.

The prognosis of WE patients depends on prompt and early intravenous administration of thiamine supplementation<sup>[3]</sup>. Sometimes WE become irreversible because the diagnosis is delayed or is misdiagnosed based on ambiguous symptoms such as dizziness, weakness, anorexia, and memory disturbance<sup>[4]</sup>. Magnetic resonance (MR) imaging may be valuable for the diagnosis especially when the clinical diagnosis is difficult.

In the periventricular regions, there is a high rate of thiamine-related glucose and oxidative metabolism, which has been considered the cause of blood-brain barrier deficiency of these regions in WE<sup>[6]</sup>.

The typical MR imaging findings in acute WE are represented by a symmetrical increased T2-weighted and fluid-attenuated inversion recovery (FLAIR) signal intensity of periaqueductal area, medial thalami, mammillary bodies, tectal plate and periventricular region of third and fourth ventricles<sup>[5]</sup>. In these areas, the maintenance of cellular osmotic gradients is considered to be strictly related to thiamine levels.

The atypical MR imaging findings are represented by abnormal signal-intensity involving the cerebellum, the cerebellar vermis, the cranial nerve nuclei, the red nuclei, the dentate nuclei, the caudate nuclei, the corpus callosum, and the cerebral cortex<sup>[5,7-21]</sup>.

In this article the typical and atypical MRI findings of alcoholic and nonalcoholic Wernicke's encephalopathy are presented and the value of MR imaging in the diagnosis and follow-up of the disorder is discussed.

## MATERIALS AND METHODS

### Patient population

The institutional review board of our institution approved this retrospective study and written informed consent was obtained from all patients. All patients were referenced with the suspect of WE. There were a total of 7 patients (2 men, 5 women; age 28-75 years; mean age, 52.3 years) that underwent MR examination between January 2012 and March 2016 in a single institution. Four out of 7 patients underwent to MR imaging follow-up within 2 mo after intravenous administration of thiamine. Demographic and epidemiologic data are summarized in Table 1.

Three patients had a history of chronic alcohol abuse: (1) patient #1 (male, 50 years) was hospitalized for fatigue, malnutrition, and stupor; clinical examination showed a bilateral paralysis of the abductens, lateral nystagmus in both eyes, mental confusion and

**Table 1 Patient population affected by Wernicke's encephalopathy**

Patient	Age (yr)	Gender	Predisposing causes
1	50	M	Alcoholic
2	55	F	Alcoholic
3	67	F	Alcoholic
4	45	F	Parental nutrition
5	75	F	Leukemia in chemotherapy treatment
6	28	F	Pregnancy
7	53	M	Stomach cancer

M: Male; F: Female.

disorientation; (2) patient #2 (female, 55 years) was hospitalized for loss of consciousness, nystagmus, bilateral lateral rectus palsies and conjugate gaze palsies; and (3) patient #3 (female, 67 years) was admitted with ataxia and global confusion.

The remaining 4 patients hadn't history of alcohol abuse: (1) patient #4 (female, of 45 years) was in parental nutrition from some weeks for acute pancreatitis, she showed sudden onset of nystagmus, disorientation, and ataxia; (2) patient #5 (female, 75 years), affected by leukemia, was treated with chemotherapy and parenteral nutrition, presented with vomiting, nausea, hallucinations, behavioral disturbances; (3) patient #6 (female, 28 years), at 32<sup>nd</sup> weeks of pregnancy, had hyperemesis gravidarum with neurological disorders; and (4) patient #7 (male, 53 years) had a stomach cancer with pyloric stenosis demonstrated at gastroscopy and was hospitalized for walking disorders, nausea, and vomiting.

### MR imaging examination

All MR examinations were performed on a 1.5T MR scanner (Signa Excite, GE Medical Systems, Milwaukee, United States). MR imaging protocol included axial and sagittal fast spin-echo (FSE) T2W [5100/110 (TR/TE)] images, axial FLAIR [8000/140/2400 (TR/TE/TI)] images, along with axial, sagittal, and coronal non-enhanced and contrast-enhanced (0.1 mmol/Kg gadobutrol - Gadovist, Bayer, Germany) FSE T1W [650/15 (TR/TE)] images with a field of view (FOV) of 22 cm, matrix 512 × 512, slice thickness 5 mm, intersection gap 1 mm, number of excitations 2. Diffusion-weighted imaging (DWI) with echo-planar (TR 6500/TE 125) technique was obtained in all patients.

## RESULTS

Typical and atypical MRI findings in WE patients are summarized in Table 2.

In all patients, high signal intensity on T2W and FLAIR sequences was demonstrated in the periaqueductal area and in the tectal plate in association with signal abnormalities around the mammillary bodies in 1 alcoholic WE (Figure 1) patient and in 2 nonalcoholics WE patients. Concomitant involvement of the medial

**Table 2 Typical and atypical sites for magnetic resonance signal abnormalities in alcoholic and nonalcoholic Wernicke's encephalopathy patients**

Patient	Typical site					Atypical site
	Periaqueductal	Thalami	Tectal plate	Floor of the fourth ventricle	Mammillary bodies	
1	X <sup>1</sup>	X	X	X		
2	X <sup>1</sup> , r	X	X		X <sup>1</sup> , r	
3	X <sup>1</sup> , r	X	X	X	r	
4	X <sup>1</sup>	X	X		X	X, r
5	X	X	X			X, r
6	X	X	X	X	X	X, r
7	X		X			X, r

<sup>1</sup>Contrast-enhancement on T1W sequences. X: High signal intensity on T2W and FLAIR MR sequences; r: Restricted diffusion; FLAIR: Fluid-attenuated inversion recovery.

thalami was seen in 2 alcoholics WE patients and in 3 nonalcoholics WE patients.

In the 4 nonalcoholics WE patients, in adjunction to the signal abnormalities in the periaqueductal area and in the tectal plate, high signal intensity on T2W and FLAIR images was seen in the cerebellar vermis and in the cerebellar hemispheres with restricted diffusion in these areas (Figure 2).

Restricted diffusion was demonstrated in the periaqueductal grey matter and around the mammillary bodies in 2 alcoholics WE patients in the acute phase of the disease (Figure 3).

Three alcoholics and 1 nonalcoholic WE patients presented contrast-enhancement of the periaqueductal grey matter. One of the 3 alcoholic WE patients presented a concomitant contrast-enhancement of the mammillary bodies in the acute phase of the disease (Figure 4).

MR imaging follow-up, performed within 6 mo after intravenous administration of thiamine in 4 (2 alcoholic and 2 nonalcoholics WE) patients, demonstrated disappearance of the signal abnormalities seen on T2-weighted, FLAIR, and diffusion-weighted images (Figure 5) previously observed concomitant with clinical recovery.

## DISCUSSION

Our results confirm that MR imaging can assist the diagnosis of WE, particularly in patients presenting with atypical clinical symptoms, or with no history of alcohol abuse, and in the acute phase of the disease by using DWI sequences and contrast-enhanced MR imaging.

The pathology of the alterations detected in Wernicke's encephalopathy was not completely understood. Thiamine deficiency could lead an inability in sustainment of osmotic gradients of cell membranes and in the maintenance of membrane integrity with following intra and extra cellular edema.

In the periventricular regions, there is a high rate of thiamine-related glucose and oxidative metabolism

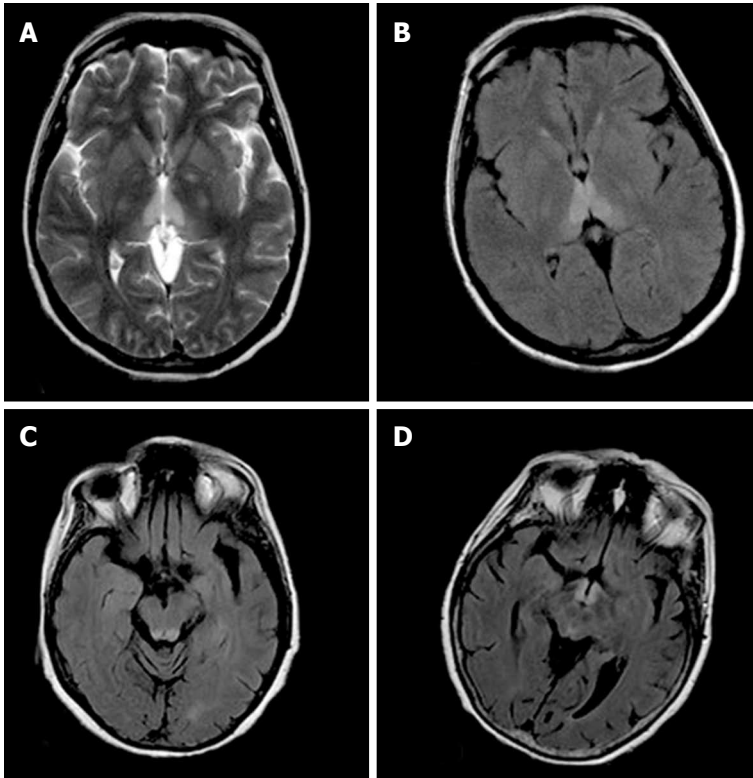


**Figure 1** Magnetic resonance images in a patient with alcoholic Wernicke's encephalopathy. A: Axial T2-weighted image shows symmetrical high signal intensity lesions in the medial thalami; B: Axial fluid-attenuated inversion recovery (FLAIR) image shows symmetrical high signal intensity lesions in the medial thalami; C: Axial FLAIR image shows symmetrical high signal intensity lesions in the periaqueductal area; D: Axial FLAIR image shows symmetrical high signal intensity lesions around the mammillary bodies.

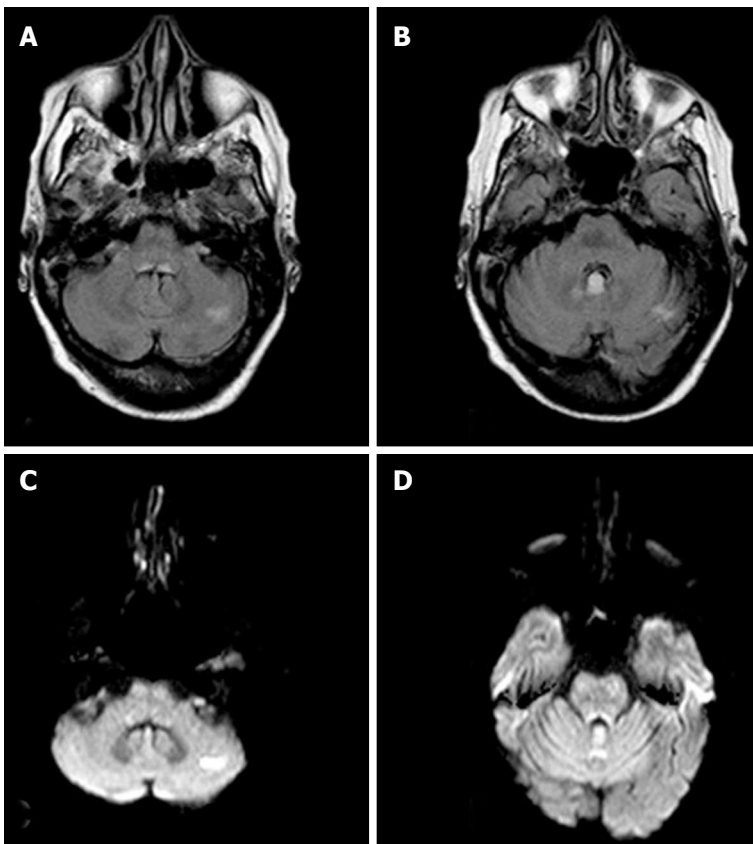


**Figure 2** Magnetic resonance images in a patient with nonalcoholic Wernicke's encephalopathy. A: Axial FLAIR image shows a high signal intensity lesion in the left cerebellar hemisphere; B: Axial FLAIR image shows a high signal intensity lesion in the cerebellar vermis; C: Axial DWI shows a high signal intensity lesion in the left cerebellar hemisphere; D: Axial DWI shows a high signal intensity lesion in the cerebellar vermis. FLAIR: Fluid-attenuated inversion recovery; DWI: Diffusion-weighted imaging.

and it can account as the cause of blood-brain barrier deficiency of these regions<sup>[11,12]</sup>.

Cytotoxic edema is considered the most distinctive lesion of acute WE, and it is easily shown on DWI images as it detects changes in the diffusion of water

molecules.

However, the presence of high signal intensities on DWI and decreased apparent diffusion coefficient values must be carefully evaluated as it could result from T2 shine-through effects<sup>[10]</sup>. Signal alterations on DWI most

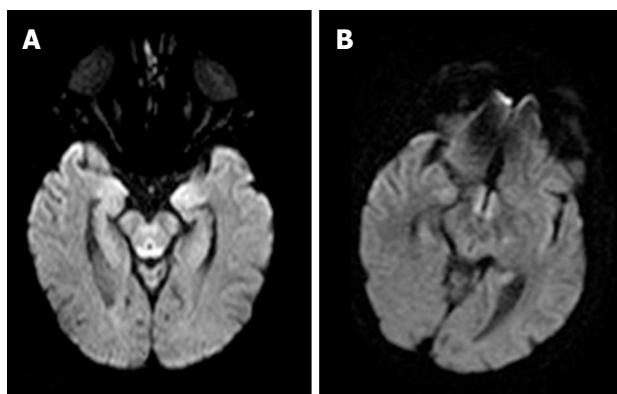


**Figure 3** Axial diffusion weighted image magnetic resonance images in a patient with alcoholic Wernicke's encephalopathy in the acute phase. A: Diffusion weighted image shows restricted diffusion in the periaqueductal grey matter; B: Diffusion weighted image shows restricted diffusion around the mammillary bodies.

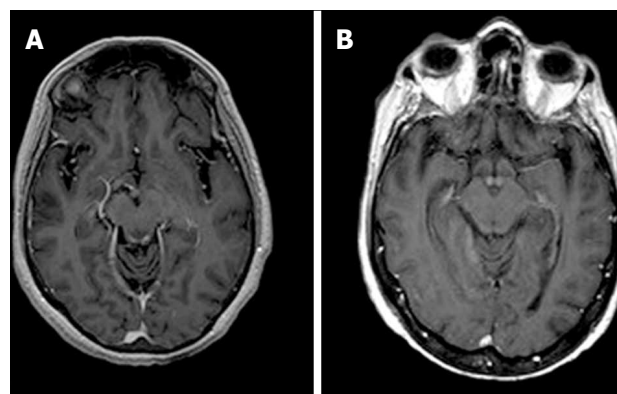


**Figure 4** Axial T1-weighted magnetic resonance images after contrast material administration in a patient with alcoholic Wernicke's encephalopathy. A: Enhanced axial T1-weighted image shows contrast-enhancement of the periaqueductal grey matter; B: Enhanced axial T1-weighted image shows contrast-enhancement around the mammillary bodies.

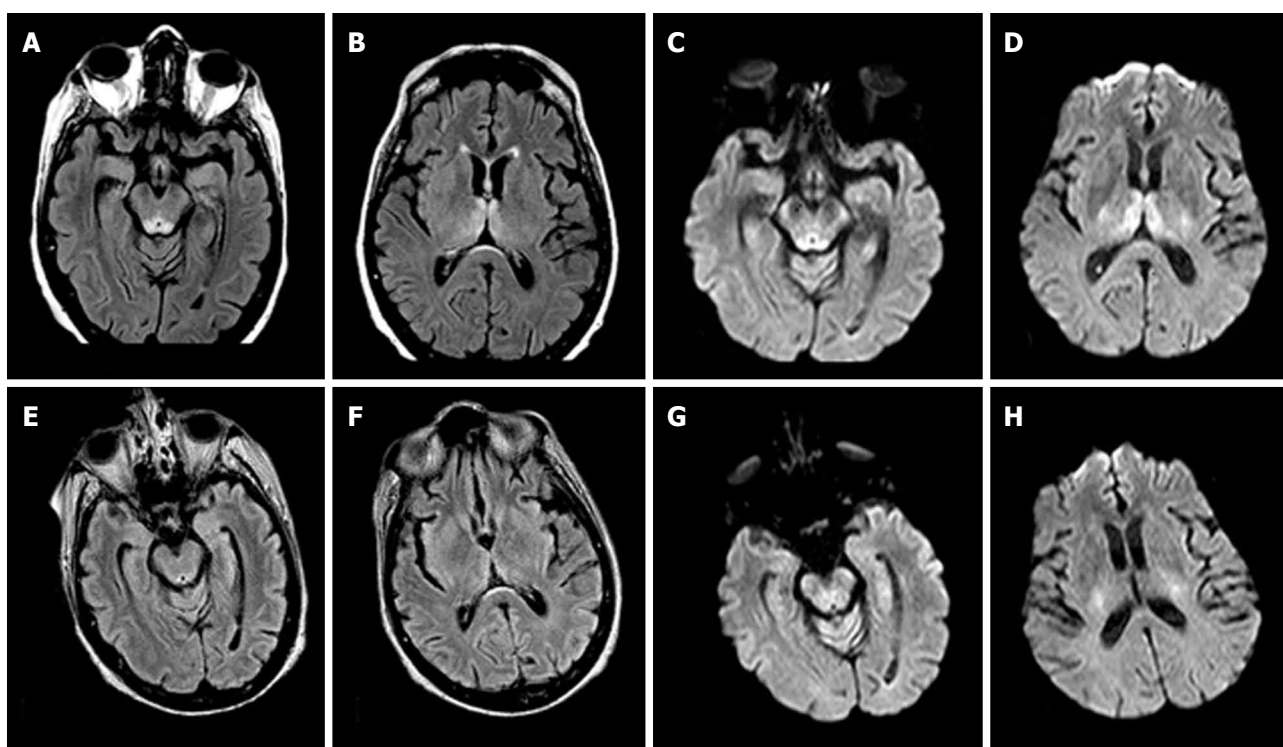


**Figure 5** Magnetic resonance images in a patient affected by alcoholic Wernicke's encephalopathy. A-D: MR images before intravenous administration of thiamine therapy; E-H: MR images after intravenous administration of thiamine therapy. Axial FLAIR images (A,B) and DWI images (C,D) show signal abnormalities in the periaqueductal area and in the medial thalami. Axial FLAIR (E,F) and DWI (G,H) follow-up MR images, after intravenous administration of thiamine therapy, show resolution of the signal abnormalities previously observed. MR: Magnetic resonance; FLAIR: Fluid-attenuated inversion recovery; DWI: Diffusion weighted image.

likely represent tissue at risk, similar to the cells in the ischemic penumbra, related to the cytotoxic edema and can be reversible<sup>[21]</sup>. In this study restricted diffusion was seen in 4 nonalcoholics and 2 alcoholics WE patients. At follow-up MR imaging obtained in 4 patients within 6 mo after thiamine therapy, resolution of these alterations was demonstrated confirming that restricted diffusion can be reversible (Figure 5).

According to previous reports<sup>[13,22]</sup>, contrast enhancement was observed more frequently in the mammillary

bodies in alcoholic patients (Figure 4), suggesting that mammillary bodies may be particularly susceptible to the toxic effects of alcohol.

Mammillary bodies enhancement, without mammillary body atrophy, is a finding that was associated with the acute phase of the disease, thus can allow an earlier diagnosis and treatment<sup>[22]</sup>.

If not treated or inappropriately treated, Wernicke's encephalopathy can lead to irreversible brain damage and, in 20% of cases, to death. Initial improvements in



acute symptoms can be observed within the first week after thiamine administration, but usually, one to 3 mo are needed to resolve<sup>[15,22]</sup>.

Our result confirms that MR signal abnormalities in WE can be reversible if a prompt therapy is established as demonstrated at follow-up MR imaging in 4 (2 alcoholic and 2 nonalcoholics WE) patients in our series (Figure 5).

The main limitation of this study is that it is a retrospective study without predefined criteria for diagnosis, which may have lead to a selection bias. Specifically, some patients with WE may not have been identified due to missed clinical diagnosis, particularly if they had atypical clinical manifestations and no history of alcohol abuse.

Despite these limitations, the diagnosis was confirmed in all patients as they clinically recovered after thiamine therapy and in 4 out of 7 patients resolution of the signal intensities abnormalities previously seen was demonstrated at follow-up MR imaging.

In conclusion, MR imaging is valuable in supporting the diagnosis of WE in patients with or without a history of alcohol abuse, especially in patients without the classic clinical presentation. Bilateral and symmetric increased T2-weighted and FLAIR MR signal intensity in the typical areas (periaqueductal area, medial thalami, mammillary bodies, tectal plate) are more often seen in alcoholic WE patients. Signal-intensity alterations in atypical sites (cerebellum, cranial nerve nuclei, and cerebral cortex) are found more frequently in nonalcoholic patients. Contrast-enhanced MR imaging and DWI MR imaging provides additional information to help diagnosis, especially in the acute phase of the disease, and should be included in the standard MR protocol in patients suspected to have WE. Knowledge of these MR imaging findings may be useful in the early diagnosis of WE and in reducing the complications associated with the disease.

## COMMENTS

### Background

Wernicke's encephalopathy (WE) is a serious neurologic disease, with acute onset, caused by thiamine deficiency. Alcohol abuse is the most common cause. Typical clinical presentation is characterized by a triad of symptoms: Ocular manifestations, ataxia and global confusion. However, this triad occurs in only 13%-18% of patients. Thus, magnetic resonance imaging (MRI) results are of utmost importance for the diagnosis of WE.

### Research frontiers

This study demonstrated that MR imaging can assist the diagnosis of WE, especially in patients with atypical clinical symptoms, or with no history of alcohol abuse.

### Applications

MR imaging is useful in supporting the diagnosis of WE. Knowledge of MR imaging findings can help radiologist in the early diagnosis, thus reducing the risk of complications.

### Terminology

Wernicke's encephalopathy: Acute neurologic disease caused by thiamine (vitamin B1) deficiency.

## Peer-review

Well written article. Nicely summarises brain imaging findings in WE including typical and atypical cases.

## REFERENCES

- 1 **Gui QP**, Zhao WQ, Wang LN. Wernicke's encephalopathy in nonalcoholic patients: clinical and pathologic features of three cases and literature reviewed. *Neuropathology* 2006; **26**: 231-235 [PMID: 16771180 DOI: 10.1111/j.1440-1789.2006.00665.x]
- 2 **Thomson AD**, Marshall EJ. The natural history and pathophysiology of Wernicke's Encephalopathy and Korsakoff's Psychosis. *Alcohol Alcohol* 2006; **41**: 151-158 [PMID: 16384871 DOI: 10.1093/alcalc/agh249]
- 3 **Zuccoli G**, Gallucci M, Capellades J, Regnicolo L, Tumiatì B, Giadàs TC, Bottari W, Mandrioli J, Bertolini M. Wernicke encephalopathy: MR findings at clinical presentation in twenty-six alcoholic and nonalcoholic patients. *AJNR Am J Neuroradiol* 2007; **28**: 1328-1331 [PMID: 17698536 DOI: 10.3174/ajnr.A0544]
- 4 **Fei GQ**, Zhong C, Jin L, Wang J, Zhang Y, Zheng X, Zhang Y, Hong Z. Clinical characteristics and MR imaging features of nonalcoholic Wernicke encephalopathy. *AJNR Am J Neuroradiol* 2008; **29**: 164-169 [PMID: 18192344 DOI: 10.3174/ajnr.A0827]
- 5 **Nolli M**, Barbieri A, Pinna C, Pasetto A, Nicosia F. Wernicke's encephalopathy in a malnourished surgical patient: clinical features and magnetic resonance imaging. *Acta Anaesthesiol Scand* 2005; **49**: 1566-1570 [PMID: 16223408 DOI: 10.1111/j.1399-6576.2-005.00879.x]
- 6 **Bonucchi J**, Hassan I, Policeni B, Kaboli P. Thyrotoxicosis associated Wernicke's encephalopathy. *J Gen Intern Med* 2008; **23**: 106-109 [PMID: 18026802 DOI: 10.1007/s11606-007-0438-3]
- 7 **Blanco-Muñoz O**, Suárez-Gauthier A, Martín-García H, Díaz-Konrad V, San Antonio-Román V, Cabello A. Unusual cortical compromise in a case of Wernicke's encephalopathy. *Rev Neurol* 2006; **42**: 596-599 [PMID: 16703527]
- 8 **Lindboe CF**, Løberg EM. Wernicke's encephalopathy in non-alcoholics. An autopsy study. *J Neurol Sci* 1989; **90**: 125-129 [PMID: 2723677 DOI: 10.1016/0022-510X(89)90095-6]
- 9 **Asato R**, Okumura R, Konishi J. "Fogging effect" in MR of cerebral infarct. *J Comput Assist Tomogr* 1991; **15**: 160-162 [PMID: 1987190 DOI: 10.1097/00004728-199101000-00029]
- 10 **Zuccoli G**, Pipitone N. Neuroimaging findings in acute Wernicke's encephalopathy: review of the literature. *AJR Am J Roentgenol* 2009; **192**: 501-508 [PMID: 19155417 DOI: 10.2214/AJR.07.3959]
- 11 **Bae SJ**, Lee HK, Lee JH, Choi CG, Suh DC. Wernicke's encephalopathy: atypical manifestation at MR imaging. *AJNR Am J Neuroradiol* 2001; **22**: 1480-1482 [PMID: 11559494]
- 12 **Gallucci M**, Bozzao A, Splendiani A, Masciocchi C, Passariello R. Wernicke encephalopathy: MR findings in five patients. *AJNR Am J Neuroradiol* 1990; **11**: 887-892 [PMID: 2120991 DOI: 10.2214/ajr.155.6.2122685]
- 13 **Sun GH**, Yang YS, Liu QS, Cheng LF, Huang XS. Pancreatic encephalopathy and Wernicke encephalopathy in association with acute pancreatitis: a clinical study. *World J Gastroenterol* 2006; **12**: 4224-4227 [PMID: 16830380 DOI: 10.3748/wjg.v12.i26.4224]
- 14 **Antunez E**, Estruch R, Cardenal C, Nicolas JM, Fernandez-Sola J, Urbano-Marquez A. Usefulness of CT and MR imaging in the diagnosis of acute Wernicke's encephalopathy. *AJR Am J Roentgenol* 1998; **171**: 1131-1137 [PMID: 9763009 DOI: 10.2214/ajr.171.4.9763009]
- 15 **Zhong C**, Jin L, Fei G. MR Imaging of nonalcoholic Wernicke encephalopathy: a follow-up study. *AJNR Am J Neuroradiol* 2005; **26**: 2301-2305 [PMID: 16219836]
- 16 **Park SH**, Kim M, Na DL, Jeon BS. Magnetic resonance reflects the pathological evolution of Wernicke encephalopathy. *J Neuroimaging* 2001; **11**: 406-411 [PMID: 11677881 DOI: 10.1111/j.1552-6569.2001.tb00070.x]
- 17 **Liu YT**, Fuh JL, Lirmg JF, Li AF, Ho DM, Wang SJ. Correlation of magnetic resonance images with neuropathology in acute Wernicke's encephalopathy. *Clin Neurol Neurosurg* 2006; **108**: 682-687

- [PMID: 15992992 DOI: 10.1016/j.clineuro.2005.05.010]
- 18 **Shogry ME**, Curnes JT. Mamillary body enhancement on MR as the only sign of acute Wernicke encephalopathy. *AJNR Am J Neuroradiol* 1994; **15**: 172-174 [PMID: 8141051]
  - 19 **D'Aprile P**, Gentile MA, Carella A. Enhanced MR in the acute phase of Wernicke encephalopathy. *AJNR Am J Neuroradiol* 1994; **15**: 591-593 [PMID: 8197963]
  - 20 **Zuccoli G**, Santa Cruz D, Bertolini M, Rovira A, Gallucci M, Carollo C, Pipitone N. MR imaging findings in 56 patients with Wernicke encephalopathy: nonalcoholics may differ from alcoholics. *AJNR Am J Neuroradiol* 2009; **30**: 171-176 [PMID: 18945789 DOI: 10.3174/ajnr.A1280]
  - 21 **Manzo G**, De Gennaro A, Cozzolino A, Serino A, Fenza G, Manto A. MR imaging findings in alcoholic and nonalcoholic acute Wernicke's encephalopathy: a review. *Biomed Res Int* 2014; **2014**: 503596 [PMID: 25050351 DOI: 10.1155/2014/503596]
  - 22 **Sparacia G**, Banco A, Lagalla R. Reversible MRI abnormalities in an unusual paediatric presentation of Wernicke's encephalopathy. *Pediatr Radiol* 1999; **29**: 581-584 [PMID: 10415181 DOI: 10.1007/s002470050652]

**P- Reviewer:** Kumar A, Prakash N   **S- Editor:** Kong JX  
**L- Editor:** A   **E- Editor:** Wu HL



## Observational Study

# Feasibility of imaging superficial palmar arch using micro-ultrasound, 7T and 3T magnetic resonance imaging

Alison N Pruzan, Audrey E Kaufman, Claudia Calcagno, Yu Zhou, Zahi A Fayad, Venkatesh Mani

Alison N Pruzan, Audrey E Kaufman, Claudia Calcagno, Yu Zhou, Zahi A Fayad, Venkatesh Mani, Translational and Molecular Imaging Institute, Department of Radiology, Icahn School of Medicine at Mount Sinai, New York, NY 10029, United States

**Author contributions:** Pruzan AN, Kaufman AE and Mani V designed the study and performed the research; Zhou Y helped perform the research and helped acquire ultrasound data; Calcagno C provided her imaging expertise and helped with MRI acquisition; Pruzan AN and Kaufman AE drafted the article and made critical revisions related to the intellectual content of the manuscript; Fayad ZA and Mani V helped with data analysis and interpretation; all authors reviewed and approved the manuscript content; Pruzan AN and Kaufman AE contributed equally to this research.

**Institutional review board statement:** This study was conducted in conformance with institutional policies with regard to human subject protections after informed consent and ethical permission were obtained.

**Conflict-of-interest statement:** There are no conflicts of interest to disclose.

**Data sharing statement:** No additional data are available.

**Open-Access:** This article is an open-access article which was selected by an in-house editor and fully peer-reviewed by external reviewers. It is distributed in accordance with the Creative Commons Attribution Non Commercial (CC BY-NC 4.0) license, which permits others to distribute, remix, adapt, build upon this work non-commercially, and license their derivative works on different terms, provided the original work is properly cited and the use is non-commercial. See: <http://creativecommons.org/licenses/by-nc/4.0/>

**Manuscript source:** Invited manuscript

**Correspondence to:** Venkatesh Mani, PhD, Translational and Molecular Imaging Institute, Department of Radiology, Icahn School of Medicine at Mount Sinai, 1470 Madison Avenue New York, NY 10029, United States. [venkatesh.mani@mssm.edu](mailto:venkatesh.mani@mssm.edu)  
Telephone: +1-212-8248538

Received: October 8, 2016

Peer-review started: October 10, 2016

First decision: December 13, 2016

Revised: December 17, 2016

Accepted: January 11, 2017

Article in press: January 14, 2017

Published online: February 28, 2017

## Abstract

### AIM

To demonstrate feasibility of vessel wall imaging of the superficial palmar arch using high frequency micro-ultrasound, 7T and 3T magnetic resonance imaging (MRI).

### METHODS

Four subjects (ages 22-50 years) were scanned on a micro-ultrasound system with a 45-MHz transducer (Vevo 2100, VisualSonics). Subjects' hands were then imaged on a 3T clinical MR scanner (Siemens Biograph MMR) using an 8-channel special purpose phased array carotid coil. Lastly, subjects' hands were imaged on a 7T clinical MR scanner (Siemens Magnetom 7T Whole Body Scanner) using a custom built 8-channel transmit receive carotid coil. All three imaging modalities were subjectively analyzed for image quality and visualization of the vessel wall.

### RESULTS

Results of this very preliminary study indicated that vessel wall imaging of the superficial palmar arch was feasible with a whole body 7T and 3T MRI in comparison with micro-ultrasound. Subjective analysis of image quality (1-5 scale, 1: poorest, 5: best) from B mode, ultrasound, 3T SPACE MRI and 7T SPACE MRI indicated that the image quality obtained at 7T was superior to both 3T MRI and micro-ultrasound. The 3D SPACE sequence at both 7T and 3T MRI with isotropic voxels allowed for multi-planar

reformatting of images and allowed for less operator dependent results as compared to high frequency micro-ultrasound imaging. Although quantitative analysis revealed that there was no significant difference between the three methods, the 7T Tesla trended to have better visibility of the vessel and its wall.

## CONCLUSION

Imaging of smaller arteries at the 7T is feasible for evaluating atherosclerosis burden and may be of clinical relevance in multiple diseases.

**Key words:** Superficial Palmar Arch; 7T and 3T magnetic resonance imaging; Micro-ultrasound; Atherosclerosis; Cardiovascular disease

© **The Author(s) 2017.** Published by Baishideng Publishing Group Inc. All rights reserved.

**Core tip:** The evaluation of smaller arteries in the hand may be clinically useful in a variety of vascular diseases. Imaging the vessel wall of such small caliber arteries (2.5 mm to 3.1 mm) requires very high spatial resolution and the use of either high frequency micro-ultrasound or 7 Tesla magnetic resonance imaging (MRI) would be the ideal tool to acquire these images. We sought to demonstrate feasibility of vessel wall imaging of the superficial palmar arch using 7T and 3T MRI in comparison with very high frequency micro-ultrasound.

Pruzan AN, Kaufman AE, Calcagno C, Zhou Y, Fayad ZA, Mani V. Feasibility of imaging superficial palmar arch using micro-ultrasound, 7T and 3T magnetic resonance imaging. *World J Radiol* 2017; 9(2): 79-84 Available from: URL: <http://www.wjgnet.com/1949-8470/full/v9/i2/79.htm> DOI: <http://dx.doi.org/10.4329/wjr.v9.i2.79>

## INTRODUCTION

A variety of pathological processes can affect the hand, including atherosclerosis, scleroderma, thromboangiitis obliterans (TO), hypothenar hammer syndrome and acute arterial thrombosis related to intraarterial injection<sup>[1]</sup>.

Atherosclerosis is a chronic complex process involving multiple factors including inflammation, oxidative stress, endothelial dysfunction, smooth muscle cell proliferation, platelet activation, and thrombosis, all leading to pathologic changes in the arterial wall with plaque formation<sup>[2]</sup>. The plaque is primarily composed of inflammatory cells, lipids, and calcium<sup>[3]</sup>. Chronic atherosclerosis can cause peripheral vascular occlusive disease in the extremities. In the upper extremity, atherosclerosis is more prevalent in the proximal subclavian artery but can occur in smaller distal vessels with resultant morbidity<sup>[4]</sup>. For example, young diabetics who have diffuse distal atherosclerosis, end-stage

renal disease and are on renal dialysis are at high risk for developing finger gangrene<sup>[5]</sup>. In the autoimmune disorder scleroderma, ultrasound evaluation has shown that the ulnar artery proximal to the wrist is specifically targeted<sup>[6]</sup>. The vasculopathy of scleroderma can cause secondary Raynaud's phenomenon, as well as digital ulcers. Doppler sonography has proven useful in assessing palmar and digital arteries in these cases<sup>[7,8]</sup>. TO also known as Buerger's disease, is a panarteritis of unknown origin, which demonstrates a strong concurrence with tobacco use. It affects both small and medium-sized vessels of the extremities. The thrombotic and inflammatory changes associated with TO cause vascular changes with associated arteriographic findings<sup>[9-11]</sup>. Hypothenar hammer syndrome, a post-traumatic pathology arising from repetitive hitting of the hypothenar region of the hand, can cause ulnar artery occlusive disease with thromboembolism and resulting ischemia to the digits<sup>[12,13]</sup>. The thrombosis secondary to TO and hypothenar hammer syndrome may be relatively localized, whereas diffuse arterial thrombosis of the hand may occur secondary to intraarterial injection of medications or illegal substances<sup>[14]</sup>. Visualizing atherosclerotic changes in small arteries such as the superficial palmar arch may provide valuable clinical insights into the progression of these disease states.

Imaging the vessel wall of smaller caliber arteries requires higher resolution imaging when compared to imaging larger vessels such as the aorta and carotid arteries. For this purpose we conducted MR evaluation of the superficial palmar arch using 7T and 3T whole body MR scanners and compared the images acquired with high frequency micro-ultrasound imaging. The superficial palmar arch is the continuation of the ulnar artery as it passes distal to the flexor retinaculum in the hypothenar region of the palm. We chose to focus on the superficial palmar arch because it is easily and consistently visualized using the modalities employed. We hypothesize that 7T MRI will provide better delineation of the vessel wall as compared to 3T and may be a suitable method to visualize small arteries in the hand. We also believe that ultrasound may be a convenient alternative compared to 3T and 7T due to its image acquisition speed and wide availability. But, conventional clinical ultrasound (about 3-7 MHz) may lack resolution, so the use of a high frequency (45-MHz) micro-ultrasound typically used in animal models may be better suited for superficial structures such as the palmar arch.

## MATERIALS AND METHODS

### Study population

Four subjects (ages 22-50 years) were scanned on a micro-ultrasound system with a 45-MHz transducer (Vevo 2100, VisualSonics, Toronto, Canada) (Figure 1A). While this system is primarily used in animal studies, it has been successfully and safely used in



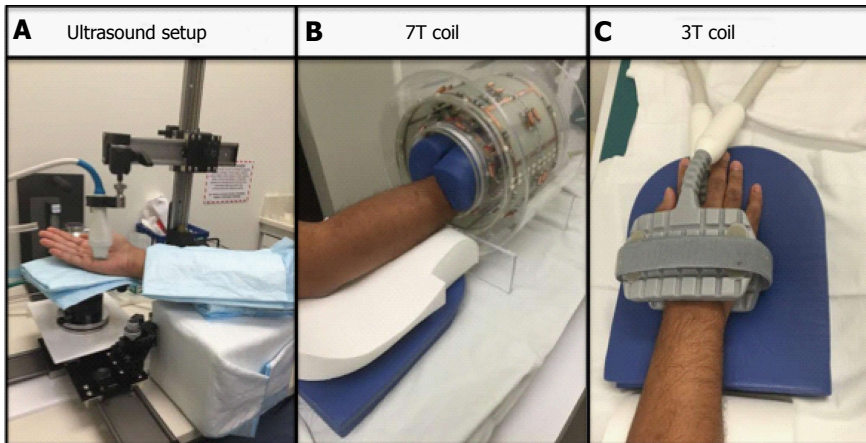


**Figure 1** The figure shows the set up for the ultrasound (A), the 7T (B) and the 3T (1) respectively.

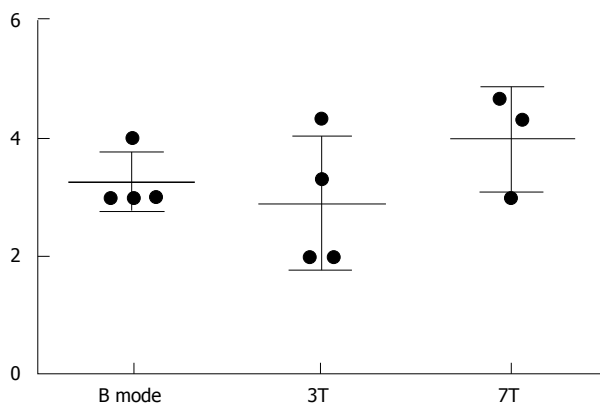


**Figure 2** Data from 3 subjective analyses of image quality (1-5 scale). Error bars included.

clinical studies, which include infants and children.<sup>[15,16]</sup> Subjects' hands were then imaged on a 3T clinical MR scanner (Siemens Biograph MMR) using an 8-channel special purpose phased array carotid coil (Figure 1C). Lastly, subjects' hands were imaged on a 7T clinical MR scanner (Siemens Magnetom 7T Whole Body Scanner) using a custom built 8-channel transmit receive carotid coil (Figure 1B).

#### Micro-ultrasound imaging and protocol

The Vevo Imaging Station (Vevo 2100, VisualSonics, Toronto, Canada) was used for mounting the transducer and for stabilizing the position of the hand. The subject was seated during the scan with the hand in supine position with slight rotation toward neutral. Padding was also used under the hand and arm for stabilization and comfort purposes (Figure 1A). With this positioning, images in B mode, Power mode, Doppler mode and M mode of the superficial palmar arch were obtained. Images were then subjectively analyzed for image quality. Three readers rated the images on a score: (1) is a non-visible vessel with non-visible walls and poor image quality; (2) represents a vessel with indistinct vessel walls and poor image quality; (3) is a vessel with adequate image quality with walls moderately well seen; (4) represents a vessel with

**Table 1** Imaging protocol for both 3T and 7T magnetic resonance imaging

Parameter	7T T2 SPACE	3T T2 SPACE	7T TOF	3T TOF
TE	101	77	2.81	3.23
TR	1500	1600	60	21
Slice thickness	625.00 $\mu$ m	630.00 $\mu$ m	160.00 mm	1.00 mm
Pixel size	0.600/0.600	0.625/0.625	0.3125/0.3125	0.234/0.234
Number of averages	2	4	1	1
Field of view	136 $\times$ 160	100 $\times$ 160	160 $\times$ 160	107 $\times$ 120

distinct vessel walls and good image quality; and (5) is excellent visualization of the vessel and image quality. Results from the three readers were averaged. Criteria used for subjective evaluation were the overall image quality, visualization of the vessel wall, adequate flow suppression and absence of artifacts. We also obtained measures of average peak Doppler velocity, intima media thickness, wall thickness, lumen diameter, and total vessel diameter.

#### MR imaging and protocol

Subjects' hands were imaged on a 3T clinical MR scanner (Siemens Biograph MMR) using an 8-channel special purpose phased array carotid coil (Figure 1C). Subjects' hands were imaged on a 7T clinical MR scanner (Siemens Magnetom 7T Whole Body Scanner) using a custom built 8-channel transmit receive carotid coil (Figure 1B). Subjects were imaged in a head first prone position with hand extended above the head. The imaging protocols between 3T and 7T were matched as closely as possible. Total scan time was approximately 20 min each. We acquired a localizer, a 3D time-of-flight (TOF) MR angiography sequence followed by a 3D T2 weighted Sampling Perfection with Application optimized Contrasts using different flip angle Evolution (SPACE) sequence<sup>[1,17,18]</sup> and a 0.6 mm isotropic resolution in all dimensions (Table 1). MR images were also subjectively analyzed for image quality and visualization of the vessel wall. The imaging criteria used were similar to that for the ultrasound. Furthermore, we also measured

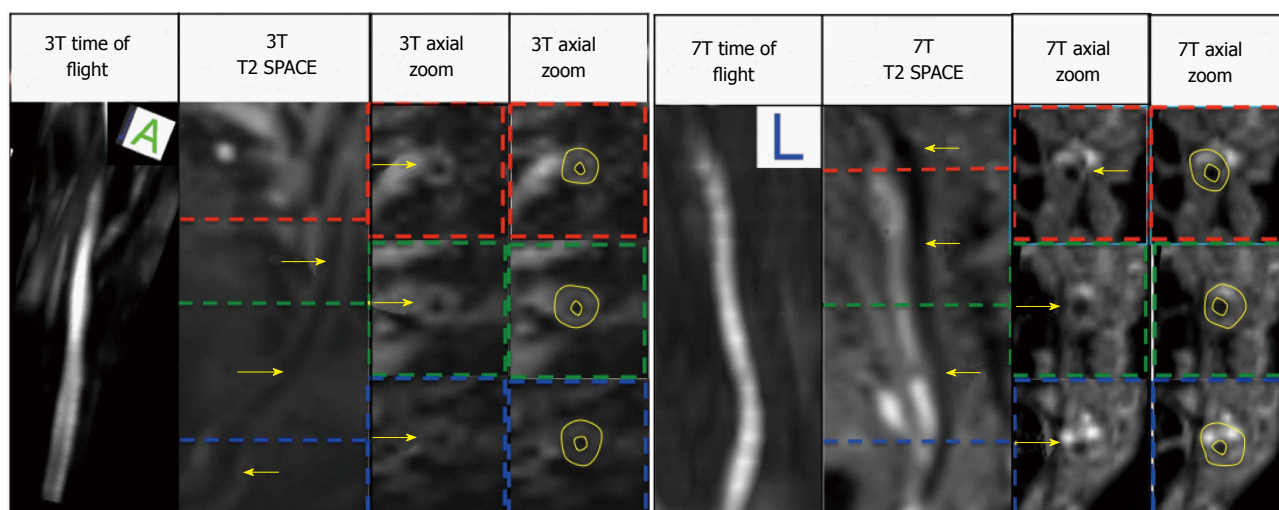


Figure 3 Displays the 3T images (Left) and the 7T images (Right) the arrows point to vessel wall.

**Table 2** Data from 3 subjective analyses of image quality with average and standard deviation

Subject	B mode	3T	7T
1	3.00	3.33	3.00
2	3.00	2.00	Not available
3	3.00	4.33	4.67
4	4.00	2.00	4.33
Average	3.25	2.92	4.00
Standard deviation	0.50	1.13	0.882

**Table 3** RM one-way ANOVA and Tukey's multiple comparisons test

Vessel wall measurements	P value
Lumen area	0.3152
Wall area	0.0628
Total vessel area	0.0573
Normalized wall index	0.0362 <sup>a</sup>
Wall thickness	0.0519

<sup>a</sup> $P < 0.05$ , significant.

wall thickness, lumen and outer diameters from the MR images. The order of the imaging tests was randomized.

### Statistical analysis

The data were expressed as the mean  $\pm$  SD. For the statistics, a RM one-way ANOVA and Tukey's multiple comparisons test were used.  $P < 0.05$  was considered as statistically significant.

## RESULTS

Subjective analysis of image quality was performed (1-5 scale, 1: Vessel non-visible, 5: Clearly visible vessel wall) from B mode, ultrasound, 3T SPACE MRI and 7T SPACE MRI. These results are shown in Table 2 and Figure 2.

In addition, lumen area, wall area, total vessel area, and wall thickness were automatically calculated by a MatLab script (MATLAB and Statistics Toolbox Release 2012b, The MathWorks, Inc., Natick, Massachusetts, United States) for the manually drawn contours on the 3T and 7T images using a customized software program (Vessel Mass Software, Leiden University Medical Center, The Netherlands) (Figure 3). Sonographic images were analyzed on the micro-ultrasound machine using the software on the B and M Mode photos (Figure 4) and data was extracted and used to calculate the aforementioned measurements by hand in Microsoft Excel.

## DISCUSSION

Qualitative analysis indicated that the image quality obtained at 7T trended to be superior to both 3T MRI and micro-ultrasound (Figure 2 and Table 2). Compared to the 3D Time of Flight, the 3D SPACE sequence with isotropic voxels allowed for multi-planar reformatting of images and allowed for less operator dependent results as compared to high frequency micro-ultrasound imaging. Although there was no significant difference between the three methods ( $P = 0.5647$ , One-Way ANOVA), the 7T Tesla trended to have better visibility of the vessel and its wall (Table 2, Figures 2 and 3).

The One-Way ANOVA between all 3 imaging modalities showed that 7T, 3T and micro-ultrasound imaging are all comparable imaging methods with no statistical difference between extracted values, (lumen area, wall area, total vessel area, wall thickness)<sup>[19,20]</sup> [ $P > 0.05$  (Table 3)]. *Post hoc* test using Tukey's correction however showed significant differences when comparing 3T and micro-ultrasound for wall thickness.

Results of this very preliminary study indicated that vessel wall imaging of the superficial palmar arch was feasible with a whole body 7T MRI with subjective evaluations indicating that the image quality obtained at 7T is superior to both 3T MRI and micro-ultrasound. The 3D SPACE sequence with isotropic voxels allowed

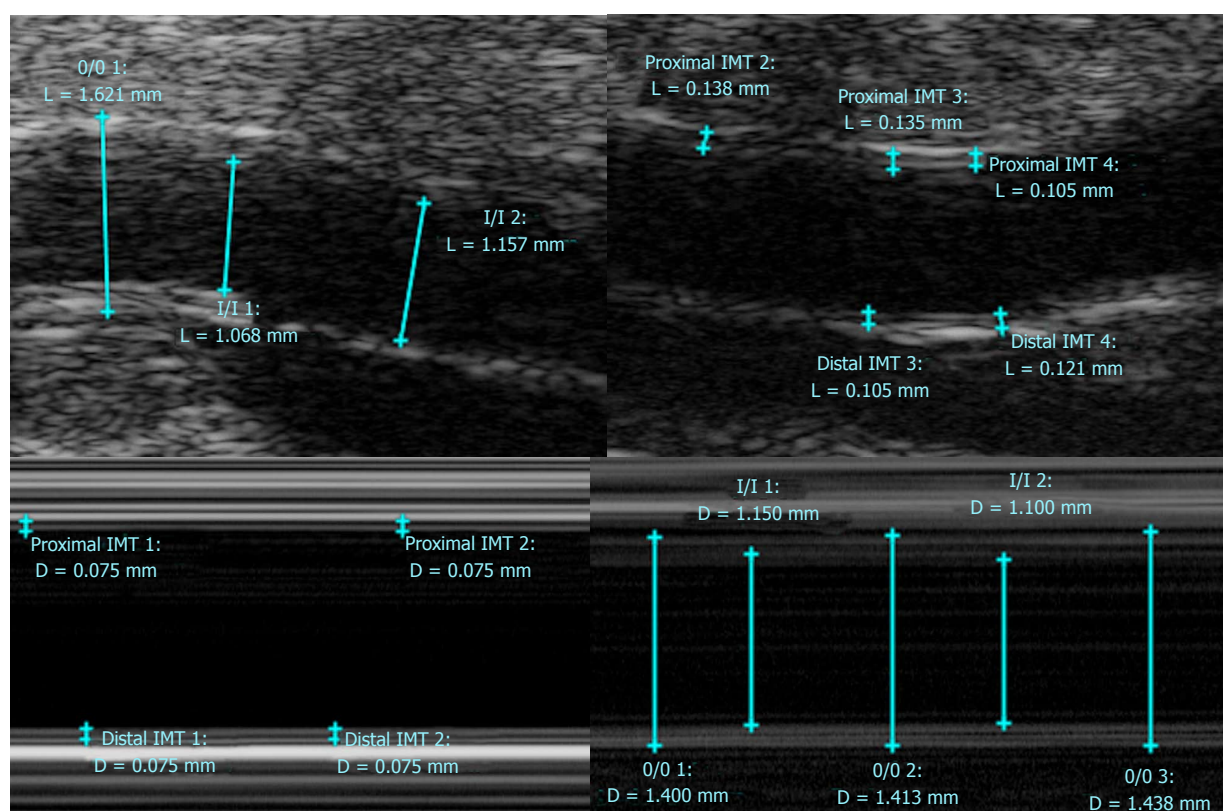


Figure 4 Ultrasound Images (B mode, M mode).

multi-planar reformatting of images and allows for less operator dependent results as compared to ultrasound imaging. Scanning time for the micro-ultrasound portion of the study approached that of the MR scan times, however with more operator experience the micro-ultrasound scan time could improve. The time spent on post-processing image analysis was similar across all modalities. Limitations of this study include a very small sample size and the fact that only healthy individuals without any atherosclerotic disease were examined. Future investigation should study individuals with diseased conditions in a larger sample size. Additionally, methods to optimize image quality could include warming the region of interest prior and during imaging to dilate the vessel and provide better contrast between the lumen and the vessel wall structures. This technique has been shown to optimize image quality in peripheral 2D TOF MRA evaluation<sup>[21]</sup>.

In conclusion, imaging of the superficial palmar arch at the 7T is feasible with high frequency micro-ultrasound, 3T and 7T MRI and should be considered for evaluating arterial pathology. This may be of clinical relevance in specific disease conditions such as atherosclerosis, scleroderma, diabetes, TO, hypothenar hammer syndrome and acute arterial thrombosis related to intraarterial injection. Future studies need to be performed in diseased individuals and in a larger number of subjects to better establish clinical feasibility of the approach.

## COMMENTS

### Background

Imaging the vessel wall of smaller caliber arteries requires higher resolution imaging when compared to imaging larger vessels such as the aorta and carotid arteries. For this purpose the authors conducted MR evaluation of the superficial palmar arch using 7T and 3T whole body MR scanners and compared the images acquired with high frequency ultrasound imaging. The author chose to focus on the superficial palmar arch because it is easily and consistently visualized using the modalities employed.

### Research frontiers

A variety of pathological processes can affect the hand, including atherosclerosis, scleroderma, thromboangitis obliterans, hypothenar hammer syndrome and acute arterial thrombosis related to intraarterial injection. These diseases are currently evaluated using sonography, arteriography, and standard 1.5 or 3T MRI. The intent of the investigation is to improve and potentially advance imaging techniques for evaluation of these diseases.

### Innovations and breakthroughs

A thorough search of medical literature shows few if any prior investigations related to imaging the superficial palmar arch on a 7T MRI and therefore this is a novel application.

### Applications

Future evaluation for atherosclerosis and other diseases may involve non-invasive 3T or 7T MR as well as micro-ultrasound imaging of the superficial palmar arch.

### Peer-review

Imaging of smaller artery is feasible using micro-ultrasound and 3T and 7T MRI. Interesting and good study enough for publication.



## REFERENCES

- 1 **Wong SK**, Mobolaji-lawal M, Arama L, Cambe J, Biso S, Alie N, Fayad ZA, Mani V. Atherosclerosis imaging using 3D black blood TSE SPACE vs 2D TSE. *World J Radiol* 2014; **6**: 192-202 [PMID: 24876923 DOI: 10.4329/wjr.v6.i5.192]
- 2 **Faxon DP**, Fuster V, Libby P, Beckman JA, Hiatt WR, Thompson RW, Topper JN, Annex BH, Rundback JH, Fabunmi RP, Robertson RM, Loscalzo J. Atherosclerotic Vascular Disease Conference: Writing Group III: pathophysiology. *Circulation* 2004; **109**: 2617-2625 [PMID: 15173044 DOI: 10.1161/01.CIR.0000128520.37674.EF]
- 3 **Alie N**, Eldib M, Fayad ZA, Mani V. Inflammation, Atherosclerosis, and Coronary Artery Disease: PET/CT for the Evaluation of Atherosclerosis and Inflammation. *Clin Med Insights Cardiol* 2014; **8**: 13-21 [PMID: 25674025 DOI: 10.4137/CMC.S17063]
- 4 **Zimmerman NB**. Occlusive vascular disorders of the upper extremity. *Hand Clin* 1993; **9**: 139-150 [PMID: 8444972]
- 5 **Yeager RA**, Moneta GL, Edwards JM, Landry GJ, Taylor LM, McConnell DB, Porter JM. Relationship of hemodialysis access to finger gangrene in patients with end-stage renal disease. *J Vasc Surg* 2002; **36**: 245-249; discussion 249 [PMID: 12170204]
- 6 **Stafford L**, Englert H, Gover J, Bertouch J. Distribution of macrovascular disease in scleroderma. *Ann Rheum Dis* 1998; **57**: 476-479 [PMID: 9797553]
- 7 **Lescoat A**, Coiffier G, Rouil A, Droitcourt C, Cazalets C, de Carlan M, Perdriger A, Jégo P. Vascular evaluation of the hand by Power Doppler Ultrasonography provides new predictive markers of ischemic digital ulcers in systemic sclerosis. *Arthritis Care Res (Hoboken)* 2016 Jul 7; Epub ahead of print [PMID: 27390194 DOI: 10.1002/acr.22965]
- 8 **Chikui T**, Izumi M, Eguchi K, Kawabe Y, Nakamura T. Doppler spectral waveform analysis of arteries of the hand in patients with Raynaud's phenomenon as compared with healthy subjects. *AJR Am J Roentgenol* 1999; **172**: 1605-1609 [PMID: 10350298 DOI: 10.2214/ajr.172.6.10350298]
- 9 **Rivera-Chavarría IJ**, Brenes-Gutiérrez JD. Thromboangiitis obliterans (Buerger's disease). *Ann Med Surg (Lond)* 2016; **7**: 79-82 [PMID: 27144003 DOI: 10.1016/j.amsu.2016.03.028]
- 10 **Gallagher KA**, Tracci MC, Scovell SD. Vascular arteritides in women. *J Vasc Surg* 2013; **57**: 27S-36S [PMID: 23522715 DOI: 10.1016/j.jvs.2012.10.119]
- 11 **Fazeli B**, Rezaee SA. A review on thromboangiitis obliterans pathophysiology: thrombosis and angiitis, which is to blame? *Vascular* 2011; **19**: 141-153 [PMID: 21652666 DOI: 10.1258/vasc.2010.ra0045]
- 12 **Marie I**, Hervé F, Primard E, Cailleux N, Levesque H. Long-term follow-up of hypothernar hammer syndrome: a series of 47 patients. *Medicine (Baltimore)* 2007; **86**: 334-343 [PMID: 18004178 DOI: 10.1097/MD.0b013e31815c95d3]
- 13 **Carpentier PH**, Biro C, Jiguet M, Maricq HR. Prevalence, risk factors, and clinical correlates of ulnar artery occlusion in the general population. *J Vasc Surg* 2009; **50**: 1333-1339 [PMID: 19837535 DOI: 10.1016/j.jvs.2009.07.076]
- 14 **Iannuzzi NP**, Higgins JP. Acute Arterial Thrombosis of the Hand. *J Hand Surg Am* 2015; **40**: 2099-2106 [PMID: 26408378 DOI: 10.1016/j.jhsa.2015.04.015]
- 15 **Ymalay R**, Sadanala U, Tinney JP, Kriss V, Keller BB. Initial Observations and Limitations of Vevo 2100 High Resolution Ultrasound Imaging in Neonates. *J Invest Med* 2012; **60**: 379
- 16 **Kaufman CL**, Ouseph R, Blair B, Kutz JE, Tsai TM, Scheker LR, Tien HY, Moreno R, Ozyurekoglu T, Banegas R, Murphy E, Burns CB, Zaring R, Cook DF, and Marvin MR. Graft Vasculopathy in Clinical Hand Transplantation. *Am J Transplant* 2012; **12**: 1004-1016 [DOI: 10.1111/j.1600-6143.2011.03915]
- 17 **Mihai G**, Chung YC, Merchant A, Simonetti OP, Rajagopalan S. T1-weighted-SPACE dark blood whole body magnetic resonance angiography (DB-WBMRA): initial experience. *J Magn Reson Imaging* 2010; **31**: 502-509 [PMID: 20099365 DOI: 10.1002/jmri.22049]
- 18 **Zhang Z**, Fan Z, Carroll TJ, Chung Y, Weale P, Jerecic R, Li D. Three-dimensional T2-weighted MRI of the human femoral arterial vessel wall at 3.0 Tesla. *Invest Radiol* 2009; **44**: 619-626 [PMID: 19692844 DOI: 10.1097/RLI.0b013e3181b4c218]
- 19 **Fayad ZA**, Mani V, Woodward M, Kallend D, Abt M, Burgess T, Fuster V, Ballantyne CM, Stein EA, Tardif JC, Rudd JH, Farkouh ME, Tawakol A. Safety and efficacy of dalcetrapib on atherosclerotic disease using novel non-invasive multimodality imaging (dal-PLAQUE): a randomised clinical trial. *Lancet* 2011; **378**: 1547-1559 [PMID: 21908036 DOI: 10.1016/S0140-6736(11)61383-4]
- 20 **Balu N**, Chu B, Hatsukami TS, Yuan C, Yarnykh VL. Comparison between 2D and 3D high-resolution black-blood techniques for carotid artery wall imaging in clinically significant atherosclerosis. *J Magn Reson Imaging* 2008; **27**: 918-924 [PMID: 18383253 DOI: 10.1002/jmri.21282]
- 21 **Blackband SJ**, Buckley DL, Knowles AJ, Gibbs P, Turnbull LW, Horsman A. Improved peripheral MR angiography with temperature regulation in healthy patients. *Radiology* 1996; **198**: 899-902 [PMID: 8628890 DOI: 10.1148/radiology.198.3.8628890]

**P- Reviewer:** Chow J, Gumustas OG, Tang GH **S- Editor:** Qi Y  
**L- Editor:** A **E- Editor:** Wu HL





## Observational Study

# Gastric blunt traumatic injuries: A computed tomography grading classification

Antonio Solazzo, Giulia Lassandro, Francesco Lassandro

Antonio Solazzo, Department of Radiology, AO Bolognini di Seriate, 24068 Seriate, Italy

Giulia Lassandro, Department of Radiology, Federico II University, 80131 Naples, Italy

Francesco Lassandro, Department of Radiology, Monaldi Hospital, 80131 Naples, Italy

**Author contributions:** Solazzo A and Lassandro G analyzed and interpreted the data and drafted the article; Lassandro F designed the study, acquired data and critically revised the article; all the authors approved the version for publication.

**Institutional review board statement:** Approved by ethical committee of SUN-Monaldi n.940 August 2, 2016.

**Informed consent statement:** Participants informed consent was not obtained to be enrolled in this study, but data are anonymized and risk of identification is low.

**Conflict-of-interest statement:** All the authors have no conflict of interests.

**Data sharing statement:** No addition data are available.

**Open-Access:** This article is an open-access article which was selected by an in-house editor and fully peer-reviewed by external reviewers. It is distributed in accordance with the Creative Commons Attribution Non Commercial (CC BY-NC 4.0) license, which permits others to distribute, remix, adapt, build upon this work non-commercially, and license their derivative works on different terms, provided the original work is properly cited and the use is non-commercial. See: <http://creativecommons.org/licenses/by-nc/4.0/>

**Manuscript source:** Invited manuscript

**Correspondence to:** Francesco Lassandro, MD, Department of Radiology, Monaldi Hospital, via Leonardo Bianchi, 80131 Naples, Italy. [f.lassandro@gmail.com](mailto:f.lassandro@gmail.com)  
Telephone: +39-081-5786114  
Fax: +39-081-5786114

Received: July 13, 2016

Peer-review started: July 16, 2016

First decision: September 2, 2016

Revised: October 30, 2016

Accepted: December 1, 2016

Article in press: December 2, 2016

Published online: February 28, 2017

## Abstract

### AIM

To produce a radiological grading of gastric traumatic injuries.

### METHODS

In our study, we retrospectively analyzed 32 cases of blunt gastric traumatic injuries and compared computed tomography (CT) data with patients' surgical or medical development. In all cases, a basal phase was acquired, and an intravenous contrast material was administered *via* an antecubital venous catheter with acquisition in the venous phase (70-90 s). In addition, a further set of delayed scans was performed 4-5 min after the first scanning session, without supplementary intravenous contrast material, to identify or better define areas of active bleeding. All CT examinations were retrospectively reviewed by two radiologists, with more than 5 years of experience in emergency radiology, to detect signs of gastric injuries and/or associated abdominal lesions according to literature data. Specific CT findings for gastric rupture include luminal content extravasation and discontinuity of the gastric wall, while CT findings suggestive of injury consisted of free peritoneal fluid, extraluminal air, pneumatosis, and thickening and hematoma of gastric wall.

### RESULTS

We found 32 gastric traumatic injuries. In 22 patients

(68.8%), the diagnosis was based on the surgical findings; in the other 10 patients (31.2%), the diagnosis was based on the clinical and CT radiological data. We observed discontinuity of the gastric wall and luminal content extravasation in 1 patient (3.1%); in 10 patients (31.2%), there was extra-luminal air in the peritoneum. In 28 patients (87.5%), there was peritoneal fluid, which was blood in 14 patients (hematoma in 11 patients and contrast material extravasation from active bleeding in 3 patients). In 15 patients (46.9%), there was gastric wall thickening. In 3 patients, it was possible to identify a prevalent involvement of the external layer of the gastric wall, whereas, in 2 patients, the inner side of the gastric wall presented with major involvement. In 3 patients (9.4%), pneumatosis of the gastric wall was detected. In 19 (59.4%) patients, the stomach was full. The fundus was the most frequently damaged part of the stomach because it was involved in 17 patients (53.1%). Based on the observed data, we identified four grades of gastric lesions.

## CONCLUSION

A radiologic score is helpful for guiding the diagnosis and management (surgical or conservative) of gastric blunt traumatic injuries and stratify patients according to short-term outcomes.

**Key words:** Gastric injuries; Blunt trauma; Computed tomography grading; Emergency radiology; Stomach rupture

© **The Author(s) 2017.** Published by Baishideng Publishing Group Inc. All rights reserved.

**Core tip:** Although a wide spectrum of computed tomography findings has been described for gastric blunt traumas, no systematic instrumental approach exists in this setting. In this study the authors produced a radiological grading of gastric traumatic injuries that might play a role in both the diagnostic phase of the emergency setting and prognostic stratification of these patients.

Solazzo A, Lassandro G, Lassandro F. Gastric blunt traumatic injuries: A computed tomography grading classification. *World J Radiol* 2017; 9(2): 85-90 Available from: URL: <http://www.wjgnet.com/1949-8470/full/v9/i2/85.htm> DOI: <http://dx.doi.org/10.4329/wjr.v9.i2.85>

## INTRODUCTION

In Europe, blunt trauma is the main cause of death in the first four decades of life, and there is a substantial rate of permanent disability<sup>[1,2]</sup>.

Blunt trauma involving the stomach is infrequent with a reported incidence of 0.4%-1.7%<sup>[3-5]</sup>; however, such trauma may cause extremely high individual and social consequences<sup>[6]</sup>.

Management of traumatic injuries requires a high index of suspicion, rapid investigation, accurate classification and well-defined treatment protocols to ensure optimal outcomes and reduce long-term disabilities<sup>[7]</sup>.

Clinical signs and symptoms of gastrointestinal injuries often require hours before they appear, and a delayed diagnosis may prolong the period of peritoneal contamination, increasing the incidence of intra-abdominal complications, such as abscess, sepsis, and mortality<sup>[8,9]</sup>. Moreover, the differentiating between injuries requiring surgery and those that can be treated conservatively may be very challenging<sup>[10]</sup>.

The widespread introduction of traumatic injury classifications, based on clinical and instrumental findings for most of the abdominal organs, has greatly improved the management of patients with traumatic injuries<sup>[7]</sup>. Although a wide spectrum of computed tomography (CT) findings has been described for gastric blunt traumas, no systematic instrumental approach exists in this setting<sup>[11]</sup>. For this reason, we sought to produce a radiological grading of gastric traumatic injuries in our study that might play a role in both the diagnostic phase of the emergency setting and prognostic stratification of these patients.

## MATERIALS AND METHODS

Over a 14-year period, from January 2002 to December 2015, a total of 32 patients (22 males and 10 females; age range 16-82 years, mean age: 41.34) with evidence of blunt gastric traumatic injuries were retrospectively identified based on the final surgical and radiological reports.

The diagnosis of gastric injury was based on the surgical findings in 22 patients, whereas the diagnosis for 10 patients was based on the clinical and radiological findings. CT scan was performed in all patients.

CT scans were performed with different scanners over time, reflecting the evolution of the technique, ranging from single slice helical CT to 64-row detector CT. In all cases, a basal phase was acquired, and an intravenous contrast material was administered *via* an antecubital venous catheter with acquisition in the venous phase (70-90 s). In addition, a further set of delayed scans was performed 4-5 min after the first scanning session, without supplementary intravenous contrast material, to identify or better define areas of active bleeding.

All CT examinations were retrospectively reviewed by two radiologists, with more than 5 years of experience in emergency radiology, to detect signs of gastric injuries and/or associated abdominal lesions according to literature data. Specific CT findings for gastric rupture include luminal content extravasation and discontinuity of the gastric wall, while CT findings suggestive of injury consisted of free peritoneal fluid, extraluminal air, pneumatosis, and thickening and hematoma of gastric wall<sup>[11]</sup>.

**Table 1** Computed tomography signs of gastric blunt traumatic injuries

CT signs of gastric blunt traumatic injuries ( <i>n.</i> 57 in 32)	
Gastric wall discontinuity	1
Extraluminal air	10
Peritoneal fluid	28
Hematoma	11
Contrast material	3
Luminal content extravasation	1
Gastric wall thickening	15
Pneumatosis of gastric wall	3

CT: Computed tomography.

**Table 2** Abdominal associated lesions

Abdominal associated lesions ( <i>n.</i> 33 in 27 patients)	
Large bowel	2
Spleen	14
Liver	9
Left kidney	3
Right kidney	1
Pancreas	1
Mesentery	3

We evaluated the relevance of each instrumental pattern of gastric blunt injury, comparing the radiological signs with surgical findings or clinical follow-up, to propose a radiologic classification for this type of injury.

## RESULTS

We found 32 gastric traumatic injuries. In 22 patients (68.8%), the diagnosis was based on the surgical findings; in the other 10 patients (31.2%), the diagnosis was based on the clinical and CT radiological data.

We observed (Table 1) discontinuity of the gastric wall and luminal content extravasation in 1 patient (3.1%); in 10 patients (31.2%), there was extra-luminal air in the peritoneum (it was linked to pneumoretroperitoneum in 2 patients and to pneumomediastinum in 1 patient). In 28 patients (87.5%), there was peritoneal fluid, which was blood in 14 patients (hematoma in 11 patients and contrast material extravasation from active bleeding in 3 patients). In 15 patients (46.9%), there was gastric wall thickening. In 3 patients, it was possible to identify a prevalent involvement of the external layer of the gastric wall, whereas, in 2 patients, the inner side of the gastric wall presented with major involvement. In 3 patients (9.4%), pneumatosis of the gastric wall was detected. In 19 (59.4%) patients, the stomach was full.

Twenty-seven patients (84.4%) presented with associated abdominal lesions. The spleen was the most frequently involved organ (43.8%), which was followed by the liver (28.1%), kidneys (12.5%), large bowel (6.3%), mesentery (9.4%) and pancreas (3.1%) (Table 2).

The fundus was the most frequently damaged part of the stomach because it was involved in 17 patients

**Table 3** Location of gastric lesions

Location of gastric lesions	
Fundus	17
Body	15
Anterior wall	7
Greater curvature	2
Small curvature	1
Posterior surface	3
Antrum	3
Not detectable	1

(53.1%) (Table 3).

All patients with extraluminal air and/or peritoneal hematic collections underwent surgery. Among the 22 patients with a surgical diagnosis of gastric lesions, 14 showed radiological signs that were directly related to gastric involvement (thickening of the gastric wall, extraluminal air in proximity to the gastric wall and discontinuity of the gastric wall) (66.6%). In the other 8 patients, a gastric lesion was diagnosed during surgery, but it was not detected on the CT scan.

Peritoneal fluid was detected in all patients who underwent surgery, but it was also present in 6 of 10 patients who were conservatively treated (60%).

Nine out of 10 patients who had not undergone surgery showed a thickened gastric wall on CT. Perigastric pneumatosis was the only sign in one patient.

Pneumatosis of the gastric wall was observed in 3 patients (9.4%), two with significant gastric lesion requiring surgery and one who recovered spontaneously.

Based on the observed data, we identified four grades of gastric lesions.

Cases with minor contusion with parietal thickening alone (Figure 1), which did not involve the fundus and was not associated with the peritoneal fluid, and only included portal pneumatosis (Figure 2) detected by CT scan, do not require surgical intervention (grade 1 lesion). Cases of minor lacerations with high attenuating focal thickening involving the mucosal side and with a small level without hematic peritoneal fluid (Figure 3) require monitoring (grade 2 lesion). Cases with partial laceration with parietal hematoma and/or stretching of the external layer and peritoneal hematic collection (Figure 4) require careful monitoring (grade 3 lesion). Cases with full thickness rupture, necrosis, food in peritoneal cavity, vascular involvement and contrast media extravasation (Figure 5) require intervention (grade 4 lesion) (Table 4).

## DISCUSSION

Trauma currently represents a major social and sanitary problem with characteristics of an epidemic illness involving especially young people and with a high residual morbidity.

Gastric blunt traumas often occur after high velocity impact involving the epigastric region when the stomach is full, in the post-prandial phase<sup>[12-14]</sup>, due to



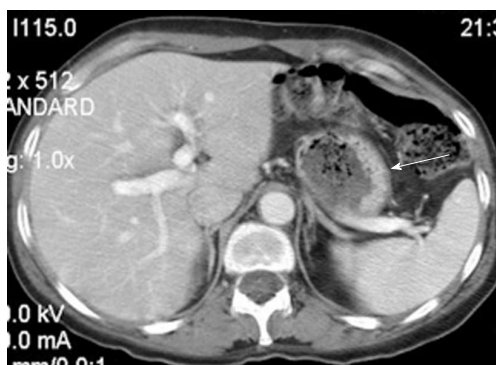


**Figure 1** Wall thickening of the gastric body (arrow). Surgery was not required. Grade 1 lesion.



**Figure 2** Isolated gastric pneumatosis after abdominal trauma (arrows). Spontaneous recovery. Grade 1 lesion.



**Figure 3** Blood in the gastric lumen (arrow). Follow-up without surgery. Grade 2 lesion.

the positive correlation between the wall pressure and cavity radius, as explained in Laplace's law. These data were confirmed by an experimental model of rats that also demonstrated a higher frequency and grade of injury of other parenchymal organs in rats with full stomachs<sup>[15]</sup>. Moreover, a full thickness rupture is more frequently observed at the level of the fundus<sup>[11,16]</sup>. The mechanisms responsible for gastric injuries in blunt trauma include tangential tearing along fixed points,

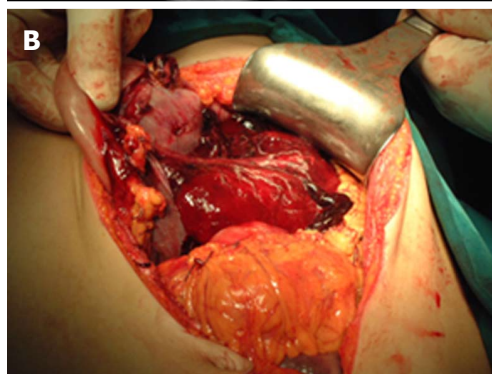


**Figure 4** Parietal hematoma. A: Parietal hematoma: Thickening with high-attenuation in the external layer of gastric wall (arrows). Grade 3 lesion. Follow-up with subsequent surgery for worsening symptoms and peritoneal reaction; B: External layer gastric wall hematoma confirmed at surgery.

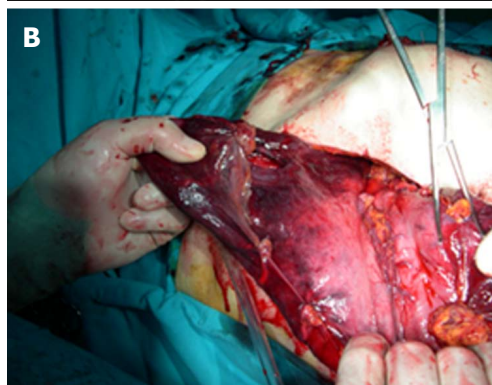
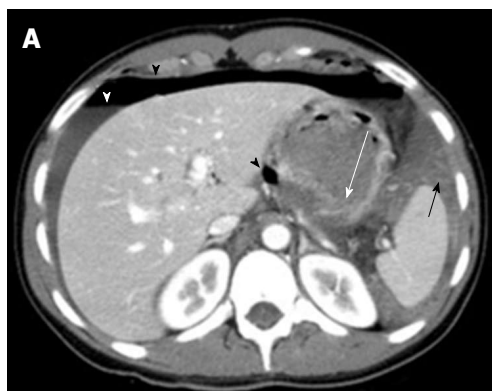


**Figure 5** Gastric rupture. A: Gastric wall rupture (white arrow): Peritoneal fluid (white arrowhead) with homogeneous hyperdense components from blood (black arrow), pneumoperitoneum with a bubble of gas located close to the gastric lesion (black arrowheads). Grade 4 lesion; B: Gastric rupture confirmed at surgery.



**Table 4** Grading computed tomography of gastric blunt traumatic injuries

	Pathology	CT signs	Treatment
Grade 1	Gastric contusion	Gastric wall thickening No peritoneal fluid	No surgery
Grade 2	Minor lacerations involving the mucosal side	Perigastric pneumatosis High-attenuation hematoma confined to the inner side, blood in the gastric lumen	Follow-up
Grade 3	Partial laceration with parietal hematoma and/or stretching of the external layer	Small amount of non-bloody peritoneal fluid Peritoneal hematoma collection, gastric wall thickening with high-attenuation of the external side	Close follow-up/ surgery
Grade 4	Full thickness rupture Vascular involvement (necrosis or active bleeding)	Extraluminal air Luminal content extravasation Contrast material extravasation	Emergency surgery

CT: Computed tomography.

increased intraluminal pressure, and crushing against vertebral bodies<sup>[17]</sup>.

In the management of trauma patients, diagnostic imaging plays a key role, especially CT, which is considered the gold standard for accurate and fast detection of abdominal injuries.

To standardize and improve clinical outcomes, especially for prompt identification of patients who need to be referred to surgery, radiological scores have been widely used.

Although they represent 0.4%-1.7% of all abdominal traumas<sup>[12,18-20]</sup>, gastric blunt traumatic injuries have rarely been described in the medical literature<sup>[12,18-21]</sup>, and a CT grading classification is not yet available. For this reason, we propose a radiological score based on our experience and literature data to better classify these lesions (Table 4).

Full thickness rupture of the stomach requires prompt surgical intervention, which is also the cases with vascular involvement, infarct or hemorrhage. However, in several cases, a parietal thickening may be observed on CT scans, bringing attention to the stomach without necessarily requiring surgery.

In some cases, the gas content of the stomach, which usually plays a protective role, can dissect the mucosal layer and pass into the gastric veins, causing perigastric pneumatosis and, subsequently, portal pneumatosis<sup>[10,11,22]</sup>, a condition that could be related to more serious conditions, such as an intestinal infarction from traumatic shock.

Extraluminal air, hematic peritoneal collection and active bleeding suggest patients should be referred to surgery. Proximal lesions with fundus involvement more often require surgery. In other cases, less aggressive treatment and surveillance may be indicated.

However, in 33.3% of our patients who required surgery, a gastric injury was detected on surgical intervention without any previous radiological suspicion. The use of a simple classification could help guide medical practice.

In conclusion, traumatic injuries require a careful and systematic treatment approach because of their economic and social relevance. For these reasons,

uncommon lesions require attention, and a meta-analysis should be performed.

## COMMENTS

### Background

Gastric injuries after blunt trauma have rarely been reported in the literature; however, preoperative recognition and staging of these lesions play a critical role in patient management.

### Research frontiers

The widespread introduction of traumatic injury classifications, based on clinical and instrumental findings for most of the abdominal organs, has greatly improved the management of patients with traumatic injuries. Although a wide spectrum of computed tomography findings has been described for gastric blunt traumas, no systematic instrumental approach exists in this setting.

### Innovations and breakthroughs

The authors produced a radiological grading of gastric traumatic injuries.

### Applications

The study results suggest that a radiological grading of gastric traumatic injuries might play a role in both the diagnostic phase of the emergency setting and prognostic stratification of these patients.

### Peer-review

The authors investigated gastric blunt traumatic injuries about computed tomography classification. The work is good and well designed.

## REFERENCES

- 1 Bode PJ, Edwards MJ, Kruit MC, van Vugt AB. Sonography in a clinical algorithm for early evaluation of 1671 patients with blunt abdominal trauma. *AJR Am J Roentgenol* 1999; **172**: 905-911 [PMID: 10587119 DOI: 10.2214/ajr.172.4.10587119]
- 2 van Beeck EF, van Roijen L, Mackenbach JP. Medical costs and economic production losses due to injuries in the Netherlands. *J Trauma* 1997; **42**: 1116-1123 [PMID: 9210552 DOI: 10.1097/00005373-199706000-00023]
- 3 Takabe K, Ohtani T, Muto I, Takano Y, Miyauchi T, Kato H, Sekido H, Ohki S, Hatakeyama K, Shimada H. Computed tomography (CT) findings of gastric rupture after blunt trauma. *Hepatogastroenterology* 2000; **47**: 901-903 [PMID: 10919058]
- 4 Oncel D, Malinoski D, Brown C, Demetriades D, Salim A. Blunt gastric injuries. *Am Surg* 2007; **73**: 880-883 [PMID: 17939417]
- 5 Bruscagin V, Coimbra R, Rasslan S, Abrantes WL, Souza HP, Neto G, Dalcin RR, Drumond DA, Ribas JR. Blunt gastric injury. A

- multicentre experience. *Injury* 2001; **32**: 761-764 [PMID: 11754882 DOI: 10.1016/S0020-1383(01)00081-X]
- 6 **Hoyt DB**, Coimbra R, Potenza BM. Trauma System, Triage, and Transport. In: Feliciano DV, Mattox KL, Moore EE, Bonnie RJ, Fulco CE, Liverman CT, editors. *Magnitude and Costs. Reducing the burden of injury. Advancing Prevention and Treatment*. Washington, DC, United States: National Academy Press, 1999
- 7 **Oniscu GC**, Parks RW, Garden OJ. Classification of liver and pancreatic trauma. *HPB* (Oxford) 2006; **8**: 4-9 [PMID: 18333232 DOI: 10.1080/13651820500465881]
- 8 **Brody JM**, Leighton DB, Murphy BL, Abbott GF, Vaccaro JP, Jagminas L, Cioffi WG. CT of blunt trauma bowel and mesenteric injury: typical findings and pitfalls in diagnosis. *Radiographics* 2000; **20**: 1525-1536; discussion 1536-1537 [PMID: 11112806 DOI: 10.1148/radiographics.20.6.g00nv021525]
- 9 **Butela ST**, Federle MP, Chang PJ, Thaete FL, Peterson MS, Dorvault CJ, Hari AK, Soni S, Branstetter BF, Paisley KJ, Huang LF. Performance of CT in detection of bowel injury. *AJR Am J Roentgenol* 2001; **176**: 129-135 [PMID: 11133551 DOI: 10.2214/ajr.176.1.1760129]
- 10 **Scaglione M**, de Lutio di Castelguidone E, Scialpi M, Merola S, Diettrich AI, Lombardo P, Romano L, Grassi R. Blunt trauma to the gastrointestinal tract and mesentery: is there a role for helical CT in the decision-making process? *Eur J Radiol* 2004; **50**: 67-73 [PMID: 15093237 DOI: 10.1016/j.ejrad.2003.11.016]
- 11 **Lassandro F**, Romano S, Rossi G, Muto R, Cappabianca S, Grassi R. Gastric traumatic injuries: CT findings. *Eur J Radiol* 2006; **59**: 349-354 [PMID: 16787728 DOI: 10.1016/j.ejrad.2006.04.028]
- 12 **Courcy PA**, Soderstrom C, Brotman S. Gastric rupture from blunt trauma. A plea for minimal diagnostics and early surgery. *Am Surg* 1984; **50**: 424-427 [PMID: 6331779]
- 13 **Siemens RA**, Fulton RL. Gastric rupture as a result of blunt trauma. *Am Surg* 1977; **43**: 229-233 [PMID: 851294]
- 14 **Takabe K**, Hatakeyama K. Computed tomography is useful for preoperative workup of gastric rupture caused by blunt trauma. *Surg Today* 2009; **39**: 1109 [PMID: 19997812 DOI: 10.1007/s00595-009-4069-7]
- 15 **Kafadar H**, Kafadar S, Tokdemir M. Comparison of internal organ injuries by blunt abdominal trauma in rats with empty or full stomach. *Ulus Travma Acil Cerrahi Derg* 2014; **20**: 395-400 [PMID: 25541917 DOI: 10.5505/tjtes.2014.92331]
- 16 **Shinkawa H**, Yasuhara H, Naka S, Morikane K, Furuya Y, Niwa H, Kikuchi T. Characteristic features of abdominal organ injuries associated with gastric rupture in blunt abdominal trauma. *Am J Surg* 2004; **187**: 394-397 [PMID: 15006569 DOI: 10.1016/j.amjsurg.2003.12.018]
- 17 **Madiba TE**, Hlophe M. Gastric trauma: a straightforward injury, but no room for complacency. *S Afr J Surg* 2008; **46**: 10-13 [PMID: 18468416]
- 18 **Brunsting LA**, Morton JH. Gastric rupture from blunt abdominal trauma. *J Trauma* 1987; **27**: 887-891 [PMID: 3612865 DOI: 10.1097/00005373-198708000-00007]
- 19 **Pikoulis E**, Delis S, Tsatsoulis P, Leppäniemi A, Derlopas K, Koukoulides G, Mantonakis S. Blunt injuries of the stomach. *Eur J Surg* 1999; **165**: 937-939 [PMID: 10574100 DOI: 10.1080/110241599750008035]
- 20 **Semel L**, Frittelli G. Gastric rupture from blunt abdominal trauma. *N Y State J Med* 1981; **81**: 938-939 [PMID: 6940012]
- 21 **Nanji SA**, Mock C. Gastric rupture resulting from blunt abdominal trauma and requiring gastric resection. *J Trauma* 1999; **47**: 410-412 [PMID: 10452486 DOI: 10.1097/00005373-199908000-00040]
- 22 **Kingsley DD**, Albrecht RM, Vogt DM. Gastric pneumatosis and hepatoportal venous gas in blunt trauma: clinical significance in a case report. *J Trauma* 2000; **49**: 951-953 [PMID: 11086792 DOI: 10.1097/00005373-200011000-00027]

**P- Reviewer:** Bazeed MF, Gao BL, Shen J **S- Editor:** Gong XM

**L- Editor:** A **E- Editor:** Wu HL





Published by **Baishideng Publishing Group Inc**

8226 Regency Drive, Pleasanton, CA 94588, USA

Telephone: +1-925-223-8242

Fax: +1-925-223-8243

E-mail: [bpgoffice@wjgnet.com](mailto:bpgoffice@wjgnet.com)

Help Desk: <http://www.wjgnet.com/esps/helpdesk.aspx>

<http://www.wjgnet.com>

